Stereochemical matching determines both helix type and handedness in α/γ-peptides with a cyclic-constrained γ-amino acid

Dayi Liu, Ali T. Mansour, Ogaritte Yazbeck, Daoud Naoufal, Sylvie Robin, Eric Gloaguen, Valérie Brenner, Michel Mons* and David J. Aitken*

SUPPORTING INFORMATION

Table of Contents

1. Theoretical chemistry

1.1 Methodology

A theoretical analysis of the relative stability of the 12 and 12/10 helical types with either left (L) or right (R) handedness was undertaken on six N-Boc capped α/γ-peptides (where Boc = *tert*-butoxycarbonyl): two tetrapeptides with a C-terminus benzylamide cap (**1A**, **3A**), two hexapeptides with a C-terminus benzyl ester cap (**2E**, **4E**) and two hexapeptides with a C-terminus benzylamide cap (**2A**, **4A**). A complete analysis of the landscape was first undertaken on the **2A** and **4A** hexapeptides and then extended to the shorter compounds, through a selection of helical structures based on the low energy structures of each backbone type found in the **2A** and **4A** compounds. Geometry optimizations were carried using the TurboMole package,[S1] at the B97-D3 level of theory[S2] using the Becke-Johnson damping and the three-body term options (B97-D3(BJ)-abc), with a def2-TZVPPD basis set.[S3, S4] The resolution-of-identity (RI) approximation[S5] and the auxiliary associated basis[S6-S8] were also used. A *m3* default grid size and a convergence threshold of 10^{-5} a.u. on the norm of the Cartesian gradient were used. Starting geometries were taken from the initial study by Hofmann and coworkers describing α/γ-peptide helices.[S9] Due to the size of the molecules studied, numerical harmonic frequencies were calculated at a more modest level of theory (RI-B97-D3(BJ)/def2-TZVP) on structures optimized at the same level of theory, since previous tests carried out on dipeptides provided frequencies similar to those obtained at the higher level. These calculations were made using the *numforce* module with the *central* option and a step length of 0.02 a.u., which allowed us to determine Gibbs enthalpies.

Structures, energetics in solution were carried out using the Conductor-like Screening Model approximation (COSMO),[S10] implemented in the Turbomole Package, where the solute molecule forms a cavity within the dielectric continuum of permittivity ε that represents the solvent. Structure optimizations were carried out at the same level of theory than in the gas phase and in presence of the solvent (RI-B97-D3(BJ)-abc/def2-TZVPPD + COSMO). For chloroform, ε was taken as 4.81. For the same reason as mentioned above, numerical harmonic vibrational frequencies were also obtained at the more modest RI-B97-D3(BJ)/def2-TZVP +COSMO level of theory, on structures optimized at the same level. For comparison with solution spectra this level of theory was tested on the 12 helical form of a related hexapeptide, well-characterized in chloroform, namely a capped octamer of *trans*-2-aminocyclobutane carboxylic acid (ACBC):[S11] it gave a satisfactory full vibrational frequency set (Figure S1-1), within a reasonable calculation time, providing that harmonic frequencies were scaled according to a region-dependent scaling procedure described in detail previously,[S12] with, for the amide A, I and II regions, scaling factors of 0.978, 1.008 and 1.004 respectively for the RI-B97-D3(BJ)/def2-TZVP + COSMO level of theory. The same values were thus applied to the present harmonic calculations on the α/γ-peptides.

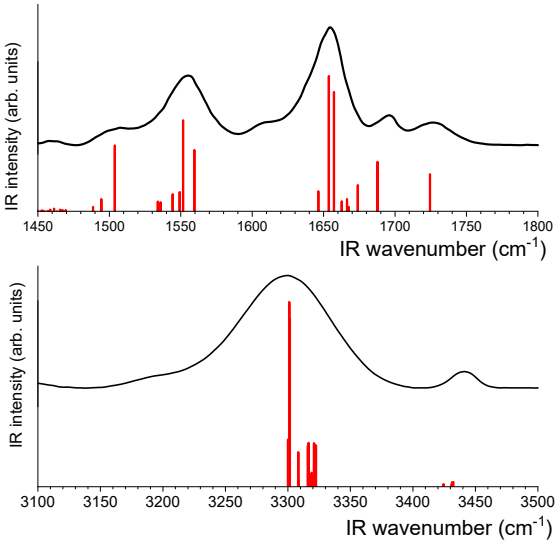

Figure S1-1. Experimental solution spectrum (black lines) of the Boc-$(ACBC)_8$-OMe molecule (a capped ACBC octamer) in the amide I and II (top panel) and amide A (lower panel) regions, used to calibrate the scaled theoretical spectra (red sticks), using region-dependent scaling factors.

1.2 Understanding configurational effects on the helix stabilities in chiral α/γ-peptides

In order to rationalize the dependence of the conformational landscape upon the Ala residue configuration in the chiral α/γ-peptides studied, a series of quantum chemistry investigations was carried out, starting from gas phase structure and energetics in a first step, eventually completed by solvation effects. In particular, the role of the *R* or *S* configuration of the Ala residue was investigated in the gas phase by comparing the structures of (*R,R,R*) and (*R,R,S*) hexapeptides **2A** and **4A** with the related hexapeptide **5** in which alanine residues are replaced by glycine and with the unsubstituted backbone hexapeptide **6** that corresponds to the Hofmann model system (see Figure S1-2).

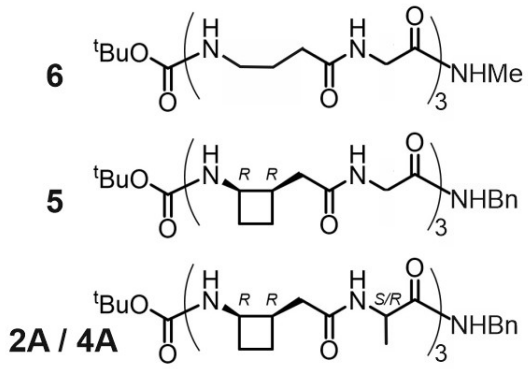

Figure S1-2. Structures of compounds examined in the Ala-dependence theoretical analysis. Hexapeptides 2A and 4A are those used in the experimental studies. In compound 5, each Ala residue of 2A/4A is replaced by Gly. In compound 6, the cyclobutane ring constraint is removed and the Bn cap is replaced by a simpler Me cap.

In compound **6**, the θ backbone dihedral of the γ residue in 12/10 and 12 helices is ± 33° and ± 53° respectively,[S9] the latter being slightly less stable by 16 kJ/mol in the gas phase (present calculations of the electronic energy at the RI-B97-D3(BJ)-abc/def2-TZVPPD level of theory). A condition to preserve the helical structures when substituting the backbone, e.g., when going from **6** to **5**, is that the constraints introduced into the backbone by the cyclic residue are not too different from these reference values. In compound **5**, the cyclobutane ring imposes a θ dihedral of ca. ± 30°,[S13] but is nevertheless accommodated within the helices at the price of a distortion of the nominal helical backbone (Table S1-2), significantly larger in 12 helices, which qualitatively explains their lower stability (Table S1-1, Figure S1-3, top center panel) compared to the 12/10 species.

The presence of the (*R,R*)-^{3,4}CB-GABA residues in compound **5** causes a degeneracy lifting between the left- and right-handed conformations of each of the helices compared to the unsubstituted α/γ-peptide **6** (see Figure S2-3, top center panel, blue arrows). As a matter of fact, R-12/10 helices, the most stable forms, are slightly favored relative to L-12/10, while the R-12 helices are strongly disfavored over L-12 forms. This latter feature correlates nicely with the presence of steric clashes (Table S1-1) involving consecutive γ-residues in the R-12 helix, as evidenced by the pictorial comparison of the two helical handednesses (Figure S1-4). In contrast, in the 12/10 helix, similar backbones are found, suggesting that the more modest difference in stability between L and R relies more on the backbone energetics, e.g., particular handedness-specific hyperconjugation effects.

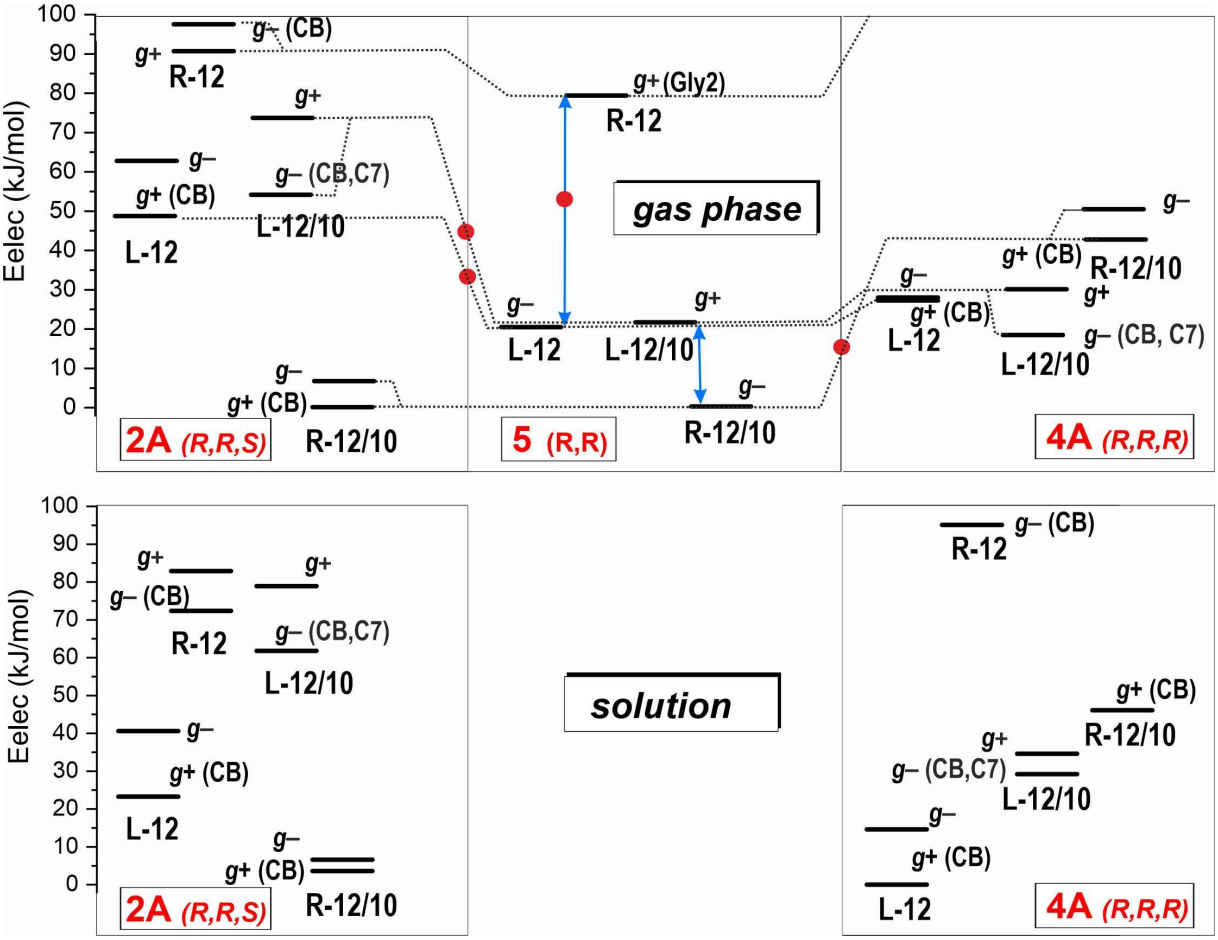

Figure S1-3: Relative energetics (RI-B97-D3(BJ)-abc/def2-TZVPPD electronic energies) of the (*R*,*R*,*R*) and (*R*,*R*,*S*) configurations of the hexapeptides 2A and 4A, in the gas phase (upper panel) and in a chloroform solution (lower panel), as obtained by quantum chemistry calculations at the B97-D3/def2-TZVPPD + COSMO model level of theory. In the upper panel, compounds 2A and 4A (left and right, resp.) are compared to compound 5 (center), where the Ala is substituted by an achiral Gly residue (see Figure S1-2). The blue arrows (center) indicate the degeneracy lift between the L and R forms for each helical type of compound 5, which is induced by the (*R*,*R*) chirality of the γ-residue. Dotted lines illustrate the relative variations in stability induced by the Ala residue. Strong variations, indicated by red dots, are all accompanied by steric clashes (see below). For the sake of comparison, the diastereoisomeric compounds 2A and 4A share the same energy reference, which is also that taken for compound 5. Same labelling as in Figure 3 of the main text.

Table S1-1. Relevant energetic data calculated for the L-12, R-12, L-12/10 and R-12/10 helical types of selected conformations of peptides 1A, 2A, 2E, 3A, 4A and 4E (all energies in kJ/mol). Electronic energies were first obtained in the gas phase at the RI-B97-D3(BJ)abc/def2-TZVPPD level of theory and in a chloroform solution using the COSMO polarizable model. Gibbs energies at 300 K were obtained for the lower conformations from a ZPE and thermal corrections calculated at the RI-B97-D3(BJ)/def2-TZVP level of theory and the COSMO model. Conformations are labelled according to the orientation of the Bn group (g+/g–), the presence of an interaction of this group with the cyclobutane of last γ-residue (CB), and the eventual replacement of a C10 H-bond by a C7 bond at the C-terminus (C7). The H-bonding network is also given from the H-bonding status of each NH group along the peptide backbone. For the hexapeptide amides 2A and 4A, the energetic stabilization due to solvation is also given together with the corresponding dipole moments (in Debye).

Compound	**2A** (R,R,S)								**4A** (R,R,R)							
helix type	L-12		R-12		L-12/10		R-12/10		L-12		R-12		L-12/10		R-12/10	
	g+ (Bn)	g-	g- (Bn)	g+	g+	g- (CB,C7)	g+ (Bn)	g-	g+ (Bn)	g-	g- (Bn)	g+	g- (CB,C7)	g+	g+ (Bn)	g-
Gas Phase Eelec (TZVPPD) (a)	48.9	62.7	98.4	90.6	74.3	54.7	0	6.7	27.3	28.0	120	127.6	18.4	30.1	42.9	50.6
Chloroform Eelec (TZVPPD) (b)	23.3	40.6	72.4	82.9	78.9	61.8	3.6	6.6	0	14.6	95.1	105.1	29.2	34.6	46.1	52.5
Solution Delta G (300K) (c)	21.7	38.1	75.1	82.9	76.1	62	2.8	2.5	0	6.4	94.6	101.0	27.3	26.5	56.5	51.7
Delta G (300K) (d)	19.2	35.5	72.7	80.5	73.6	59.6	0.3	0	0	6.4	94.6	101.0	27.3	26.5	56.5	51.7
Eelec (solution) - Eelec (gas)	-87.6	-84.1	-88.0	-69.7	-57.5	-54.8	-58.5	-62.2	-89.4	-75.5	-86.9	-84.5	-51.4	-57.6	-58.8	-60.1
dipole PG (De)	24.4	24.5	25.1	25.2	4.3	5.2	4.2	4.3	24.6	22.4	24.7	23.7	4.0	3.5	3.0	3.2
dipole solution (De)	29.8	30.2	30.4	30.3	5.5	7.7	5.5	5.5	29.7	30.1	30.2	29.6	4.2	4.3	4.2	4.6

Compound	**2E** (R,R,S)						**4E** (R,R,R)							
helix type	L-12		R-12	L-12/10	R-12/10		L-12		R-12		L-12/10		R-12/10	
	g+ (Bn)		g- (Bn)	g+	g+ (Bn)	g-	g+ (Bn)	g-		g+	g- (CB,C7)	g+	g+ (Bn)	g-
Gas Phase Eelec (TZVPPD) (a)	67.5	75.4	110.6	67.6	0	3.0	46.7	65.5		132.1	30.5	27.7	47.6	43.6
Chloroform Eelec (TZVPPD) (b)	37.1	45.7			0	0.0	18.6	34.1			31.4	28.2	41.2	42.9
Solution Delta G (300K) (c)	38.3	45.1			18.5	0	22.4	26.2			40.4	30.3	49.6	51.9
Delta G (300K) (d)	38.3	45.1			18.5	0	0	3.8			20.9	10.9	27.2	29.5

Compound	**1A** (R,R,S)						**3A** (R,R,R)							
helix type	L-12		R-12	L-12/10	R-12/10		L-12		R-12		L-12/10		R-12/10	
	g+ (Bn)	g-	g- (Bn)	g- (CB,C7)	g+ (Bn)	g-	g+ (Bn)	g-	g- (Bn)		g- (CB,C7)	g+	g+ (Bn)	g-
Gas Phase Eelec (TZVPPD) (a)	28.6	41.9	61.7	28.3	0	6.5	13.6	14.4	75.7		8.7	21.2	25.3	32.8
Chloroform Eelec (TZVPPD) (b)	17.1	30.7	50.2	39.2	7.3	10.8	0	15.3	66.6		22.2	28.2	34.0	38.7
Solution Delta G (300K) (c)	22.9	28.8	60.2	53.6	16.3	13.5	0	12.7	76.6		31.0	31.0	49.1	44.6
Delta G (300K) (d)	9.4	15.3	46.8	40.2	2.8	0	0	12.7	76.6		31.0	31.0	49.1	44.6

a) Eelec (RI-B-97-D3(BJ)-abc/def2-TZVPPD) level)

b) Eelec sol (RI-B-97-D3(BJ)-abc/def2-TZVPPD) + COSMO level)

c) Delta G (Eelec sol (RI-B-97-D3(BJ)-abc/def2-TZVPPD) + COSMO level) + Chem pot (RI-B-97-D3(BJ)/def2-TZVP) + COSMO level)

d) Energy scale origins specific to each enantiomeric compound

Table S1-2. Comparison of the helical structures in α/γ-hexapeptides (compounds 2A, 4A and 5) with the canonical gas phase structures as defined by Hofmann and co-workers.[S9] For each compound, the backbone structure of each helical type studied is characterized by the average values (in degrees) of the four (φ, θ, ζ, ψ) and two (φ, ψ) backbone dihedrals (same terminology as Fig. 1 in manuscript) for the γ and α residues respectively, given for one of the most stable conformers of the corresponding helix (indicated by the g+/g– label). The distortion of the helix relative to the canonical structures[S9] is estimated from the signed difference between the dihedral values (δ) ; data are then synthesized, separately for each residue type (γ and α), by the root-mean square value < δ > of the δ values of the corresponding residue. δ values corresponding to differences larger than 15 are indicated by a pink background. Distortions < δ > greater than their counterparts in other compounds are indicated in yellow and demonstrate the effect of a steric shift (cf. red dots in Fig S1-2).

Hofmann helices gas phase HF/6-31G*		**2A** this work gas phase RI-B-97-D3(BJ,abc)/def2-TZVPPD				**4A** this work gas phase RI-B-97-D3(BJ,abc)/def2-TZVPPD				**5** this work gas phase RI-B-97-D3(BJ,abc)/def2-TZVPPD			
R-12/10		**R-12/10**	**g+**			**R-12/10**	**g+**			**R-12/10**	**g-**		
		dihedrals	average	δ	< δ >	dihedrals	average	δ	< δ >	dihedrals	average	δ	< δ >
65		φ	79	14	γ	φ	76	11	γ	φ	76	11	γ
33		θ	14	-19	**15**	θ	16	-17	**14**	θ	14	-19	**13**
48		ζ	56	8		ζ	55	7		ζ	54	6	
-130		ψ	-116	14		ψ	-112	18		ψ	-116	14	
-67		φ	-64	3	α	φ	-56	11	α	φ	-66	1	α
148		ψ	142	-6	**5**	ψ	137	-11	**11**	ψ	150	2	**2**
L-12/10		**L-12/10**	**g-**			**L-12/10**	**g-**			**L-12/10**	**g+**		
		dihedrals	average	δ	< δ >	dihedrals	average	δ	< δ >	dihedrals	average	δ	< δ >
-65		φ	-63	2	γ	φ	-66	-1	γ	φ	-65	0	γ
-33		θ	-14	19	**11**	θ	-14	19	**13**	θ	-13	20	**13**
-48		ζ	-50	-2		ζ	-64	-16		ζ	-64	-16	
130		ψ	118	-12		ψ	123	-7		ψ	122	-8	
67		φ	62	-5	α	φ	67	0	α	φ	68	1	α
-148		ψ	-119	**29**	**21**	ψ	-149	-1	**1**	ψ	-152	-4	**3**
L-12		**L-12**	**g+**			**L-12**	**g+**			**L-12**	**g+**		
		dihedrals	average	δ	< δ >	dihedrals	average	δ	< δ >	dihedrals	average	δ	< δ >
123		φ	110	-13	γ	φ	106	-17	γ	φ	106	-17	γ
-53		θ	-27	26	**18**	θ	-28	25	**19**	θ	-29	24	**19**
-63		ζ	-81	-18		ζ	-84	-21		ζ	-85	-22	
124		ψ	111	-13		ψ	113	-11		ψ	115	-9	
72		φ	58	-14	α	φ	65	-7	α	φ	69	-3	α
28		ψ	42	14	**14**	ψ	35	7	**7**	ψ	31	3	**3**
R-12		**R-12**	**g+**			**R-12**				**R-12**	**g+**		
		dihedrals	average	δ	< δ >	dihedrals	average	δ	< δ >	dihedrals	average	δ	< δ >
-123		φ	-102	21	γ	φ	-106	17	γ	φ	-104	19	γ
53		θ	29	-24	**17**	θ	28	-25	**15**	θ	28	-25	**16**
63		ζ	72	9		ζ	68	5		ζ	72	9	
-124		ψ	-121	3		ψ	-124	0		ψ	-122	2	
0													
-72		φ	-74	-2	α	φ	-74	-2	α	φ	-79	-7	α
-28		ψ	-22	6	**5**	ψ	-17	11	**8**	ψ	-14	14	**11**

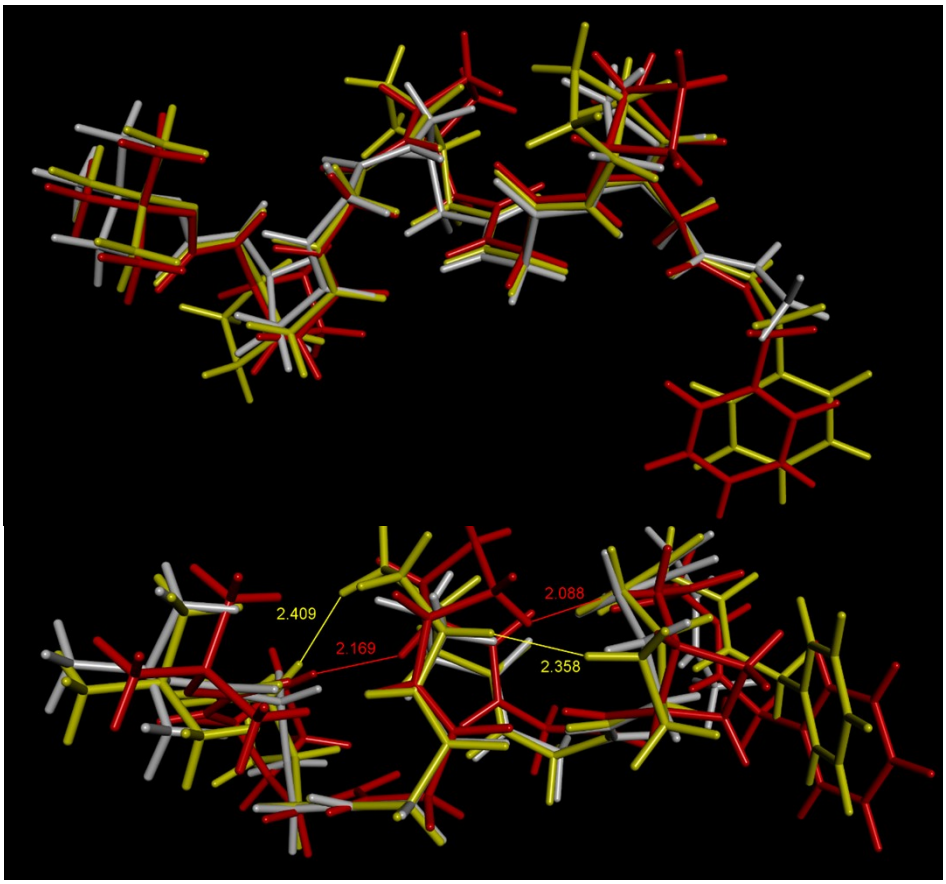

Figure S1-4. Variations in the helical structures due to the presence of the (*R*,*R*)-^{3,4}CB-GABA residue in compound 5, compared to compound 6, as illustrated for 12/10 and 12 helices (upper and lower panels, respectively). For the sake of comparison of helices of 5 with different handedness (L or R, shown in yellow and red respectively), mirror images of the right-handed helices were superimposed with the left-handed helices; the corresponding L-handed helix of compound 6 is also given in white. Relevant distances are given in Å. The 12/10 helix does not show any significant difference in backbone distortions compared to 6, in contrast to the 12 helix where, in addition to distortions, the R form exhibits short γ-γ distances compared to the L form, demonstrating the effects of a steric clash.

At this level, one can assess the implication of the configuration of the Ala residue in the evolution of the conformational landscape. The comparison of the four helical forms of (*R,R*,*R*) and (*R,R*,*S*) structures of compounds **2A** and **4A** (Figure S1-2, top lateral panels) with that of **5** (Figure S1-2, top central panel) provides immediate evidence for the presence of steric clashes involving the Ala methyl group, depending upon the Ala configuration. Indeed, further structural analysis (Figure S1-5) demonstrates that for each helical type considered, one of the **2A** or **4A** compound exhibits a backbone geometry close to that of its **5** counterpart, whereas the other appears distorted, specifically on the Ala residue. More precisely, this gas phase

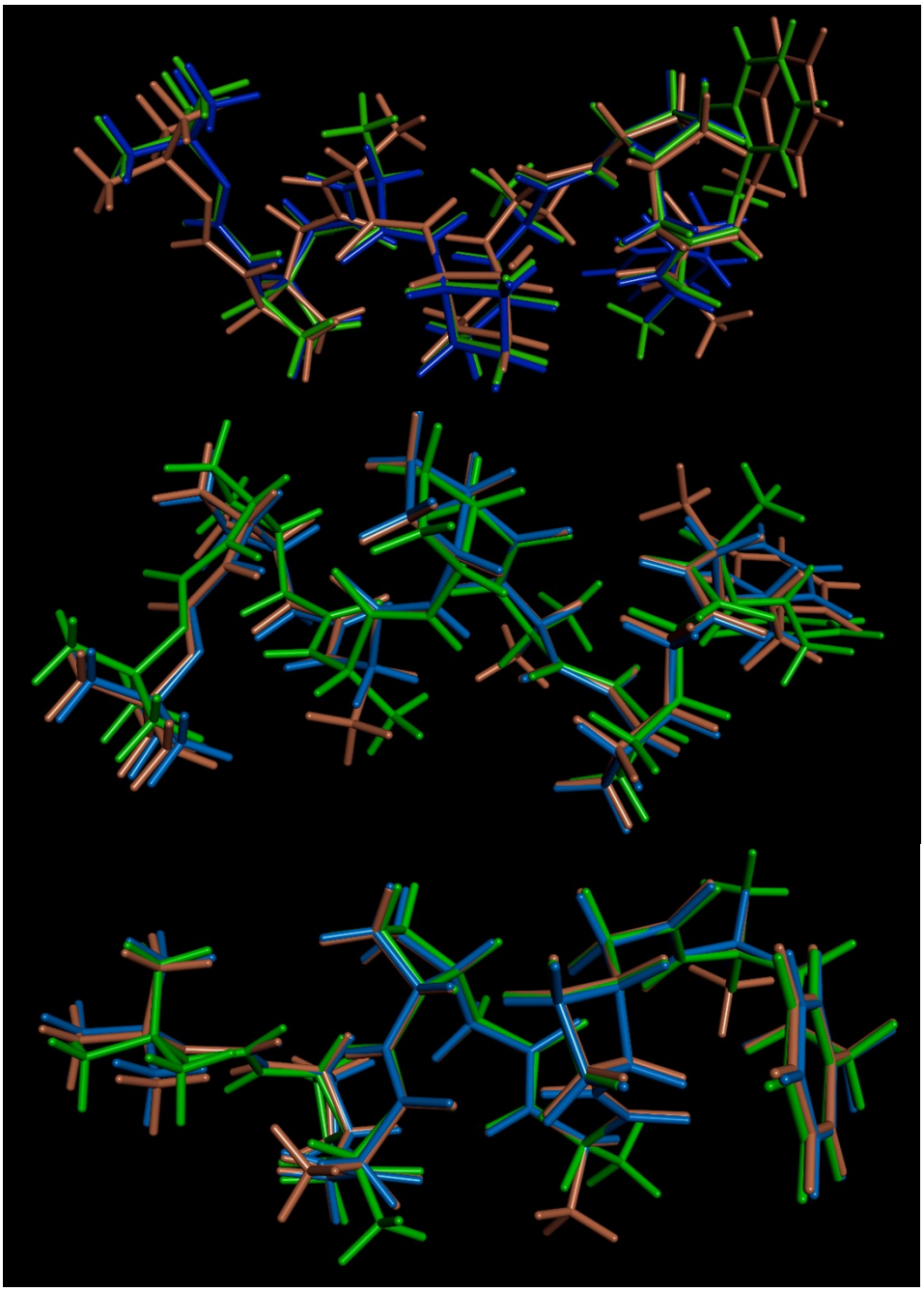

Figure S1-5. Backbone variations in the helical structures due to the presence of *R*- or *S*-Ala residues in compound 2A and 4A respectively, compared to compound 5, as illustrated for R-12/10 (top panel), L-12/10 (central panel) and L-12 helices (lower panel). For the sake of comparison, backbones have been superimposed. Helices of compounds 2A and 4A (*R*,*R*,*S* and *R*,*R*,*R* series, respectively) are drawn in green and brown respectively, while those of in compound 5 (*R*,*R*) appear in blue. Backbone distortions are especially visible on the Ala residues. The configurations giving rise to these distortions (and thus to destabilization) are found to depend upon the chirality of the helix considered: the *R*,*R*,*S* configuration (in green) in L-helices, and the *R*,*R*,*R* (in brown) in R-12/10 helices.

analysis enables us to rationalize the fact that the R-12/10 helix, which is the most stable form in **5** and **2A** (*R,R,S*), undergoes a significant destabilization in **4A** (*R,R,R*), leaving an open (*R,R,S*) gas phase landscape where R-12/10, L-12 and L-12/10 are competing in the gas phase (Figure S1-3). In contrast the L-12 and L-12/10 helices undergo a destabilization in the (*R,R,S*) species, leaving the R-12/10 species rather unchallenged.

The role of solvation was revealed as being of paramount importance in the competition between helical forms. As already remarked by Hofmann and coworkers,[S9] the 12 and 12/10 helices exhibit very different dipole moments due to their specific type of H-bonding networks: 12 helices exhibit two parallel daisy chains of H-bonds oriented in the same direction, thus leading to a macro-dipole (typically 30 Debye), whereas 12/10 helices have two anti-parallel chains of H-bonds, which endows them with much more modest dipole moments (ca. 5 D). This has a prominent differential effect (see Table S1-1) on the solvation process, which can amount up to 30 kJ/mol in hexapeptides. Consequently, the L-12 helix becomes the prominent species for (*R,R,R*) series peptides in solution. In the (*R,R,S*) series, however, the solvation effect is not sufficient to fully compensate the steric clashes which destabilize the L-12 helix and the R-12/10 form remains the most stable form, by typically 20 kJ/mol. It is noteworthy that, despite this dramatic effect on energetics, solvation barely changes the structure of the helices.

Regarding the effect of the orientation of the benzyl group (Bn) relative to the backbone, the free Bn conformations of the 12 helices tend to be less stable at the energetic level due to the self-solvation of the benzyl group, which minimizes the penalty induced by solvation of a hydrophobic moiety. Finally, when thermal corrections are taken into account (ΔG's at 300 K, see Table S1-1), this difference is reduced due to a differential entropic effect. In passing, it can be noted that in the case of L-12/10 helices, the Bn-CB interaction at the C-terminus causes an elongation of the first C10 H-bond of the helix that tends to facilitate the formation of a C7 bond originating from the last NH group.

1.3 IR Spectroscopy

1.3.1 Focusing on the CO stretch region.

As expected from general IR spectroscopy considerations, the CO stretch region (amide I) of peptides is exquisitely sensitive to the relative orientation of the CO groups within the peptides, due to the overwhelming effect of the vibrational coupling occurring between them, but is relatively insensitive to the H-bonding network. In contrast, the NH stretch region (amide A) is controlled by the strength of the H-bonds. Regarding the potential of these two regions in terms of diagnosis of the helical type present in the peptides studied experimentally in this work using IR spectroscopy, the CO stretch region appears as the most promising to distinguish the very different geometrical CO orientations of the 12 and 12/10 helices.

This is revealed by the synthesis figures (Figure S1-6), where the signatures of the amide I and II regions are plotted separately for the most stable forms of the 12 and 12/10 helix types for peptides **1A**, **2E**, **2A**, **3A**, **4E** and **4A**. A close examination shows that the 1650-1680 cm^{-1} region (blue zone) comprises a vast majority of the most intense CO stretch bands of all the L-12 species encountered. In contrast, the 1620-1650 cm^{-1} region (pink zone) is where the most intense CO stretch bands of the 12/10 helices are found. Despite their proximity, these two zones enable a differential diagnosis of the presence of these two helical types since the 12 helix does not exhibit any feature in the pink zone and the 12/10 type presents only weak bands in the blue zone. This diagnosis can be cross-checked from the NH bending region (amide II), where a narrow zone (1490-1515 cm^{-1}, in blue) exhibits significant amide II bands for the 12 helices but is devoid of any strong absorption signature for 12/10 helices.

As can be anticipated for (nearly) mirror image helices, L- and R-12/10 helix types give rise to similar patterns, which precludes distinguishing between them by experimental IR spectroscopy.

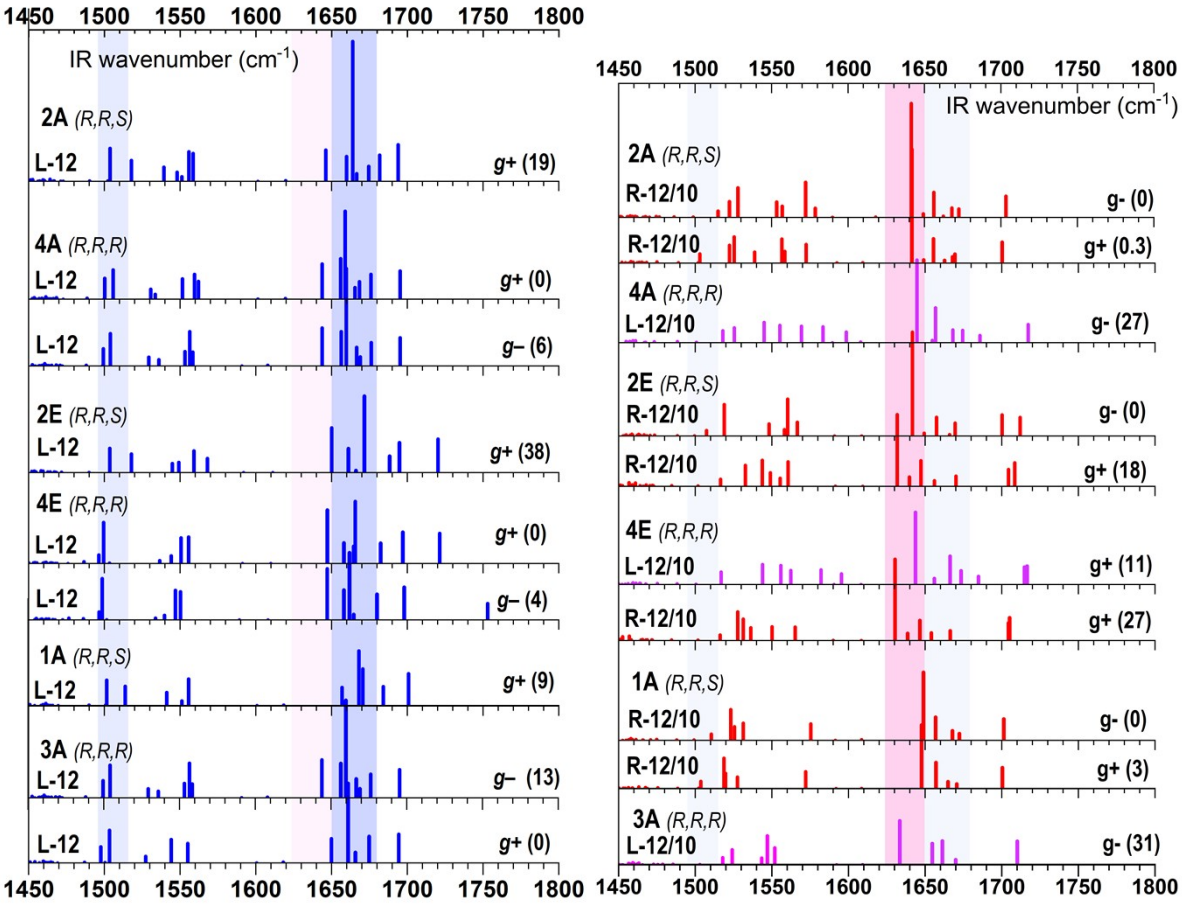

Figure S1-6: Theoretical amide I and II stick spectra of selected low energy conformations of 12 helices (left panel) and 12/10 helices (right panel) in peptides 1A, 2E, 2A, 3A, 4E and 4A. The dark colored zones indicate spectral features specific to each helix type (blue for 12 and pink for 12/10), whereas light colors illustrate the absence of strong transitions of the alternative type.

1.3.2 Assignment of the experimental solution phase IR absorption spectra.

Experimental data were acquires as indicated in Section S3.1. The experimental absorption spectra in the amide I and II regions are shown in Figure S1-7, together with the theoretical spectra of the lower energy helical conformation for each peptide analyzed: **1A**, **2E**, **2A**, **3A**, **4E** and **4A.**

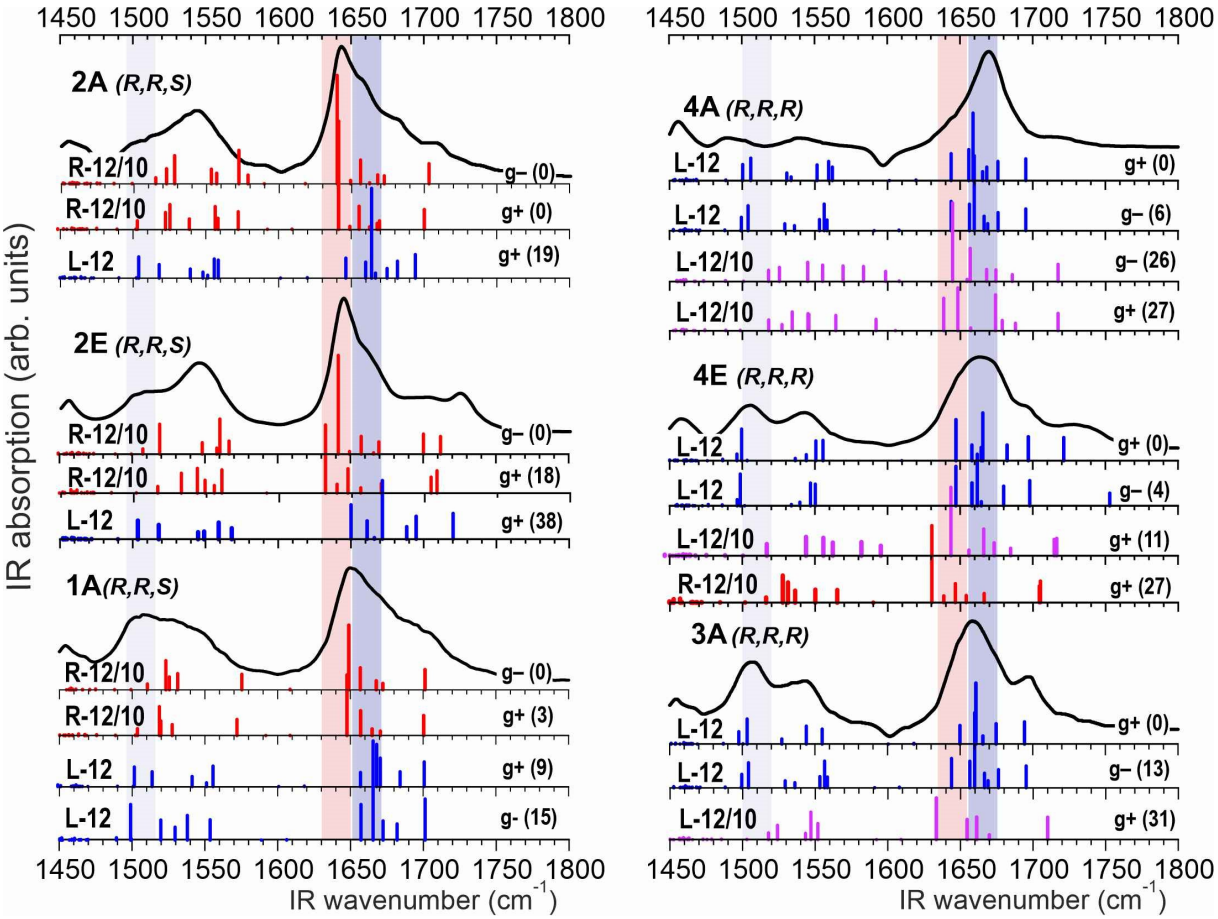

Figure S1-7. Experimental absorption spectra in the amide I and II regions (black traces) compared with the lower energy helical conformations of each (*R,R,S*) (left panel) and (*R,R,R*) (right panel) peptide studied. The theoretical spectra of L-12, R-12/10 and L-12/10 helices are shown as colored sticks (blue, red and magenta, respectively). The colored (blue and pink) zones are specific to the 12 and 12/10 helical backbones respectively (see Figure S1-6).

The amide I feature of the (*R,R,R*) peptides around 1660 cm^{-1} fits the main absorption bands calculated for the lower energy L-12 conformations (Figure S1-7, right panel, blue zone). The same observation holds for the weaker amide II feature at 1505 cm^{-1} (at least for compounds **3A** and **4E**; the poor solubility of **4A** yielded a poor-quality IR spectrum, precluding a precise analysis). Combined with the low experimental absorption level in the pink zone that is specific to the 12 species, the IR spectrum of the (*R,R,R*) species can be assigned confidently to a major L-12 helical conformation.

In contrast, the maximum of the amide I feature of the (*R,R,S*) peptides around 1640 cm^{-1} fits the main absorption bands calculated for the lower energy R-12/10 conformations (Figure S1-7, left panel, pink zone). A detailed inspection, however, shows that for the tetrapeptide **1A**, this band is broader than in the hexapeptides **2E** and **2A** and is located at the interface between the blue and pink zones, suggesting a mixture between L-12 and R-12/10 helices for **1A**. This contention is corroborated by a significant absorption in the amide II blue zone around 1505 cm^{-1}, specific to the 12 helix backbone. The decrease of this absorption in **2E** and **2A**, concomitant with the increase in another amide II band at 1540 cm^{-1}, suggests that the population of the 12 helix diminishes in the hexapeptides leaving the R-12/10 helix as the major conformation. These interpretations are in line with the relative energetics of the 12 and 12/10 backbones illustrated in Figure S1-2 and Table S1-1.

These assignments are supported by the amide A region spectral data (Figure S1-8). A fair match is obtained for the (*R,R,R*) peptides **3A**, **4E** and **4A**, between the broad amide A absorption and the calculated L-12 backbone frequencies (Figure S1-8, right panel). For the (*R,R,S*) peptides **1A**, **2E** and **2A**, the maximum of the experimental band is red-shifted compared to the (*R,R,R*) species and this red-shift seems to increase with the peptide size. This observation suggests that the R-12/10 backbone absorption is red-shifted compared to that of the L-12, in qualitative agreement with the calculated bands for 12-10 helices (Figure S1-8, left panel). However, this red-shift seems to be overestimated, by typically 50 cm^{-1}, which might indicate weaknesses in the description of the H-bonding of the 12-10 type at the level of theory used.

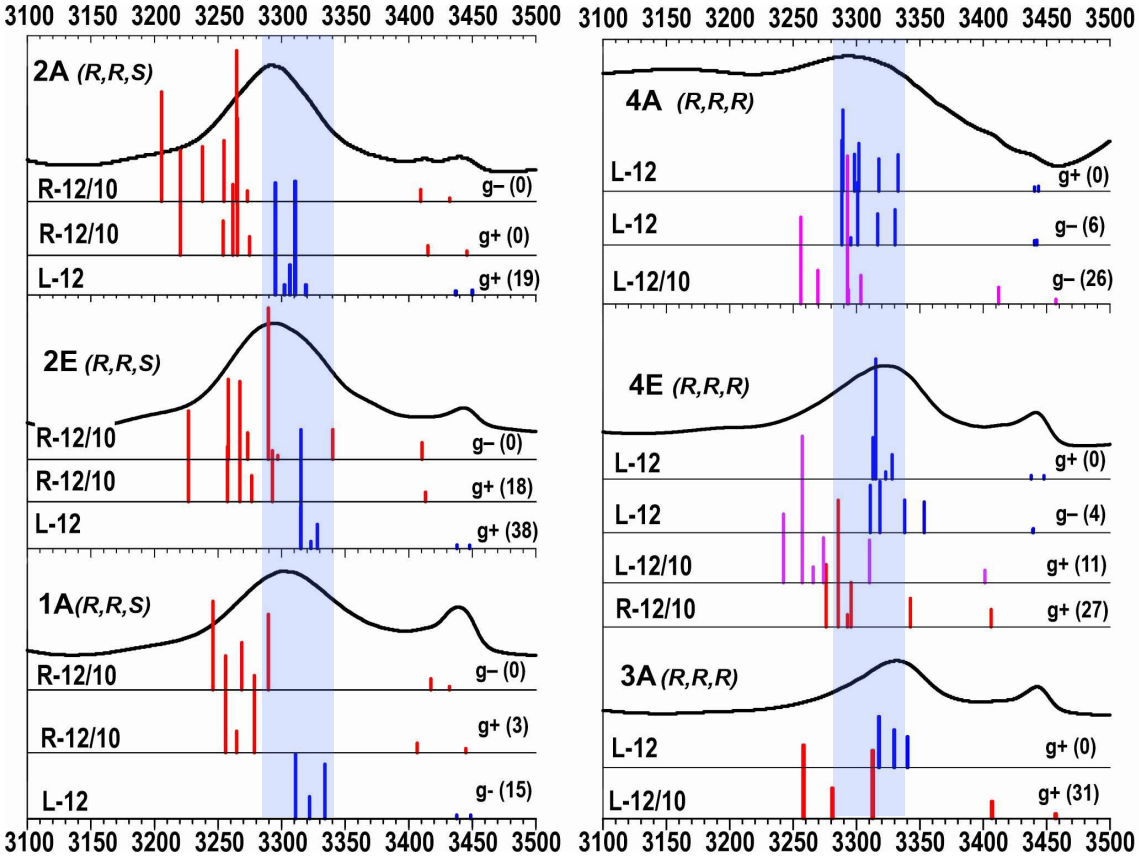

Figure S1-8. Experimental absorption spectra in the amide A region (black traces) compared with the lower energy helical conformations of each (*R,R,S*) (left panel) and (*R,R,R*) (right panel) compound studied. The theoretical spectra of L-12, R- and L-12-10 helices are shown as colored sticks (blue, red and magenta, respectively). The colored blue region is more specific to the 12 helical backbone.

2. Synthesis

2.1 Materials and instrumentation

Melting points (Mp) were measured in open capillary tubes on a Büchi B-540 apparatus and are uncorrected. Routine ^{1}H and ^{13}C NMR spectra were recorded on Bruker spectrometers operating at 600/400/360/300 MHz (for ^{1}H) or at 100/90/75 MHz (for ^{13}C). For ^{1}H NMR spectra, chemical shifts (δ) are reported in parts per million (ppm) with reference to residual protonated solvent (δ = 7.26 ppm for $CHCl_3$; δ = 8.71, 7.58, 7.21 ppm for pyridine; δ = 2.50 ppm for DMSO). ^{1}H signals are designated as s (singlet), d (doublet), t (triplet), q (quartet), m (multiplet), br (broad), or bs (broad singlet); coupling constants (J) are reported in hertz (Hz). For ^{13}C NMR spectra, chemical shifts (δ) are reported in parts per million (ppm) with reference to the deuterated solvent (δ = 77.16 ppm for $CDCl_3$; δ = 150.35, 135.91, 123.87 ppm for pyridine-d_5; δ = 39.51 ppm for DMSO-d_6). Routine infrared (IR) spectra were recorded neat for solid samples on a Fourier-transform Perkin Elmer Spectrum Two instrument equipped with an ATR diamond accessory; maximum absorbances (ν) are given in cm^{-1}. High-resolution mass spectra (HRMS; [ESI(+)]) were recorded on a Bruker MicroTOF-Q spectrometer equipped with an electrospray ionization source in positive mode. Optical rotations were measured on a Specord 205 instrument (Analytik-Jena) using a 10 cm quartz cell; values for $[\alpha]_D^T$ were obtained with the D-line of sodium at the indicated temperature T, using solutions of concentration (c) in units of g·100 mL^{-1}.

Flash chromatography was performed on silica gel columns (40-63 µm) purchased from Macherey-Nagel. Fractions were analyzed using TLC plates that were visualized by fluorescence at 254 nm then revealed using a ninhydrin solution (14 mM in EtOH) or a $KMnO_4$ solution (7.5% in water). Retention factors (R_f) are given for such TLC analysis.

Preparative HPLC was performed on an Agilent 1260 Infinity HPLC apparatus equipped with a VL G1311C quaternary pump with an online degasser, an ALS G1329B semi-preparative autosampler, a G1315D column oven, a DAD VL G1315D diode array detector and an AS G1364C collector, piloted using ChemStation OpenLab CPL version C.01.04 software. Hexane and ethanol were HPLC grade. The mobile phase was filtered through a 0.45 µm PTFE membrane, while injected solutions were filtered through a 0.22 µm PTFE membrane. Separations were performed using a lux cellulose-1 column by Phenomenex® (250 mm × 10 mm; particle size 5 µm) and a mobile phase flowrate of 5 mL/min. The mobile phase and the column were thermostated at 30 ± 2 °C. Detection was performed at 210 nm.

2-((1*R*,2*R*)-2-((*tert*-Butoxycarbonyl)amino)cyclobutyl)acetic acid [abbreviated as Boc-(*R*,*R*)-^{3,4}CB-GABA-OH] **I** was obtained according to the published procedure.[S13] All other reagents and solvents were standard grade for synthesis. For use in synthetic procedures, CH_2Cl_2 was passed through a column of alumina, DMF was distilled from CaH_2 under reduced pressure.

2.2 Synthesis of peptides

2.2.1 General procedures for synthesis.

Procedure A for removal of a Boc group.

In an argon-flushed flask, **Boc-X^1-OBn/NHBn** (1 eq.) was dissolved in CH_2Cl_2 (5 mL/mmol) then TFA (30 eq.) was added and the mixture was stirred at room temperature for 1 h. CH_2Cl_2 was removed under reduced pressure, then TFA was removed by co-evaporation with $CHCl_3$ several times and the resulting residue was held under vacuum for 2 h. The salt **TFA·H-X^1-OBn/NHBn** was digested with CH_2Cl_2 (5 mL/mmol) under argon and DIPEA (6 eq., viz. sufficient quantity to reach pH 9) was added. The resulting solution of the free amine **H-X^1-OBn/NHBn** was used directly in a subsequent coupling reaction.

Procedure B for removal of a benzyl ester group.

To a solution of **Boc-X^2-OBn** (1 eq.) in CH_2Cl_2/EtOAc (4/1; 33 mL/mmol) was added Pd-C (125 mg/mmol). The suspension was degassed then stirred under H_2 at atmospheric pressure for 4 h. The mixture was filtered through a celite pad, and the celite pad was washed through with small portions of EtOAc. The filtrate was concentrated under reduced pressure to afford **Boc-X^2-OH** that was used directly in a subsequent coupling reaction.

Procedure C for coupling reactions.

Synthesis of dipeptides: To a solution of **Boc-X^2-OH** (1 eq.) in CH_2Cl_2/DMF (4/1; 10 mL/mmol) in an argon-flushed flask were added DIPEA (2 eq.) then HATU (1.05 eq.). The mixture was stirred for 10 min at room temperature during which time the color changed from light to dark brown. A solution of **H-X^1-OBn/NHBn** (1 eq.) was added and the reaction mixture was stirred at room temperature for 24 h.

Synthesis of tetrapeptides and hexapeptides: To a solution of **Boc-X^2-OH** (1 eq.) in CH_2Cl_2/DMF (3/1; 10 mL/mmol) in an argon-flushed flask were added in succession DIPEA (2 eq.), then a solution of **H-X^1-OBn/NHBn** (1 eq.), then HATU (1.05 eq.). The resulting mixture was stirred at room temperature for 24 h.

Reaction work-up and isolation of all peptides: After the reaction time, most of the solvent was removed under reduced pressure and the remaining DMF was removed by co-evaporation with heptane several times. The residue was dissolved in CH_2Cl_2 (100 mL/mmol) and the solution was washed successively with saturated aqueous sodium bicarbonate (20 mL/mmol), brine (20 mL/mmol), 1 M HCl (20 mL/mmol) and brine (20 mL/mmol). The solution was then dried over sodium sulfate, filtered and concentrated under reduced pressure. Purification was carried out either by flash chromatography or by preparative HPLC to afford **Boc-X^2-X^1- OBn/NHBn**.

Procedure D for preparation of benzylamides.

To a solution of **Boc-X^2-OH** (1 eq.) in CH_2Cl_2 or CH_2Cl_2/DMF (10 mL/mmol) in an argon-flushed flask were added in succession benzylamine (1.02 eq.), then DIPEA (3 eq.), then HATU (1.05

eq.). The mixture was stirred at room temperature for 48 h. Most of the solvent was removed under reduced pressure and the remaining DMF was removed by co-evaporation with heptane several times. The residue was dissolved in CH_2Cl_2 (100 mL/mmol) and the solution was washed successively with saturated aqueous sodium bicarbonate (20 mL/mmol), brine (20 mL/mmol), 1 M HCl (20 mL/mmol) and brine (20 mL/mmol). The solution was then dried over sodium sulfate, filtered and concentrated under reduced pressure. Purification was carried out by flash chromatography to afford **Boc-X²-NHBn**.

2.2.2 Synthesis of dipeptides.

(*R,R,S*) series

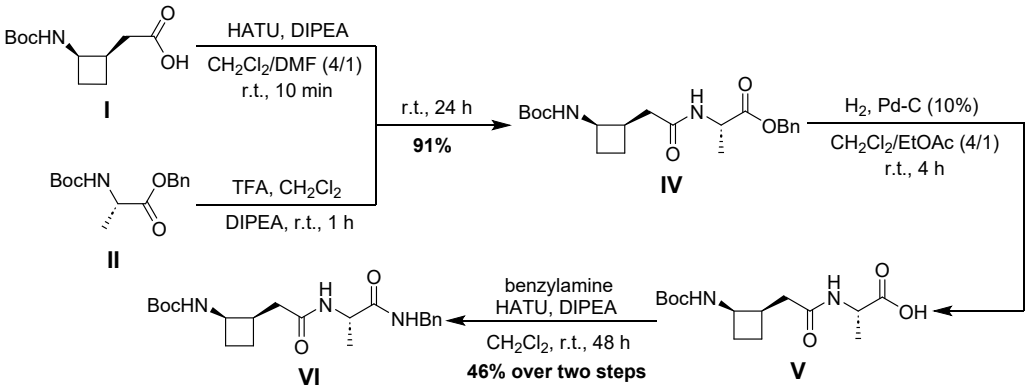

Benzyl (2-((1*R*,2*R*)-2-((*tert*-butoxycarbonyl)amino)cyclobutyl)acetyl)-(*S*)-alaninate (IV).

According to the general procedure A, Boc-(*S*)-Ala-OBn **II** (243 mg, 0.87 mmol, 1 eq.) in CH_2Cl_2 (4 mL) and TFA (2 mL, 26.1 mmol, 30 eq.) gave TFA·H-(*S*)-Ala-OBn. Digestion of this salt in CH_2Cl_2 (4 mL) and DIPEA (0.91 mL, 5.22 mmol, 6 eq.) gave a solution of H-(*S*)-Ala-OBn.

According to the general procedure C, a solution of Boc-(*R*,*R*)-^{3,4}CB-GABA-OH **I** (200 mg, 0.87 mmol, 1 eq.) in CH_2Cl_2/DMF (4/1; 8 mL) was treated with DIPEA (303 µL, 1.74 mmol, 2 eq.) and HATU (347 mg, 0.91 mmol, 1.05 eq.). After stirring for 10 min, the above-described H-(*S*)-Ala-OBn solution was added. After the reaction time, flash chromatography (PE/EtOAc = 3/2) gave Boc-(*R*,*R*)-^{3,4}GABA-(*S*)-Ala-OBn **IV** as a white solid (309 mg, 91%).

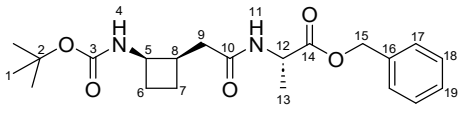

IV

R_f = 0.31 (PE/EtOAc = 3/2)

Mp = 157-158 °C

^{1}H NMR (360 MHz, $CDCl_3$, 300 K) δ 7.40-7.27 (m, 5H, H^{Ar}), 6.40 (bs, 1H, NH^{11}), 5.37 (bs, 1H, NH^4), 5.17 (dd, *J* = 20.0, 12.2 Hz, 2H, H^{15}), 4.61 (p, *J* = 7.2 Hz, 1H, H^{12}), 4.31-4.12 (m, 1H, H^5),

2.90-2.77 (m, 1H, H^8), 2.46 (dd, *J* = 14.6, 7.6 Hz, 1H, H^9), 2.36-2.28 (m, 1H, H^6), 2.27 (dd, *J* = 14.6, 7.6 Hz, 1H, H^9), 2.03-1.90 (m, 1H, H^6), 1.90-1.78 (m, 1H, H^7), 1.65-1.51 (m, 1H, H^7), 1.41 (s, 9H, H^1), 1.40 (d, *J* = 6.2 Hz, 3H, H^{13}).

^{13}C NMR (90 MHz, $CDCl_3$, 300 K) *δ* 173.08 (C^{14}), 172.12 (C^{10}), 155.64 (C^3), 135.44 (C^{16}), 128.71, 128.53, 128.23 ($C^{17, 18, 19}$), 79.40 (C^2), 67.22 (C^{15}), 48.24 (C^{12}), 47.42 (C^5), 37.56 (C^8), 36.50 (C^9), 28.49 (C^1), 27.65 (C^6), 21.59 (C^7), 18.40 (C^{13}).

IR (neat) *v* 3358, 3271, 2978, 2931, 1720, 1710, 1652, 1553, 1535, 1497 cm^{-1}.

HRMS [ESI(+)] *m/z* $[M+Na]^+$ calculated for $[C_{21}H_{30}N_2NaO_5]^+$: 413.2047, found: 413.2035.

$[\alpha]_D^{21}$ = +36.3 (c. 0.60 in $CHCl_3$).

tert-Butyl ((1*R*,2*R*)-2-(2-(((*S*)-1-(benzylamino)-1-oxopropan-2-yl)amino)-2-oxoethyl) cyclobutyl)carbamate (VI).

According to the general procedure B, Boc-(*R*,*R*)-^{3,4}CB-GABA-(*S*)-Ala-OBn **1E** (422 mg, 1.08 mmol, 1 eq.), Pd-C (135 mg) and CH_2Cl_2/EtOAc (4/1, 36 mL) were employed to afford Boc-(*R*,*R*)-^{3,4}CB-GABA-(*S*)-Ala-OH **V** as a white solid.

According to the general procedure D, a solution of the above-described sample of **V** in CH_2Cl_2 (10 mL) was reacted with benzylamine (120 µL, 1.1 mmol, 1.02 eq.), DIPEA (564 µL, 3.24 mmol, 3 eq.) and HATU (431 mg, 1.1 mmol, 1.05 eq.). Flash chromatography (EtOAc/PE = 3/1) afforded Boc-(*R*,*R*)-^{3,4}CB-GABA-(*S*)-Ala-NHBn **VI** as a white solid (194 mg, 46%).

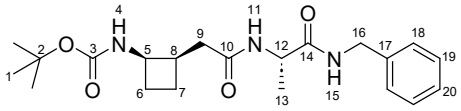

VI

***R**$_f$* = 0.48 (EtOAc/PE = 3/1)

Mp = 194-195 °C

^{1}H NMR (600 MHz, $CDCl_3$, 300 K) *δ* 7.42-7.12 (m, 5H, H^{Ar}), 6.81 (bs, 1H, NH^{15}), 6.52 (d, *J* = 7.4 Hz, 1H, NH^{11}), 5.23 (d, *J* = 7.2 Hz, 1H, NH^4), 4.51 (p, *J* = 7.2 Hz, 1H, H^{12}), 4.41 (d, *J* = 5.8 Hz, 2H, H^{16}), 4.30-4.11 (m, 1H, H^5), 2.92-2.69 (m, 1H, H^8), 2.44 (dd, *J* = 14.6, 7.6 Hz, 1H, H^9), 2.37-2.27 (m, 1H, H^6), 2.23 (dd, *J* = 14.6, 7.6 Hz, 1H, H^9), 2.03-1.88 (m, 1H, H^7), 1.88-1.78 (m, 1H, H^6), 1.62-1.48 (m, 1H, H^7), 1.42 (s, 9H, H^1), 1.39 (d, *J* = 7.0 Hz, 3H, H^{13}).

^{13}C NMR (90 MHz, $CDCl_3$, 300 K) *δ* 173.14 (C^{14}), 172.87 (C^{10}), 155.89 (C^3), 137.87 (C^{17}), 128.53, 127.42, 127.30 ($C^{18, 19, 20}$), 79.33 (C^2), 48.66 (C^{12}), 46.87 (C^5), 43.24 (C^{16}), 37.51 (C^8), 35.95 (C^9), 28.23 (C^1), 27.08 (C^6), 20.92 (C^7), 17.92 (C^{13}).

IR (neat) *v* 3325, 3311, 2957, 2937, 2865, 1757, 1735, 1682, 1639, 1528 cm^{-1}.

HRMS [ESI(+)] *m/z* $[M+Na]^+$ calculated for $[C_{21}H_{31}N_3NaO_4]^+$: 412.2207, found: 412.2189.

$[\alpha]_D^{22}$ = +13.4 (c. 0.50 in $CHCl_3$).

(*R,R,R*) series

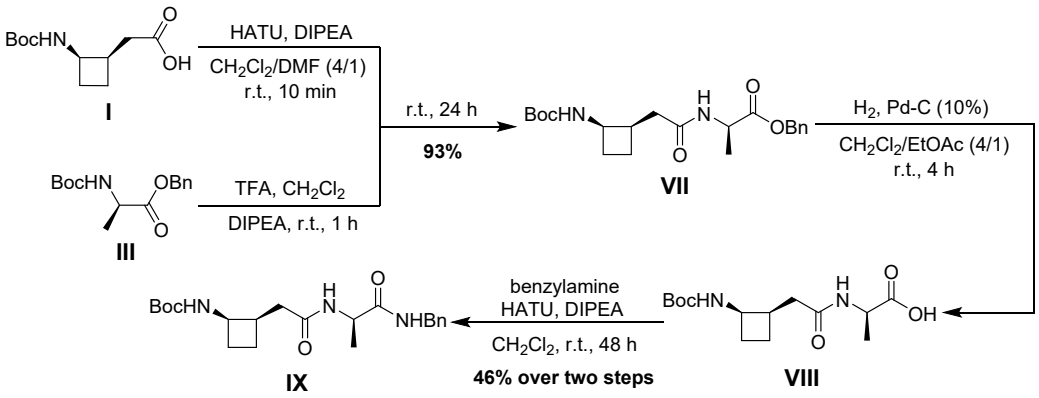

Benzyl (2-((1*R*,2*R*)-2-((*tert*-butoxycarbonyl)amino)cyclobutyl)acetyl)-(*R*)-alaninate (VII).

According to the general procedure A, Boc-(*R*)-Ala-OBn **III** (243 mg, 0.87 mmol, 1 eq.) in CH_2Cl_2 (4 mL) and TFA (2 mL, 26.1 mmol, 30 eq.) gave TFA·H-(*R*)-Ala-OBn. Digestion of this salt in CH_2Cl_2 (4 mL) and DIPEA (0.91 mL, 5.22 mmol, 6 eq.) gave a solution of H-(*R*)-Ala-OBn.

According to the general procedure C, a solution of Boc-(*R*,*R*)-^{3,4}CB-GABA-OH **I** (200 mg, 0.87 mmol, 1 eq.) in CH_2Cl_2/DMF (4/1; 8 mL) was treated with DIPEA (303 µL, 1.74 mmol, 2 eq.) and HATU (347 mg, 0.91 mmol, 1.05 eq.). After stirring for 10 min, the above-described H-(*R*)-Ala-OBn solution was added. After the reaction time, flash chromatography (PE/EtOAc = 3/2) gave Boc-(*R*,*R*)-^{3,4}GABA-(*R*)-Ala-OBn **VII** as a white solid (316 mg, 93%).

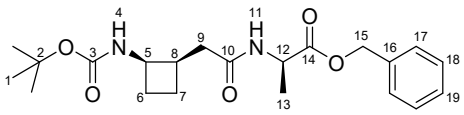

VII

R_f = 0.31 (PE/EtOAc = 3/2)

Mp = 145-146 °C

^{1}H NMR (360 MHz, $CDCl_3$, 300 K) δ 7.43-7.27 (m, 5H, H^{Ar}), 6.41 (bs, 1H, NH^{11}), 5.25 (bs, 1H, NH^4), 5.18 (dd, *J* = 18.8, 12.2 Hz, 2H, H^{15}), 4.61 (p, *J* = 7.2 Hz, 1H, H^{12}), 4.41-4.02 (m, 1H, H^5), 2.99-2.64 (m, 1H, H^8), 2.46 (dd, *J* = 14.6, 7.6 Hz, 1H, H^9), 2.37-2.28 (m, 1H, H^6), 2.26 (dd, *J* = 14.6, 7.6 Hz, 1H, H^9), 2.04-1.90 (m, 1H, H^7), 1.90-1.77 (m, 1H, H^6), 1.65-1.53 (m, 1H, H^7), 1.42 (s, 9H, H^1), 1.40 (d, *J* = 6.2 Hz, 3H, H^{13}).

^{13}C NMR (90 MHz, $CDCl_3$, 300 K) δ 173.02 (C^{14}), 172.09 (C^{10}), 155.73 (C^3), 135.48 (C^{16}), 128.74, 128.55, 128.30 ($C^{17, 18, 19}$), 79.50 (C^2), 67.24 (C^{15}), 48.26 (C^{12}), 47.66 (C^5), 37.50 (C^8), 36.64 (C^9), 28.50 (C^1), 27.60 (C^6), 21.93 (C^7), 18.32 (C^{13}).

IR (neat) *v* 3338, 3312, 2990, 2956, 1734, 1708, 1675, 1638, 1545, 1514 cm^{-1}.

HRMS [ESI(+)] *m/z* $[M+Na]^+$ calculated for $[C_{21}H_{30}N_2NaO_5]^+$: 413.2047, found: 413.2032.

$[\alpha]_D^{20}$ = +49.7 (c. 0.58 in $CHCl_3$).

***tert*-Butyl ((1*R*,2*R*)-2-(2-(((*R*)-1-(benzylamino)-1-oxopropan-2-yl)amino)-2-oxoethyl) cyclobutyl)carbamate (IX).**

According to the general procedure B, Boc-(*R*,*R*)-^{3,4}CB-GABA-(*R*)-Ala-OBn **VII** (422 mg, 1.08 mmol, 1 eq.), Pd-C (135 mg) and CH_2Cl_2/EtOAc (4/1, 36 mL) were employed to afford Boc-(*R*,*R*)-^{3,4}GABA-(*R*)-Ala-OH **VIII** as a white solid.

According to the general procedure D, a solution of the above-described sample in CH_2Cl_2 (10 mL) was reacted with benzylamine (120 µL, 1.1 mmol, 1.02 eq.), DIPEA (564 µL, 3.24 mmol, 3 eq.) and HATU (431 mg, 1.1 mmol, 1.05 eq.). Flash chromatography (EtOAc/PE = 3/1) afforded Boc-(*R*,*R*)-^{3,4}CB-GABA-(*R*)-Ala-NHBn **IX** as a white solid (194 mg, 46%).

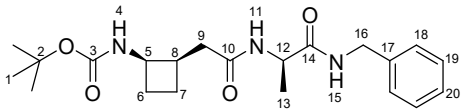

IX

R_f = 0.36 (EtOAc/PE = 3/1)

Mp = 166-167 °C

^{1}H NMR (600 MHz, $CDCl_3$, 300 K) δ 7.34-7.19 (m, 5H, H^{Ar}), 6.86 (bs, 1H, NH^{15}), 6.50 (d, *J* = 7.4 Hz, 1H, NH^{11}), 5.14 (d, *J* = 7.2 Hz, 1H, NH^4), 4.48 (p, *J* = 7.2 Hz, 1H, H^{12}), 4.45-4.36 (m, 2H, H^{16}), 4.12 (p, *J* = 7.2 Hz, 1H, H^5), 2.93-2.62 (m, 1H, H^8), 2.39 (dd, *J* = 14.6, 7.6 Hz, 1H, H^9), 2.31-2.24 (m, 1H, H^6), 2.24-2.16 (m, 1H, H^9), 2.02-1.85 (m, 1H, H^7), 1.82-1.73 (m, 1H, H^6), 1.63-1.51 (m, 1H, H^7), 1.42 (s, 9H, H^1), 1.38 (d, *J* = 7.0 Hz, 3H, H^{13}).

^{13}C NMR (90 MHz, $CDCl_3$, 300 K) δ 173.18 (C^{14}), 172.82 (C^{10}), 156.03 (C^3), 137.87 (C^{17}), 128.51, 127.43, 127.28 ($C^{18, 19, 20}$), 79.36 (C^2), 48.77 (C^{12}), 47.11 (C^5), 43.21 (C^{16}), 37.43 (C^8), 35.96 (C^9), 28.19 (C^1), 26.91 (C^6), 21.18 (C^7), 17.89 (C^{13}).

IR (neat) *v* 3331, 2976, 2959, 2935, 2859, 1737, 1681, 1659, 1637, 1530 cm^{-1}.

HRMS [ESI(+)] *m/z* $[M+Na]^+$ calculated for $[C_{21}H_{31}N_3NaO_4]^+$: 412.2207, found: 412.2191.

$[\alpha]_D^{20}$ = +56.8 (c. 0.52 in $CHCl_3$).

2.2.3 Synthesis of tetrapeptides.

(*R,R,S*) series

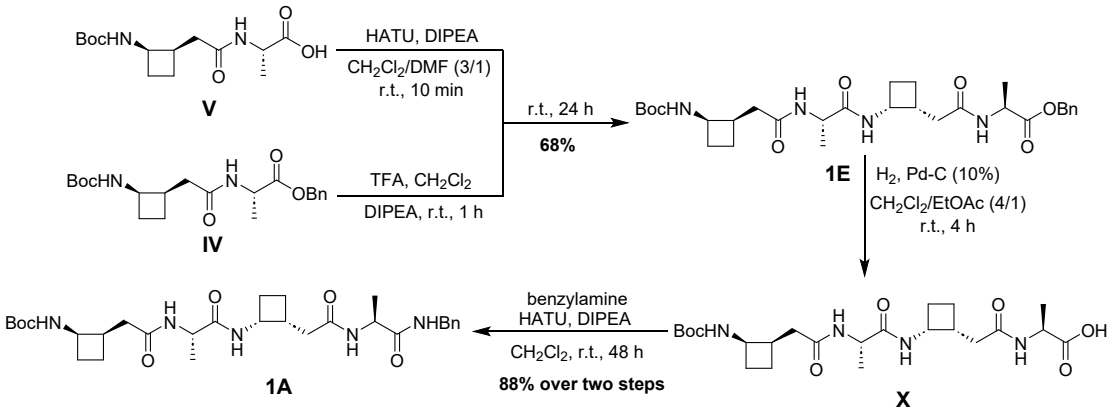

Benzyl (2-((1*R*,2*R*)-2-((*S*)-2-(2-((1*R*,2*R*)-2-((*tert*-butoxycarbonyl)amino)cyclobutyl) acetamido)propanamido)cyclobutyl)acetyl)-(*S*)-alaninate (1E).

According to the general procedure A, Boc-(*R*,*R*)-^{3,4}CB-GABA-(*S*)-Ala-OBn **IV** (117 mg, 0.3 mmol, 1 eq.) in CH_2Cl_2 (2 mL) and TFA (689 µL, 9 mmol, 30 eq.) gave TFA·H-(*R*,*R*)-^{3,4}CB-GABA-(*S*)-Ala-OBn. Digestion of this salt in CH_2Cl_2 (2 mL) and DIPEA (314 µL, 1.8 mmol, 6 eq.) gave a solution of H-(*R*,*R*)-^{3,4}CB-GABA-(*S*)-Ala-OBn.

According to the general procedure C, a solution of Boc-(*R*,*R*)-^{3,4}CB-ABA-(*S*)-Ala-OH **V** (90 mg, 0.3 mmol, 1 eq.) in CH_2Cl_2/DMF (3/1, 3 mL) was treated with DIPEA (105 µL, 0.6 mmol, 2 eq.), then the above-described H_2N-(*R*,*R*)-^{3,4}CB-GABA-(*S*)-Ala-OBn solution, then HATU (122 mg, 0.32 mmol, 1.05 eq.). After the reaction time, flash chromatography (CH_2Cl_2/MeOH = gradient from 100/1 to 100/4) gave Boc-[(*R*,*R*)-^{3,4}CB-GABA-(*S*)-Ala]$_2$-OBn **1E** as a white solid (116 mg, 68%).

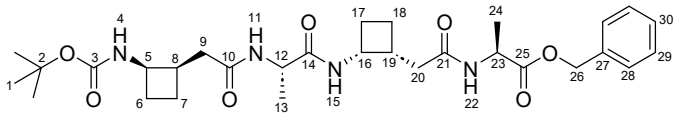

1E

R_f = 0.31 (CH_2Cl_2/MeOH = 100/4)

Mp = 198-199 °C

^{1}H NMR (360 MHz, $CDCl_3$, 300 K) δ 8.00 (d, J = 5.8 Hz, 1H, NH^{22}), 7.85 (d, J = 8.4 Hz, 1H, H^{15}), 7.57-7.26 (m, 5H, H^{Ar}), 6.86 (d, J = 6.0 Hz, 1H, H^{11}), 5.67 (d, J = 6.8 Hz, 1H, H^4), 5.19 (dd, J = 23.0,

12.4 Hz, 2H, H^{26}), 4.64 (p, *J* = 7.4 Hz, 1H, H^{23}), 4.58-4.42 (m, 1H, H^{16}), 4.36-4.04 (m, 2H, $H^{5, 12}$), 2.95-2.74 (m, 2H, $H^{19, 8}$), 2.48 (dd, *J* = 14.0, 7.8 Hz, 1H, H^{9}), 2.40-2.09 (m, 6H, $H^{20, 6, 9, 20, 17, 18}$), 2.08-1.90 (m, 3H, $H^{17, 18, 7}$), 1.90-1.78 (m, 1H, H^{6}), 1.65-1.51 (m, 1H, H^{7}), 1.50-1.39 (m, 12H, $H^{24, 1}$), 1.35 (d, *J* = 7.2 Hz, 3H, H^{13}).

^{13}C NMR (90 MHz, $CDCl_3$, 300 K) *δ* 175.50 (C^{25}), 173.43 (C^{10}), 173.23 (C^{21}), 172.67 (C^{14}), 155.64 (C^{3}), 135.37 (C^{27}), 128.75, 128.56, 128.18 ($C^{28, 29, 30}$), 79.43 (C^{2}), 67.49 (C^{26}), 49.66 (C^{12}), 48.28 (C^{23}), 47.41 (C^{5}), 46.90 (C^{16}), 37.98 (C^{8}), 37.86 (C^{19}), 36.53 (C^{9}), 35.34 (C^{20}), 28.55 (C^{1}), 27.67 (C^{6}), 26.78 (C^{17}), 21.41 (C^{7}), 19.92 (C^{18}), 17.69 (C^{13}), 17.07 (C^{24}).

IR (neat) *v* 3325, 3315, 2983, 2943, 2868, 1731, 1682, 1649, 1638, 1537 cm^{-1}.

HRMS [ESI(+)] *m/z* $[M+Na]^+$ calculated for $[C_{30}H_{44}N_4NaO_7]^+$: 595.3102, found: 595.3078.

$[\alpha]_D^{23}$ = +83.9 (c. 0.53 in $CHCl_3$).

tert-Butyl ((1*R*,2*R*)-2-(2-(((*S*)-1-(((1*R*,2*R*)-2-(2-(((*S*)-1-(benzylamino)-1-oxopropan-2-yl)amino)-2-oxoethyl)cyclobutyl)amino)-1-oxopropan-2-yl)amino)-2-oxoethyl) cyclobutyl)carbamate (1A).

According to the general Procedure B, Boc-[(*R*,*R*)-^{3,4}CB-GABA-(*S*)-Ala]$_2$-OBn **1E** (80 mg, 0.14 mmol, 1 eq.), Pd-C (18 mg) and CH_2Cl_2/EtOAc (4/1, 5 mL) were employed to afford Boc-[(*R*,*R*)-^{3,4}CB-GABA-(*S*)-Ala]$_2$-OH **X** as a white solid.

According to the general procedure D, Boc-[(*R*,*R*)-^{3,4}CB-GABA-(*S*)-Ala]$_2$-OH **X** (0.14 mmol, 1 eq.) in CH_2Cl_2 (2 mL) was reacted with benzylamine (16 µL, 0.14 mmol, 1.02 eq.), DIPEA (73 µL, 0.42 mmol, 3 eq.) and HATU (56 mg, 0.15 mmol, 1.05 eq.). Flash chromatography (CH_2Cl_2/MeOH = gradient from 100/1 to 100/4) afforded Boc-[(*R*,*R*)-^{3,4}CB-GABA-(*S*)-Ala]$_2$-NHBn **1A** as a white solid (70 mg, 88%).

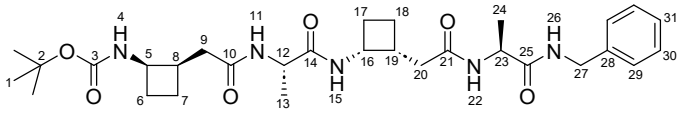

1A

***R*$_f$** = 0.35 (CH_2Cl_2/MeOH = 100/5)

Mp = 222-223 °C

^{1}H NMR (400 MHz, pyridine-d_5, 300 K) *δ* 9.51 (t, *J* = 5.8 Hz, 1H, NH^{26}), 9.17 (d, *J* = 7.4 Hz, 1H, NH^{22}), 9.10 (d, *J* = 6.8 Hz, 1H, NH^{11}), 9.07 (d, *J* = 7.8 Hz, 1H, NH^{15}), 7.80 (d, *J* = 7.2 Hz, 1H, NH^{4}), 7.54-7.46 (m, 2H, H^{Ar}), 7.32 (t, *J* = 7.6 Hz, 2H, H^{Ar}), 7.28-7.23 (m, 1H, H^{Ar}), 5.02 (p, *J* = 7.2 Hz, 1H, H^{23}), 4.94-4.89 (m, 1H, H^{12}), 4.86-4.81 (m, 1H, H^{16}), 4.71 (d, *J* = 5.8 Hz, 2H, H^{27}), 4.67-4.53 (m, 1H, H^{5}), 3.29-3.14 (m, 1H, H^{8}), 3.14-3.03 (m, 1H, H^{19}), 2.86 (dd, *J* = 14.2, 6.2 Hz, 1H, H^{9}), 2.76-2.57 (m, 3H, $H^{9, 20, 20}$), 2.37-2.15 (m, 4H, $H^{18, 17, 17, 6}$), 2.17-2.04 (m, 1H, H^{6}), 2.04-1.79 (m, 3H, $H^{7, 18, 7}$), 1.64 (d, *J* = 7.2 Hz, 3H, H^{24}), 1.49 (d, *J* = 6.2 Hz, 3H, H^{13}), 1.48 (s, 9H, H^{1}).

^{13}C NMR (100 MHz, pyridine-d_5, 300 K) δ 175.36 (C^{25}), 173.82 (C^{10}), 173.51 (C^{21}), 173.51 (C^{14}), 156.45 (C^{3}), 140.28 (C^{28}), 129.22, 128.21, 127.68 ($C^{29, 30, 31}$), 78.53 (C^{2}), 50.44 (C^{12}), 50.22 (C^{23}), 48.20 (C^{5}), 47.67 (C^{16}), 43.85 (C^{27}), 39.15 (C^{8}), 39.15 (C^{19}), 36.75 (C^{9}), 36.23 (C^{20}), 28.90 (C^{1}), 27.61 (C^{6}), 27.13 (C^{17}), 22.11 (C^{7}), 21.19 (C^{18}), 18.70 (C^{24}), 18.50 (C^{13}).

IR (neat) *v* 3325, 3300, 3062, 2976, 2932, 1680, 1658, 1639, 1532 cm^{-1}.

HRMS [ESI(+)] *m/z* $[M+Na]^+$ calculated for $[C_{30}H_{45}N_5NaO_6]^+$: 594.3262, found: 594.3241.

$[\alpha]_D^{26}$ = +68.4 (c. 0.28 in CH_2Cl_2/MeOH =1/1)

(*R,R,R*) series

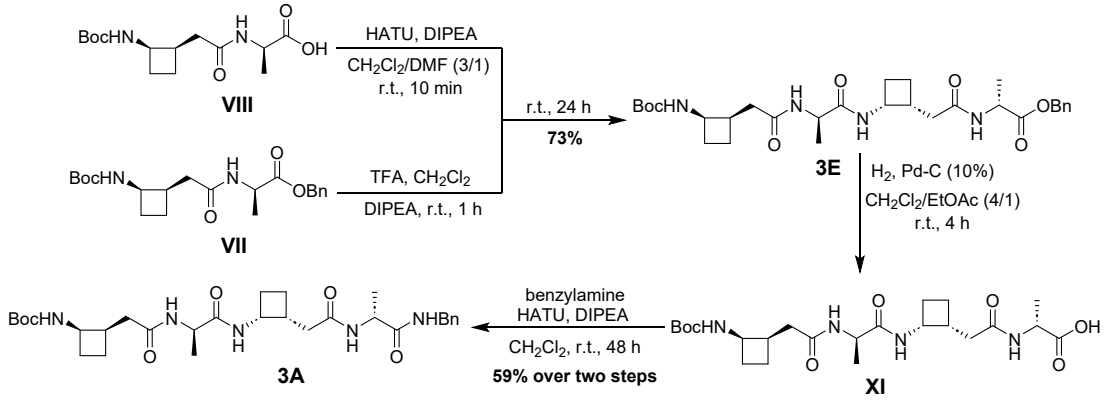

Benzyl (2-((1*R*,2*R*)-2-((*R*)-2-(2-((1*R*,2*R*)-2-((*tert*-butoxycarbonyl)amino)cyclobutyl) acetamido)propanamido)cyclobutyl)acetyl)-(*R*)-alaninate (3E).

According to the general procedure A, Boc-(*R*,*R*)-^{3,4}CB-GABA-(*R*)-Ala-OBn **VII** (117 mg, 0.3 mmol, 1 eq.) in CH_2Cl_2 (2 mL) and TFA (689 µL, 9 mmol, 30 eq.) gave TFA·H-(*R*,*R*)-^{3,4}CB-GABA-(*R*)-Ala-OBn. Digestion of this salt in CH_2Cl_2 (2 mL) and DIPEA (314 µL, 1.8 mmol, 6 eq.) gave a solution of H-(*R*,*R*)-^{3,4}CB-GABA-(*R*)-Ala-OBn.

According to the general procedure C, a solution of Boc-(*R*,*R*)-^{3,4}CB-GABA-(*R*)-Ala-OH **VIII** (90 mg, 0.3 mmol, 1 eq.) in CH_2Cl_2/DMF (3/1, 3 mL) was treated with DIPEA (105 µL, 0.6 mmol, 2 eq.), then the above-described H-(*R*,*R*)-^{3,4}CB-GABA-(*R*)-Ala-OBn solution, then HATU (122 mg, 0.32 mmol, 1.05 eq.). After the reaction time, flash chromatography (CH_2Cl_2/MeOH = gradient from 100/1 to 100/4) gave Boc-[(*R*,*R*)-^{3,4}CB-GABA-(*R*)-Ala]$_2$-OBn **3E** as a white solid (125 mg, 73%).

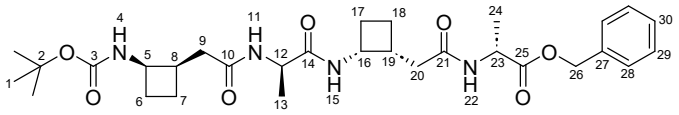

3E

R_f = 0.31 (CH_2Cl_2/MeOH = 100/4)

Mp = 209-210 °C

^{1}H NMR (360 MHz, $CDCl_3$, 300 K) δ 7.67 (d, J = 6.8 Hz, 1H, NH^{15}), 7.48-7.27 (m, 5H, H^{Ar}), 6.85 (d, J = 7.6 Hz, 1H, H^{22}), 6.41 (d, J = 6.8 Hz, 1H, H^{11}), 5.31 (d, J = 7.0 Hz, 1H, H^{4}), 5.18 (dd, J = 21.6, 12.4 Hz, 2H, H^{26}), 4.59 (p, J = 7.2 Hz, 1H, H^{23}), 4.50-4.32 (m, 2H, $H^{16, 12}$), 4.32-4.10 (m, 1H, H^{5}), 3.11-2.70 (m, 2H, $H^{19, 8}$), 2.61-2.40 (m, 2H, $H^{20, 9}$), 2.40-2.16 (m, 4H, $H^{9, 6, 17, 20}$), 2.14-1.90 (m, 3H, $H^{7, 17, 18}$), 1.84-1.75 (m, 1H, H^{6}), 1.73-1.51 (m, 2H, $H^{7, 18}$), 1.49-1.37 (m, 12H, $H^{1, 24}$), 1.35 (d, J = 7.0 Hz, 3H, H^{13}).

^{13}C NMR (90 MHz, $CDCl_3$, 300 K) δ 173.27 (C^{25}), 172.58 (C^{21}), 172.51 (C^{10}), 172.25 (C^{14}), 155.80 (C^{3}), 135.53 (C^{27}), 128.75, 128.55, 128.29 ($C^{28, 29, 30}$), 79.56 (C^{2}), 67.28 (C^{26}), 49.50 (C^{12}), 48.42 (C^{23}), 47.89 (C^{5}), 46.92 (C^{16}), 37.47 (C^{8}), 37.36 (C^{19}), 36.99 (C^{20}), 36.82 (C^{9}), 28.53 (C^{1}), 27.42 (C^{6}), 27.17 (C^{17}), 22.27 ($C^{7, 18}$), 18.69 (C^{13}), 17.97 (C^{24}).

IR (neat) ν 3328, 3310, 2982, 2942, 2868, 1728, 1682, 1638, 1537, 1499 cm^{-1}.

HRMS [ESI(+)] m/z $[M+Na]^+$ calculated for $[C_{30}H_{44}N_4NaO_7]^+$: 595.3102, found: 595.3093.

$[\alpha]_D^{20}$ = +47.8 (c. 0.55 in $CHCl_3$); $[\alpha]_D^{22}$ = +156.5 (c. 0.23 in MeOH).

tert-Butyl ((1*R*,2*R*)-2-(2-(((*R*)-1-(((1*R*,2*R*)-2-(2-(((*R*)-1-(benzylamino)-1-oxopropan-2-yl)amino)-2-oxoethyl)cyclobutyl)amino)-1-oxopropan-2-yl)amino)-2-oxoethyl) cyclobutyl)carbamate (3A).

According to the general procedure B, Boc-[(*R*,*R*)-^{3,4}CB-GABA-(*R*)-Ala]$_2$-OBn **3E** (80 mg, 0.14 mmol, 1 eq.), Pd-C (18 mg) and CH_2Cl_2/EtOAc (4/1, 5 mL) were employed to afford Boc-[(*R*,*R*)-^{3,4}CB-GABA-(*R*)-Ala]$_2$-OH **XI** as a white solid.

According to the general procedure D, Boc-[(*R*,*R*)-^{3,4}CB-GABA-(*R*)-Ala]$_2$-OH **XI** (0.14 mmol, 1 eq.) in CH_2Cl_2 (2 mL) was reacted with benzylamine (16 µL, 0.14 mmol, 1.02 eq.), DIPEA (73 µL, 0.42 mmol, 3 eq.) and HATU (56 mg, 0.15 mmol, 1.05 eq.). Flash chromatography (CH_2Cl_2/MeOH = gradient from 100/1 to 100/4) afforded Boc-[(*R*,*R*)-^{3,4}CB-GABA-(*R*)-Ala]$_2$-NHBn **3A** as a white solid (47 mg, 59%).

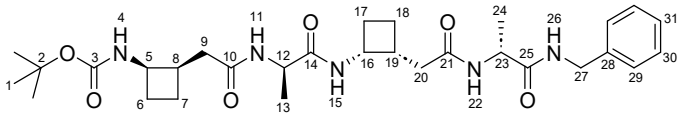

3A

R_f = 0.35 (CH_2Cl_2/MeOH = 100/5)

Mp = 214-215 °C

^{1}H NMR (400 MHz, pyridine-d_5, 300 K) δ 9.15 (s, 1H, NH^{26}), 8.96 (d, J = 5.8 Hz, 1H, NH^{22}), 8.85 (d, J = 5.4 Hz, 1H, NH^{11}), 8.81 (d, J = 7.6 Hz, 1H, NH^{15}), 8.10 (d, J = 7.0 Hz, 1H, NH^{4}), 7.56-7.46 (m, 2H, H^{Ar}), 7.33 (t, J = 7.4 Hz, 2H, H^{Ar}), 7.28-7.24 (m, 1H, H^{Ar}), 5.06-5.02 (m, 1H, H^{23}), 4.82 (dd, J = 14.8, 6.2 Hz, 1H, H^{27}), 4.78-4.61 (m, 3H, $H^{27, 16, 12}$), 4.59-4.43 (m, 1H, H^{5}), 3.45-3.11 (m, 2H, $H^{8, 19}$), 2.99-2.73 (m, 2H, $H^{9, 20}$), 2.68-2.42 (m, 2H, $H^{9, 20}$), 2.37-2.24 (m, 1H, H^{6}), 2.24-2.14 (m,

1H, H^{17}), 2.14-2.01 (m, 2H, $H^{17, 6}$), 2.00-1.81 (m, 4H, $H^{7, 18, 18, 7}$), 1.66 (d, *J* = 7.2 Hz, 3H, H^{24}), 1.47 (d, *J* = 7.2 Hz, 3H, H^{13}), 1.46 (s, 9H, H^{1}).

^{13}C NMR (100 MHz, pyridine-d_5, 300 K) δ 174.10 (C^{25}), 173.94 (C^{14}), 173.93 (C^{10}), 173.24 (C^{21}), 156.93 (C^{3}), 140.93 (C^{28}), 129.21, 128.36, 127.60 ($C^{29, 30, 31}$), 78.90 (C^{2}), 51.28 (C^{12}), 50.94 (C^{23}), 49.26 (C^{5}), 47.90 (C^{16}), 43.72 (C^{27}), 38.76 (C^{8}), 38.70 (C^{19}), 37.49 (C^{9}), 36.94 (C^{20}), 28.96 (C^{1}), 27.15 (C^{6}), 26.69 (C^{17}), 23.79 (C^{7}), 23.60 (C^{18}), 19.08 (C^{24}), 18.95 (C^{13}).

IR (neat) *v* 3325, 3297, 3064, 2977, 2937, 1714, 1680, 1660, 1639, 1528 cm^{-1}.

HRMS [ESI(+)] *m/z* [M+Na]$^+$ calculated for $[C_{30}H_{45}N_5NaO_6]^+$: 594.3262, found: 594.3239.

$[\alpha]_D^{24}$ = +54.0 (c. 0.26 in CH_2Cl_2/MeOH = 1/1)

2.2.4 Synthesis of hexapeptides.

(*R,R,S*) series

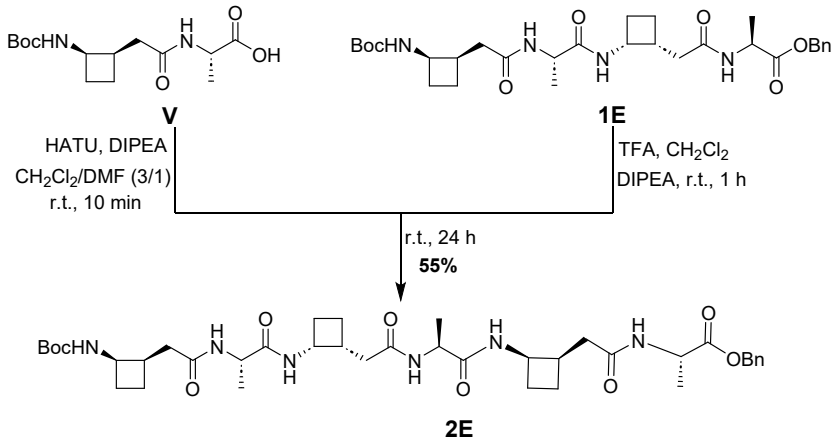

Benzyl (2-((1*R*,2*R*)-2-((*S*)-2-(2-((1*R*,2*R*)-2-((*S*)-2-(2-((1*R*,2*R*)-2-((*tert*-butoxycarbonyl) amino)cyclobutyl)acetamido)propanamido)cyclobutyl)acetamido)propanamido)cyclobutyl)a cetyl)-(*S*)-alaninate (2E).

According to the general procedure A, Boc-[(*R*,*R*)-^{3,4}CB-GABA-(*S*)-Ala]$_2$-OBn **1E** (132 mg, 0.23 mmol, 1 eq.) in CH_2Cl_2 (5 mL) and TFA (528 µL, 6.9 mmol, 30 eq.) gave TFA·H-[(*R*,*R*)-^{3,4}CB-GABA-(*S*)-Ala]$_2$-OBn. Digestion of this salt in CH_2Cl_2 (5 mL) and DIPEA (240 µL, 1.38 mmol, 6 eq.) gave a solution of H-[(*R*,*R*)-^{3,4}CB-GABA-(*S*)-Ala]$_2$-OBn.

According to the general procedure C, a solution of Boc-(*R*,*R*)-^{3,4}CB-GABA-(*S*)-Ala-OH **V** (69 mg, 0.23 mmol, 1 eq.) in CH_2Cl_2/DMF (3/1, 3 mL) was treated with DIPEA (80 µL, 0.46 mmol, 2 eq.), then the above-described H-[(*R*,*R*)-^{3,4}CB-GABA-(*S*)-Ala]$_2$-OBn solution, then HATU (92 mg, 0.24 mmol, 1.05 eq.). After the reaction time, flash chromatography (CH_2Cl_2/MeOH = gradient from 100/1 to 100/4) gave Boc-[(*R*,*R*)-^{3,4}CB-GABA-(*S*)-Ala]$_3$-OBn **2E** as a white solid (95 mg, 55%).

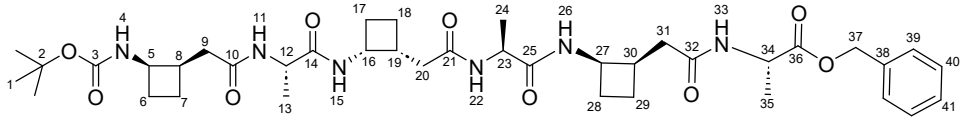

2E

R_f = 0.43 (CH_2Cl_2/MeOH = 100/6)

Mp = 245-246 °C

^{1}H NMR (400 MHz, pyridine-d_5, 310 K) δ 9.13 (d, J = 7.2 Hz, 1H, H^{22}), 9.06 (d, J = 7.0 Hz, 1H, H^{33}), 9.02 (d, J = 6.8 Hz, 1H, H^{11}), 8.96 (d, J = 7.6 Hz, 1H, H^{15}), 8.80 (d, J = 7.6 Hz, 1H, H^{26}), 7.69 (s, 1H, H^4), 7.49-7.26 (m, 5H, H^{Ar}), 5.29 (dd, J = 25.6, 12.6 Hz, 2H, H^{37}), 4.95-4.86 (m, 1H, H^{34}), 4.89-4.80 (m, 3H, $H^{16, 12, 27}$), 4.72-4.67 (m, 1H, H^{23}), 4.65-4.52 (m, 1H, H^5), 3.31-2.98 (m, 3H, $H^{8, 30, 19}$), 2.87-2.55 (m, 6H, $H^{9, 31, 20}$), 2.35-2.04 (m, 7H, $H^{17, 18, 28, 6}$), 2.04-1.81 (m, 5H, $H^{29, 18', 7}$), 1.56 (d, J = 7.2 Hz, 3H, H^{24}), 1.52 (d, J = 7.2 Hz, 3H, H^{13}), 1.49 (s, 9H, H^1), 1.47 (d, J = 7.2 Hz, 3H, H^{35}).

^{13}C NMR (100 MHz, pyridine-d_5, 300 K) δ [174.98, 174.77, 173.98, 173.98, 173.49, 173.46 ($C^{10, 14, 21, 25, 32, 36}$)], 156.46 ($C^3$), 136.91 ($C^{38}$), [129.30, 128.91, 128.79 ($C^{39, 40, 41}$)], 78.56 (C^2), 67.38 (C^{37}), [50.55, 50.43, 49.26, 48.27, 47.75, 47.75 ($C^{5, 12, 16, 23, 27, 34}$) , [40.07, 39.15, 38.96 ($C^{8, 19, 30}$)], [36.74, 36.18, 36.08 ($C^{9, 20, 31}$)], 28.92 (C^1), [27.61, 26.99, 26.96 ($C^{6, 17, 28}$)], [22.16, 21.77, 21.07 ($C^{7, 18, 29}$)], [18.44, 18.30, 17.62 ($C^{13, 24, 35}$)].

IR (neat) v 3282, 3064, 2976, 2953, 2937, 1736, 1680, 1634, 1525 cm^{-1}.

HRMS [ESI(+)] m/z $[M+Na]^+$ calculated for $[C_{39}H_{58}N_6NaO_9]^+$: 777.4157, found: 777.4127.

$[\alpha]_D^{26}$ = +106.5 (c. 0.26 in CH_2Cl_2/MeOH = 1/1).

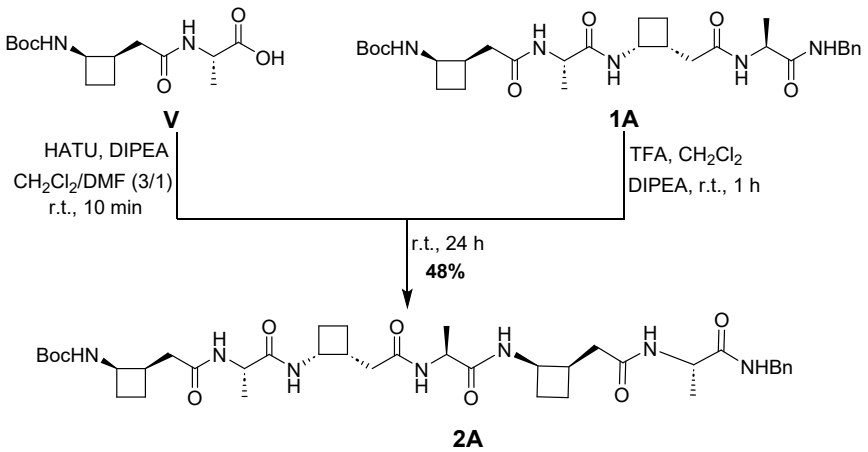

***tert*-Butyl ((1*R*,2*R*)-2-(2-(((*S*)-1-(((1*R*,2*R*)-2-(2-(((*S*)-1-(((1*R*,2*R*)-2-(2-(((*S*)-1-(benzyl amino)-1-oxopropan-2-yl)amino)-2-oxoethyl)cyclobutyl)amino)-1-oxopropan-2-yl)amino)-2-oxoethyl)cyclobutyl)amino)-1-oxopropan-2-yl)amino)-2-oxoethyl)cyclobutyl)carbamate (2A).**

According to the general procedure A, Boc-[(*R*,*R*)-^{3,4}CB-GABA-(*S*)-Ala]$_2$-NHBn **1A** (51 mg, 0.09 mmol, 1 eq.) in CH_2Cl_2 (5 mL) and TFA (207 µL, 2.7 mmol, 30 eq.) gave TFA·H-[(*R*,*R*)-^{3,4}CB-GABA-(*S*)-Ala]$_2$-NHBn. Digestion of this salt in CH_2Cl_2 (5 mL), and DIPEA (94 µL, 0.54 mmol, 6 eq.) gave a solution of H-[(*R*,*R*)-^{3,4}CB-GABA-(*S*)-Ala]$_2$-NHBn.

According to the general procedure C, a solution of Boc-(*R*,*R*)-^{3,4}CB-GABA-(*S*)-Ala-OH **V** (27 mg, 0.09 mmol, 1 eq.) in CH_2Cl_2/DMF (3/1, 2 mL) was treated with DIPEA (31 µL, 0.18 mmol, 2 eq.), then the above-described H-[(*R*,*R*)-^{3,4}CB-GABA-(*S*)-Ala]$_2$-NHBn solution, then HATU (38 mg, 0.1 mmol, 1.05 eq.). After the reaction time, preparative HPLC (hexane/EtOH = 40/60; product elution at 6.7 min) gave Boc-[(*R*,*R*)-^{3,4}CB-GABA-(*S*)-Ala]$_3$-NHBn **2A** as a white solid (32 mg, 48%).

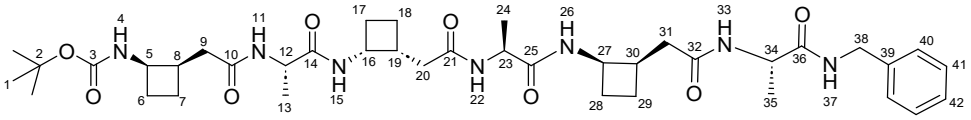

2A

R_f = 0.51 (CH_2Cl_2/MeOH = 100/6)

Mp = 255-257 °C

^{1}H NMR (400 MHz, pyridine-d_5, 330 K) δ 9.30 (s, 1H, H^{37}), 9.13 (d, *J* = 7.8 Hz, 1H, H^{26}), 9.08 (d, *J* = 6.2 Hz, 1H, H^{22}), 8.96 (d, *J* = 7.4 Hz, 1H, H^{33}), 8.89 (d, *J* = 7.8 Hz, 1H, H^{15}), 8.83 (d, *J* = 6.6 Hz, 1H, H^{11}), 7.49 (d, *J* = 7.6 Hz, 2H, H^{Ar}), 7.41 (s, 1H, H^4), 7.33 (t, *J* = 7.6 Hz, 2H, H^{Ar}), 7.28-7.24 (m, 1H, H^{Ar}), 5.01-4.91 (m, 1H, H^{34}), 4.91-4.75 (m, 4H, H$^{23, 16, 12, 27}$), 4.73-4.66 (m, 2H, H^{38}), 4.52-4.51 (m, 1H, H^5), 3.23-3.12 (m, 1H, H^8), 3.12–2.99 (m, 2H, H$^{30, 19}$), 2.83 (dd, *J* = 14.2, 6.4 Hz, 1H, H^9), 2.77-2.60 (m, 4H, H$^{31, 20, 9', 31'}$), 2.55 (dd, *J* = 14.2, 6.2 Hz, 1H, H$^{20'}$), 2.46-2.17 (m, 7H, H$^{28, 17, 17', 6, 18, 29, 28'}$), 2.17-2.05 (m, 1H, H$^{6'}$), 2.05-1.91 (m, 3H, H$^{29, 18', 7}$), 1.91-1.80 (m, 1H, H$^{7'}$), 1.61 (d, *J* = 7.4 Hz, 3H, H^{35}), 1.59 (d, *J* = 7.0 Hz, 3H, H^{24}), 1.52 (d, *J* = 7.6 Hz, 3H, H^{13}), 1.50 (s, 9H, H^1).

^{13}C NMR (100 MHz, pyridine-d_5, 300 K) δ 175.71 (C^{36}), [174.65, 174.15, 173.81, 173.29 (C$^{10, 21, 25, 32}$)], 173.09 (C^{14}), 156.04 (C^3), 139.72 (C^{39}), [128.84, 127.78, 127.30 (C$^{40, 41, 42}$)], 78.13 (C^2), 50.35 (C^{12}), 50.35 (C^{34}), 49.99 (C^{23}), 47.87 (C^5), 47.58 (C^{16}), 47.36 (C^{27}), 43.52 (C^{38}), 38.83 (C$^{8, 19, 30}$), 36.25 (C^9), 35.45 (C^{20}), 35.31 (C^{31}), 28.51 (C^1), 27.21 (C^6), 26.46 (C^{17}), 26.46 (C^{28}), 21.73 (C^7), 20.30 (C^{18}), 20.11 (C^{29}), 18.09 (C^{24}), 17.95 (C^{35}), 17.70 (C^{13}).

IR (neat) *v* 3286, 3061, 2979, 2935, 2869, 1737, 1711, 1680, 1638, 1531 cm^{-1}.

HRMS [ESI(+)] *m/z* [M+Na]$^+$ calculated for [$C_{39}H_{59}N_7NaO_8$]$^+$: 776.4317, found: 776.4279.

$[\alpha]_D^{26}$ = +108.0 (c. 0.26 in CH_2Cl_2/MeOH = 1/1).

(*R,R,R*) series

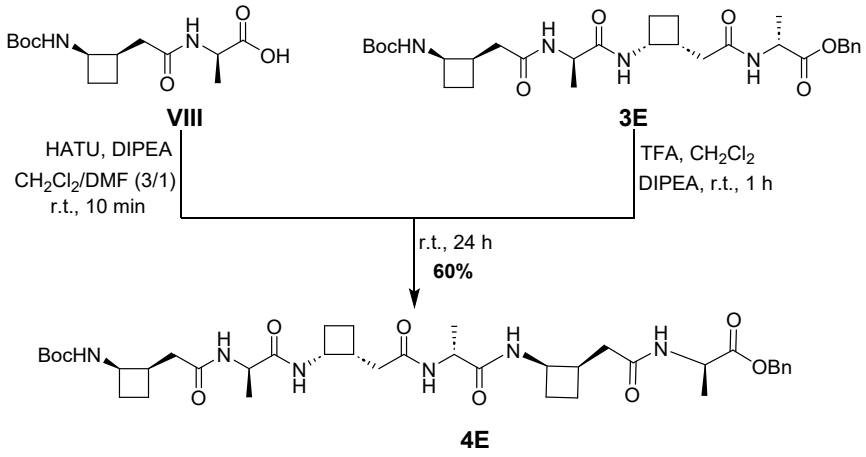

Benzyl (2-((1*R*,2*R*)-2-((*R*)-2-(2-((1*R*,2*R*)-2-((*R*)-2-(2-((1*R*,2*R*)-2-((*tert*-butoxycarbonyl) amino)cyclobutyl)acetamido)propanamido)cyclobutyl)acetamido)propanamido)cyclobutyl)a cetyl)-(*R*)-alaninate (4E).

According to the general procedure A, Boc-[(*R*,*R*)-^{3,4}CB-GABA-(*R*)-Ala]$_2$-OBn **3E** (132 mg, 0.23 mmol, 1 eq.) in CH_2Cl_2 (5 mL) and TFA (528 µL, 6.9 mmol, 30 eq.) gave TFA·H-[(*R*,*R*)-^{3,4}CB-GABA-(*R*)-Ala]$_2$-OBn. Digestion of this salt in CH_2Cl_2 (5 mL), and DIPEA (240 µL, 1.38 mmol, 6 eq.) gave a solution of H-[(*R*,*R*)-^{3,4}CB-GABA-(*R*)-Ala]$_2$-OBn.

According to the general procedure C, a solution of Boc-(*R*,*R*)-^{3,4}CB-GABA-(*R*)-Ala-OH **VIII** (69 mg, 0.23 mmol, 1 eq.) in CH_2Cl_2/DMF (3/1, 3 mL) was treated with DIPEA (80 µL, 0.46 mmol, 2 eq.), then the above-described H-[(*R*,*R*)-^{3,4}CB-GABA-(*R*)-Ala]$_2$-OBn solution, then HATU (92 mg, 0.24 mmol, 1.05 eq.). After the reaction time, preparative HPLC (hexane/EtOH = 65/35; product elution at 14.6 min) gave Boc-[(*R*,*R*)-^{3,4}CB-GABA-(*R*)-Ala]$_3$-OBn **4E** as a white solid (104 mg, 60%).

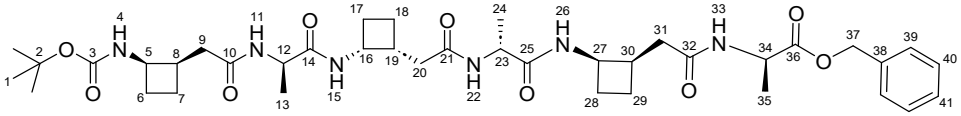

4E

R_f = 0.43 (CH_2Cl_2/MeOH = 100/6)

Mp = 233-234 °C

^{1}H NMR (600 MHz, DMSO-d_6, 350 K) δ 8.34 (d, J = 7.2 Hz, 1H), 8.07 (d, J = 7.8 Hz, 1H), 8.03 (d,

J = 7.2 Hz, 1H), 7.98 (d, *J* = 7.8 Hz, 1H), 7.95 (d, *J* = 7.8 Hz, 1H), 7.53-7.20 (m, 5H), 7.06 (d, *J* = 8.4 Hz, 1H), 5.10 (dd, *J* = 15.0, 12.3 Hz, 2H), 4.37-4.26 (m, 3H), 4.25-4.18 (m, 2H), 4.11-4.00 (m, 1H), 2.72-2.63 (m, 3H), 2.25-2.17 (m, 4H), 2.12-1.99 (m, 8H), 1.84-1.72 (m, 3H), 1.56-1.47 (m, 3H), 1.37 (s, 9H), 1.28 (d, *J* = 7.2 Hz, 3H), 1.19 (d, *J* = 2.4 Hz, 3H), 1.18 (d, *J* = 2.4 Hz, 3H).

^{13}C NMR (150 MHz, DMSO-d_6, 350 K) δ [171.48, 171.43, 171.39, 171.19, 171.13, 170.89 ($C^{10, 14, 21, 25, 32, 36}$)], 154.50 ($C^{3}$), 135.76 ($C^{38}$), [127.97, 127.53, 127.24 ($C^{39, 40, 41}$)], 77.24 (C^{2}), 65.43 (C^{37}), [47.94, 47.92, 47.33 ($C^{12, 23, 34}$)], [46.67, 45.24, 45.06 ($C^{5, 16, 27}$)], [37.00, 36.91, 36.85 ($C^{8, 19, 30}$)], [34.98, 34.98, 34.73 ($C^{9, 20, 31}$)], 27.92 (C^{1}), [25.78, 25.53, 25.53 ($C^{6, 17, 28}$)], [21.06, 20.79, 20.58 ($C^{7, 18, 29}$)], [18.17, 16.56, 15.85 ($C^{13, 24, 35}$)].

IR (neat) *v* 3320, 3297, 2988, 2958, 2926, 2853, 1738, 1679, 1661, 1641, 1554, 1531 cm^{-1}.

HRMS [ESI(+)] *m/z* [M+Na]$^+$ calculated for $[C_{39}H_{58}N_6NaO_9]^+$: 777.4157, found: 777.4141.

$[\alpha]_D^{25}$ = +36.5 (c. 0.25 in CH_2Cl_2/MeOH = 1/1).

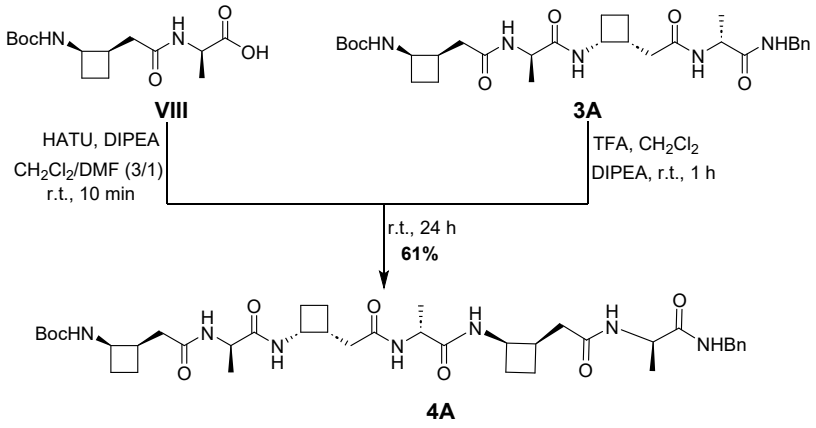

***tert*-Butyl ((1*R*,2*R*)-2-(2-(((*R*)-1-(((1*R*,2*R*)-2-(2-(((*R*)-1-(((1*R*,2*R*)-2-(2-(((*R*)-1-(benzyl amino)-1-oxopropan-2-yl)amino)-2-oxoethyl)cyclobutyl)amino)-1-oxopropan-2-yl)amino)-2-oxoethyl)cyclobutyl)amino)-1-oxopropan-2-yl)amino)-2-oxoethyl)cyclobutyl)carbamate (4A).**

According to the general procedure A, Boc-[(*R*,*R*)-^{3,4}CB-GABA-(*R*)-Ala]$_2$-NHBn **3A** (51 mg, 0.09 mmol, 1 eq.) in CH_2Cl_2 (5 mL) and TFA (207 µL, 2.7 mmol, 30 eq.) gave TFA·H-[(*R*,*R*)-^{3,4}CB-GABA-(*R*)-Ala]$_2$-NHBn. Digestion of this salt in CH_2Cl_2 (5 mL), and DIPEA (94 µL, 0.54 mmol, 6 eq.) gave a solution of H-[(*R*,*R*)-^{3,4}CB-GABA-(*R*)-Ala]$_2$-NHBn.

According to the general procedure C, a solution of Boc-(*R*,*R*)-^{3,4}CB-GABA-(*R*)-Ala-OH **VIII** (27 mg, 0.09 mmol, 1 eq.) in CH_2Cl_2/DMF (3/1, 2 mL) was treated with DIPEA (31 µL, 0.18 mmol, 2 eq.), then the above-described H-[(*R*,*R*)-^{3,4}CB-GABA-(*R*)-Ala]$_2$-NHBn solution, then HATU (38 mg, 0.1 mmol, 1.05 eq.). After the reaction time, preparative HPLC (hexane/EtOH = 40/60;

product elution at 10.5 min) gave Boc-[(*R*,*R*)-^{3,4}CB-GABA-(*R*)-Ala]$_3$-NHBn **4A** as a white solid (41 mg, 61%).

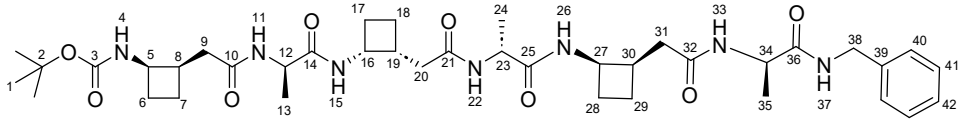

4A

R_f = 0.51 (CH_2Cl_2/MeOH = 100/6)

Mp = 245-246 °C

^{1}H NMR (400 MHz, DMSO-d_6, 350 K) δ 8.08 (d, J = 5.2 Hz, 1H), 7.86 (d, J = 7.6 Hz, 1H), 7.83 (d, J = 7.8 Hz, 1H), 7.75 (d, J = 7.2 Hz, 1H), 7.69 (d, J = 7.2 Hz, 2H), 7.38-7.11 (m, 5H), 6.74 (s, 1H), 4.34-4.22 (m, 7H), 4.11-4.03 (m, 1H), 2.81-2.70 (m, 3H), 2.29-2.19 (m, 6H), 2.18-2.08 (m, 3H), 2.02-1.94 (m, 3H), 1.90-1.77 (m, 3H), 1.62-1.52 (m, 3H), 1.39 (s, 9H), 1.28-1.21 (m, 9H).

^{13}C NMR (100 MHz, DMSO-d_6, 350 K) δ [172.00, 171.57, 171.57, 171.24, 171.09, 171.01 ($C^{10, 14, 21, 25, 32, 36}$)], 154.54 ($C^3$), 139.13 ($C^{39}$), [127.79, 126.70, 126.27 ($C^{40, 41, 42}$)], 77.27 (C^2), [48.15, 48.15, 48.06 ($C^{12, 23, 34}$)], [46.68, 45.37, 45.32 ($C^{5, 16, 27}$)], 41.79 (C^{38}), [37.02, 36.85, 36.85 ($C^{8, 19, 30}$)], [35.05, 35.02, 35.01 ($C^{9, 20, 31}$)], 27.93 (C^1), [25.79, 25.45, 25.43 ($C^{6, 17, 28}$)], [21.20, 21.16, 20.61 ($C^{7, 18, 29}$)], [18.13, 18.06, 17.81 ($C^{13, 24, 35}$)].

IR (neat) v 3320, 3297, 2988, 2958, 2926, 2853, 1738, 1679, 1661, 1641, 1554, 1531 cm^{-1}.

HRMS [ESI(+)] m/z [M+Na]$^+$ calculated for $[C_{39}H_{59}N_7NaO_8]^+$: 776.4317, found: 777.4283.

$[\alpha]_D^{26}$ = +7.1 (c. 0.12 in CH_2Cl_2/MeOH = 1/1).

2.3 Copies of ^{1}H and ^{13}C NMR spectra

Compound **IV** (in $CDCl_3$)

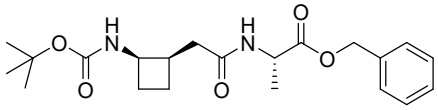

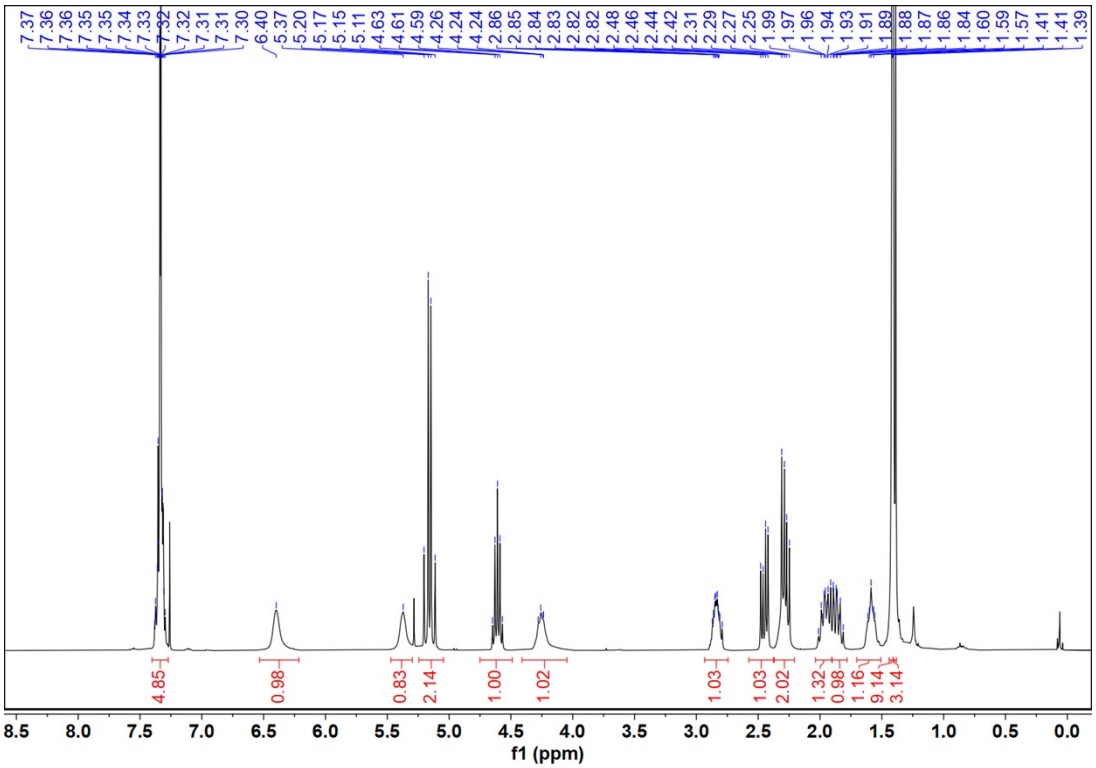

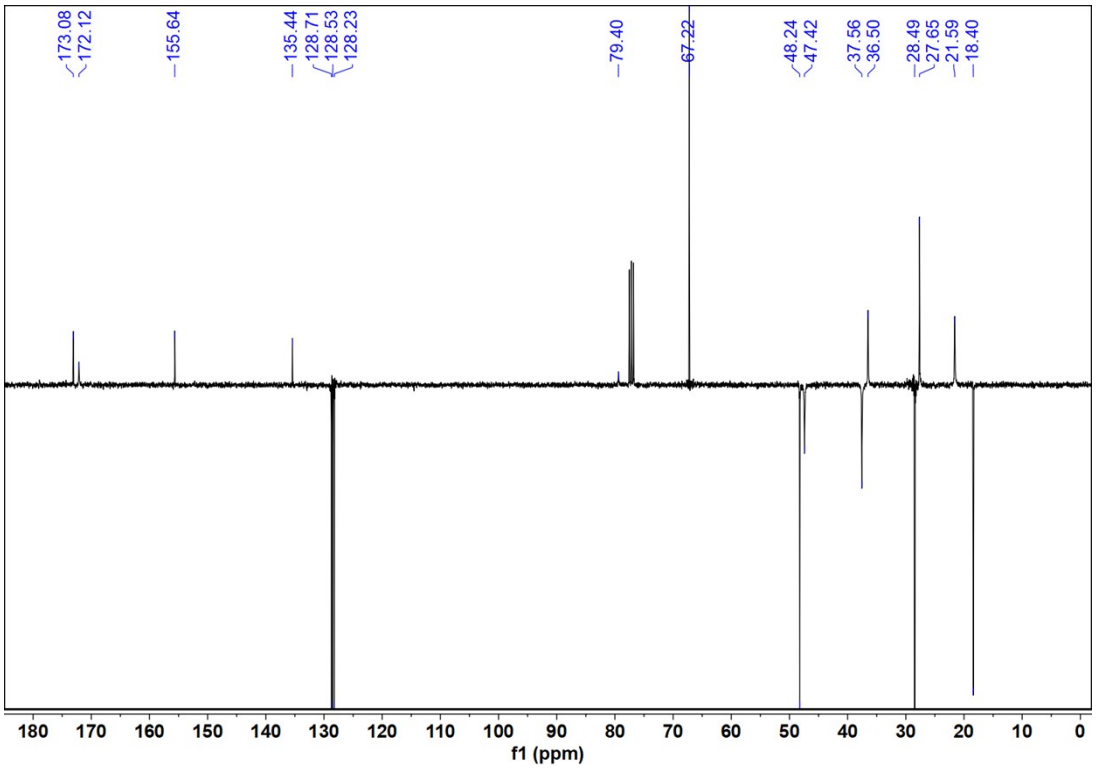

Compound **VI** (in $CDCl_3$)

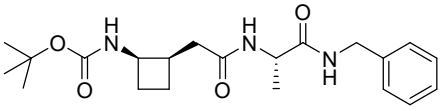

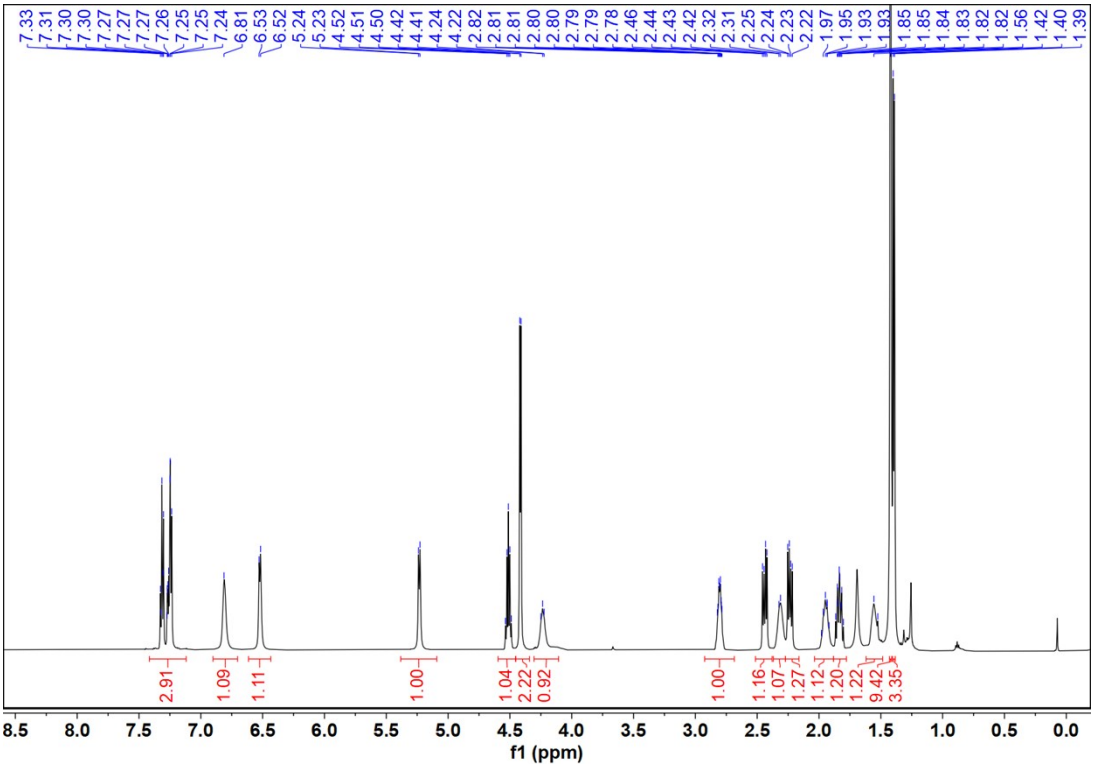

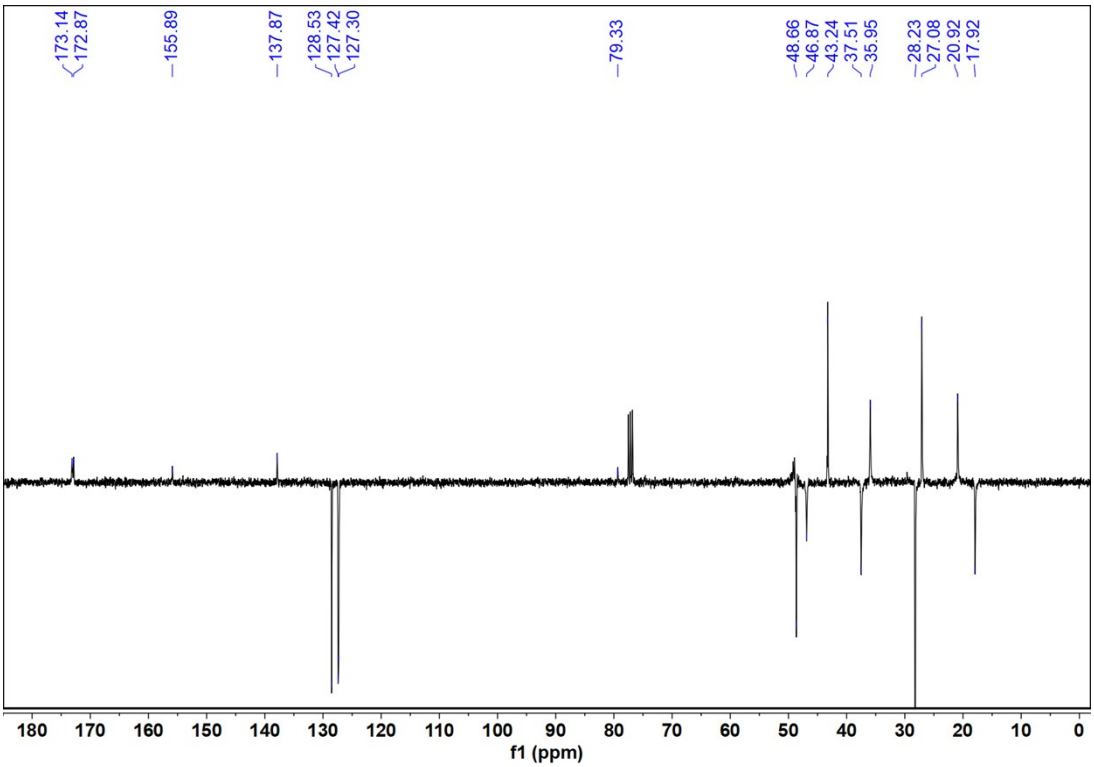

Compound **VII** (in $CDCl_3$)

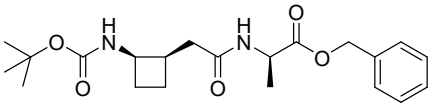

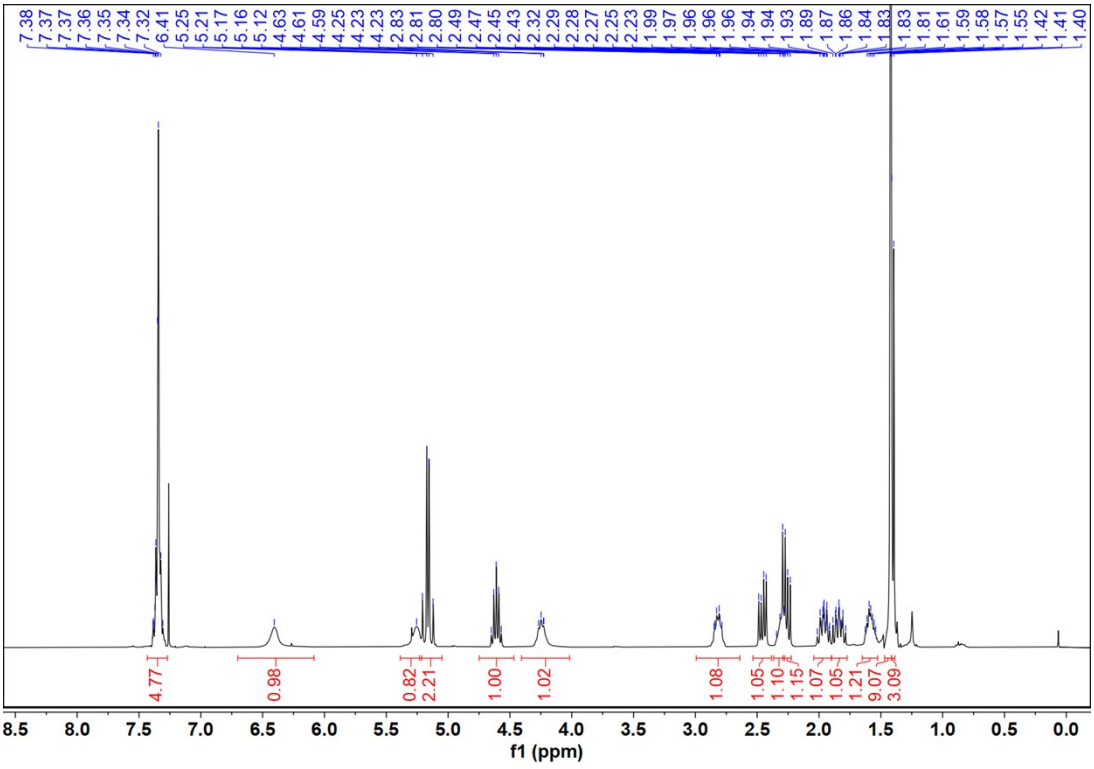

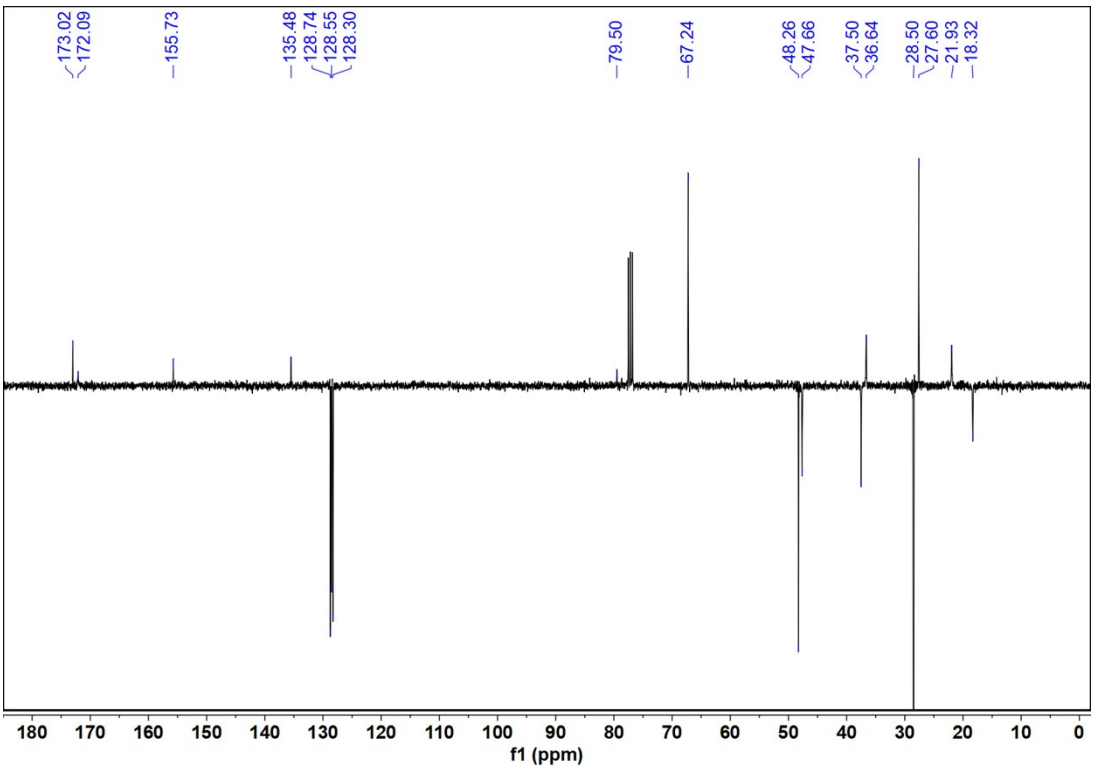

Compound **IX** (in $CDCl_3$)

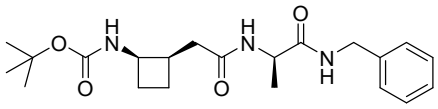

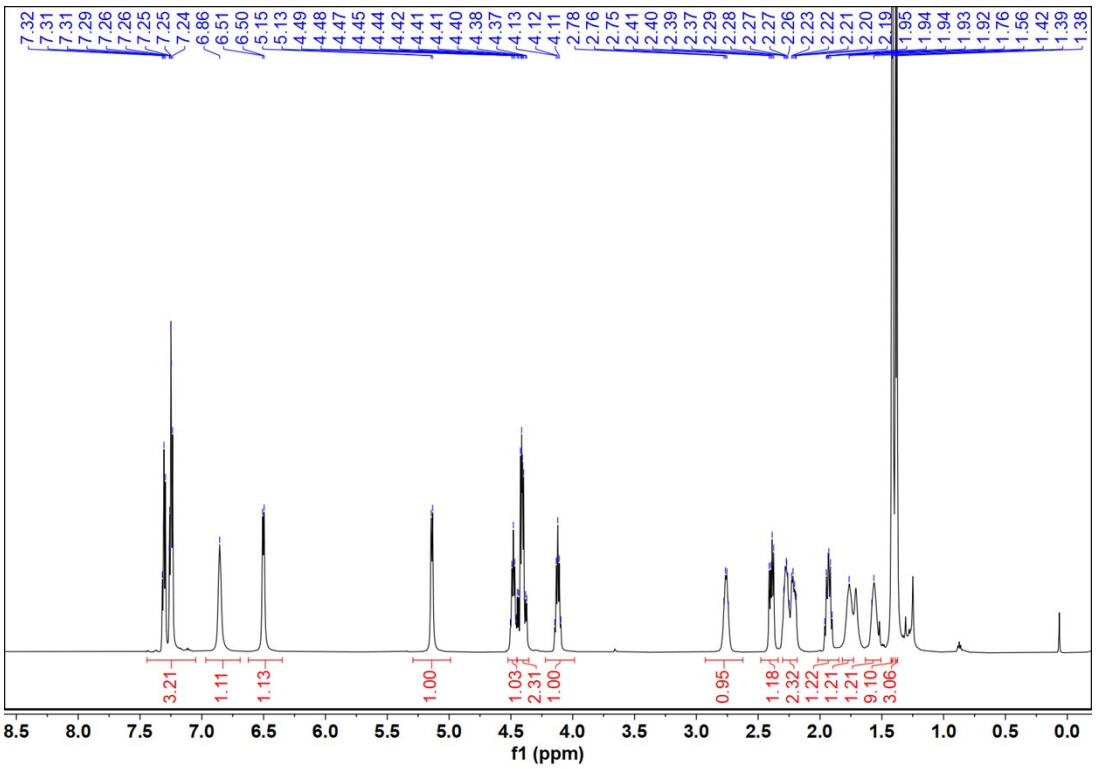

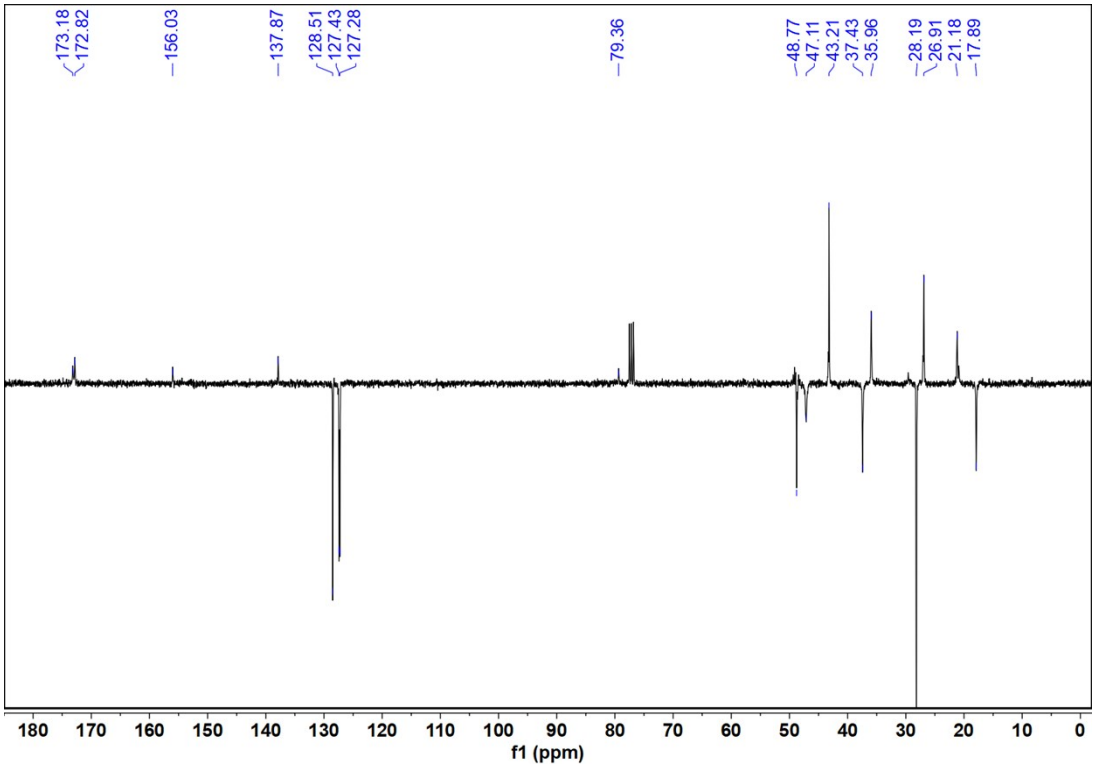

Tetrapeptide ester **1E** (in $CDCl_3$)

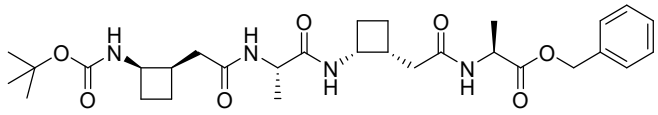

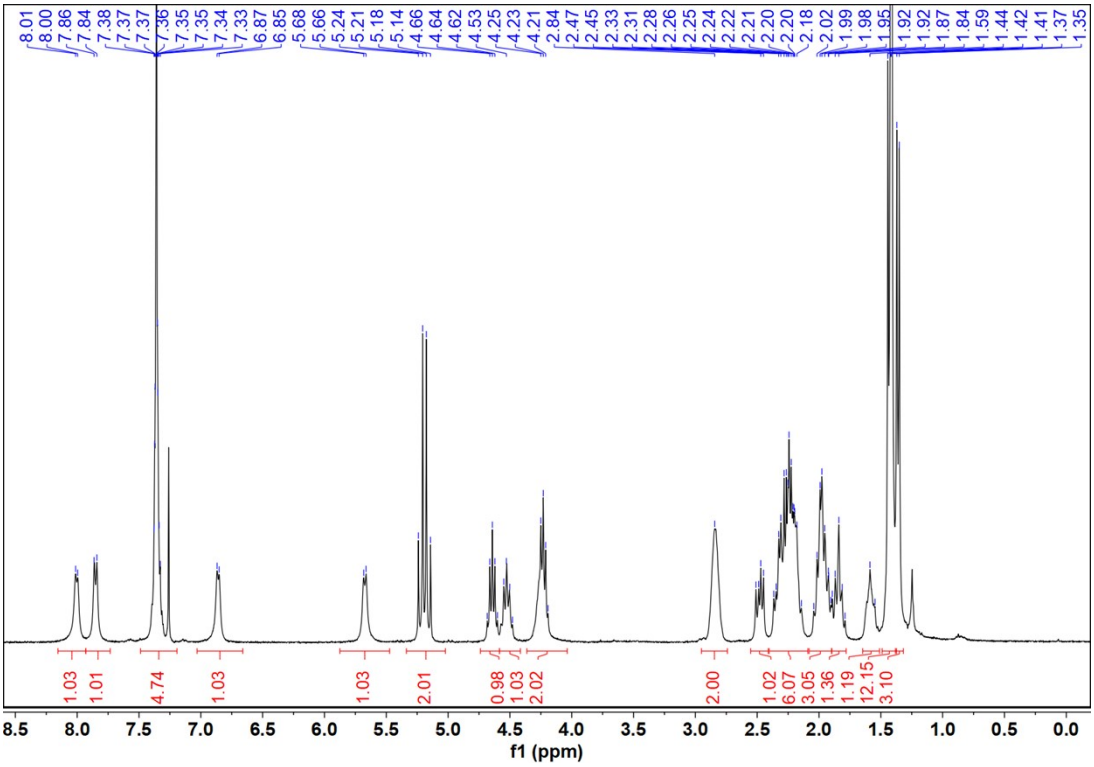

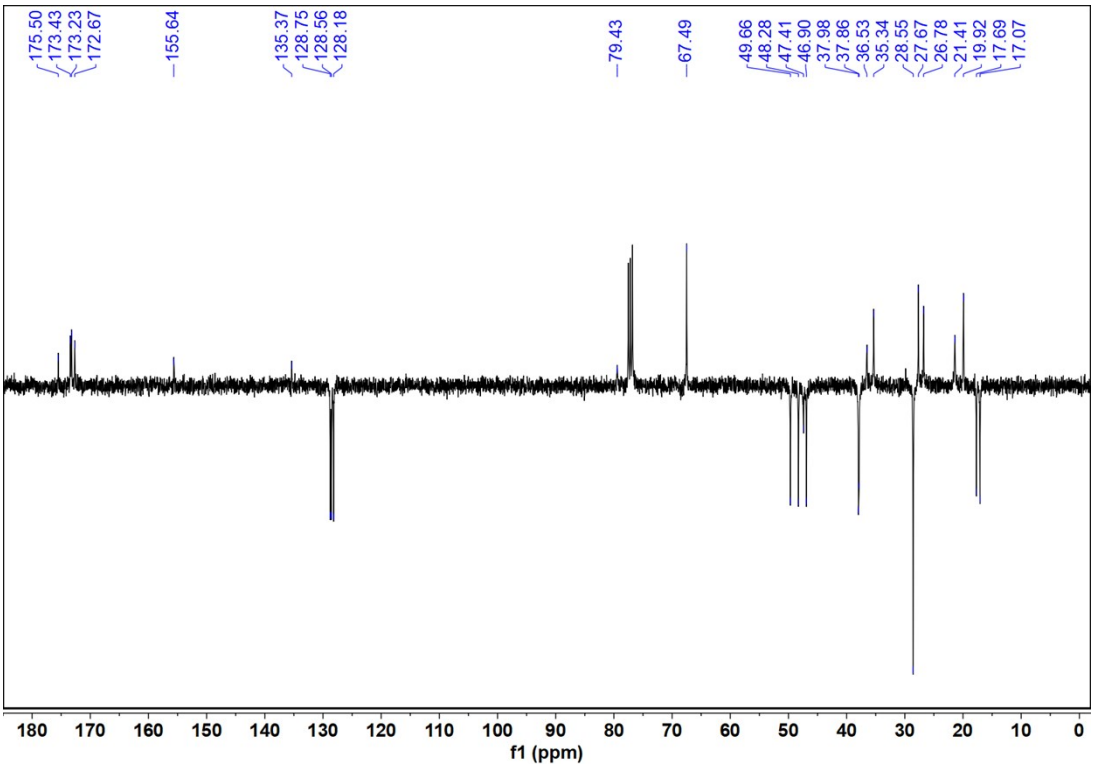

Tetrapeptide amide **1A** (in pyridine-d_5)

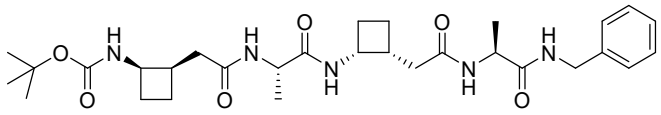

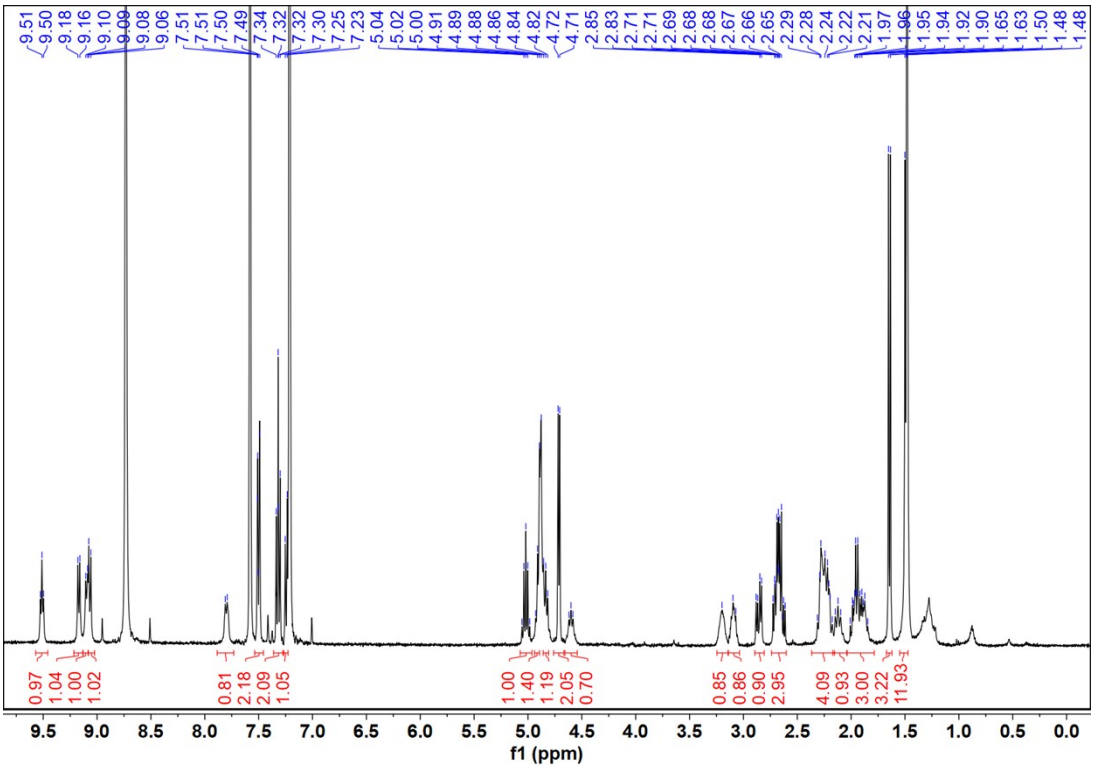

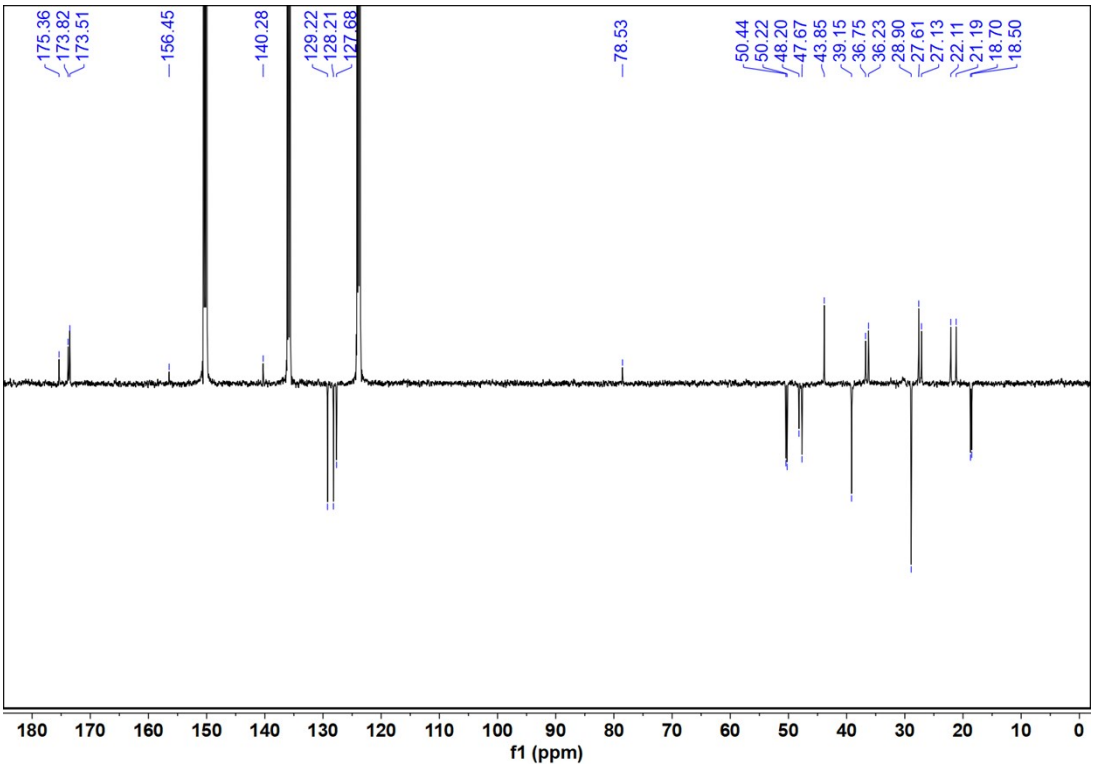

Hexapeptide ester **2E** (in pyridine-d_5)

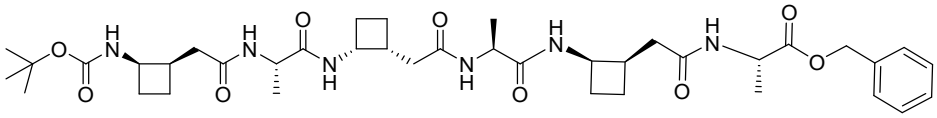

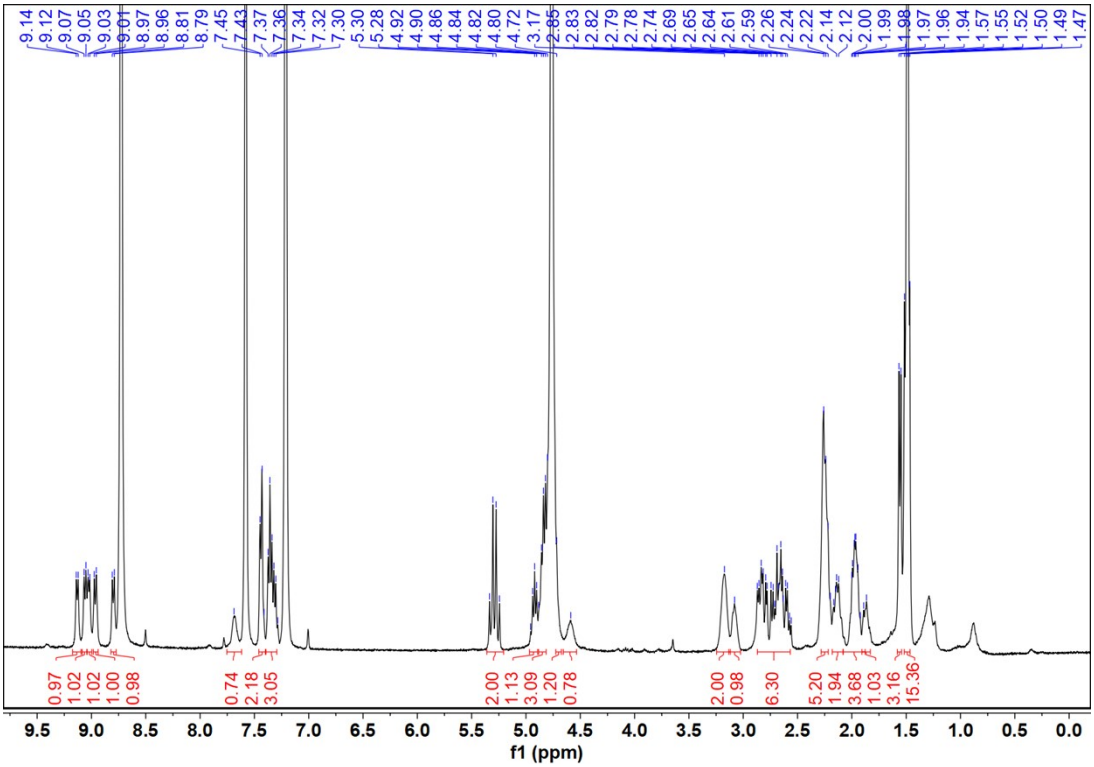

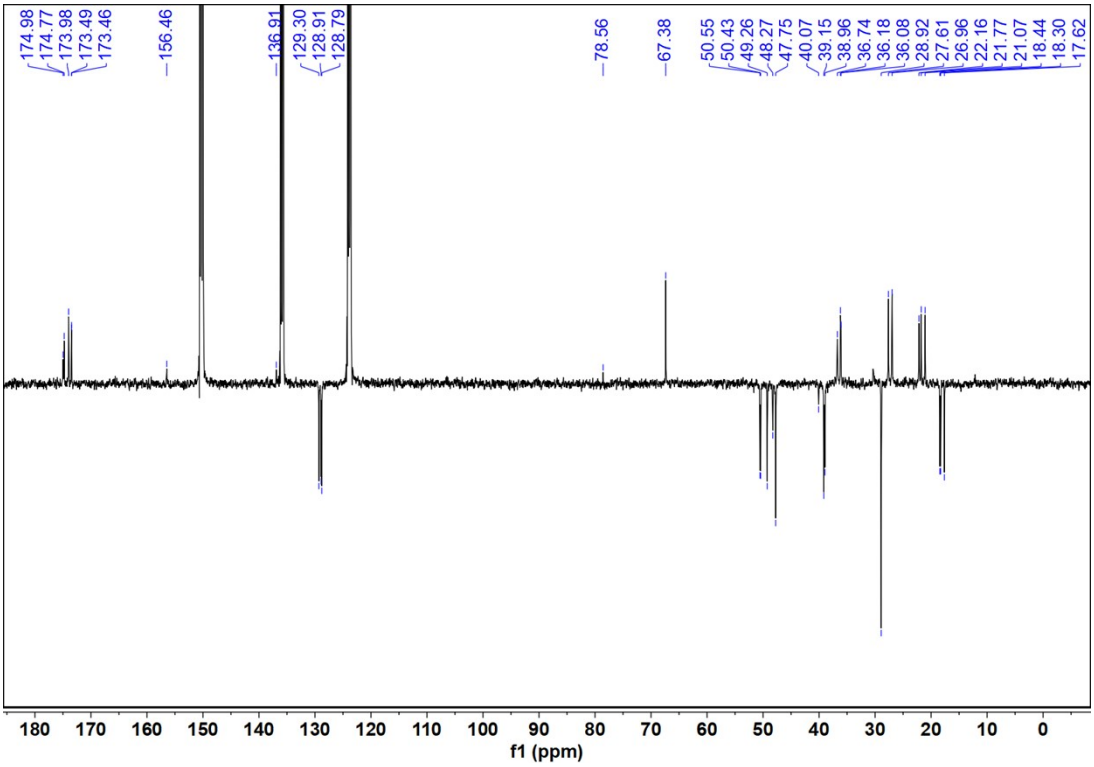

Hexapeptide amide **2A** (in pyridine-d_5)

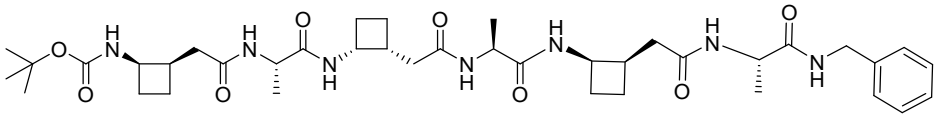

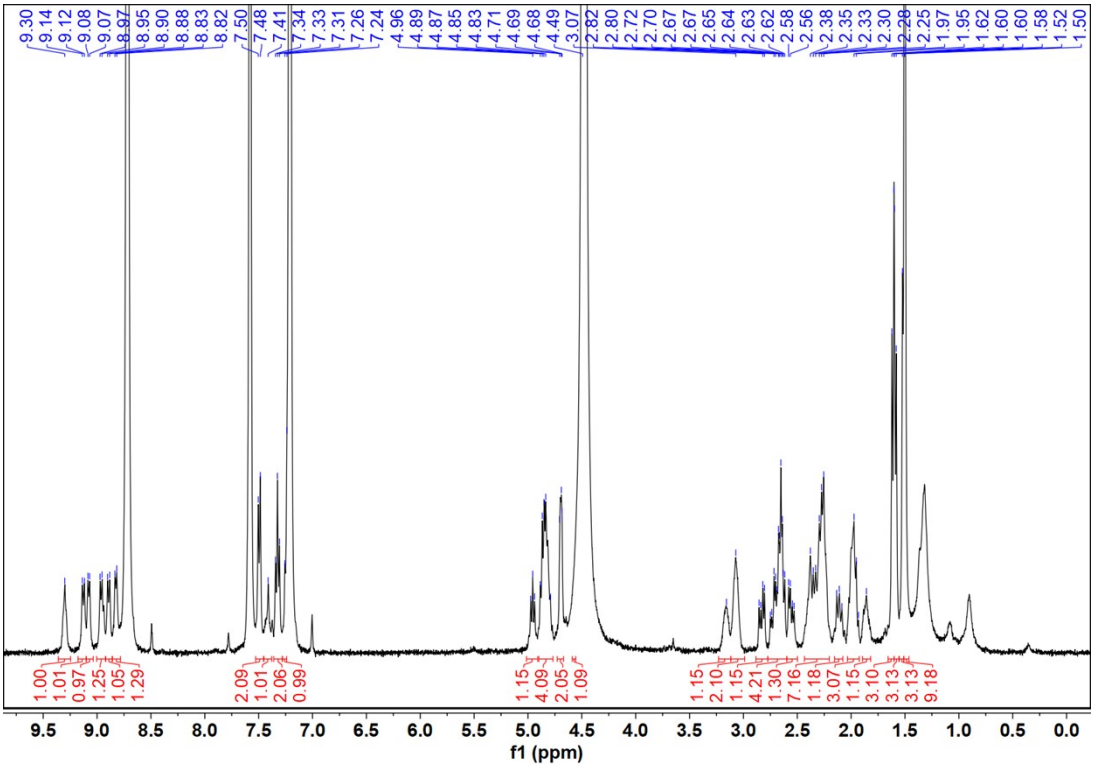

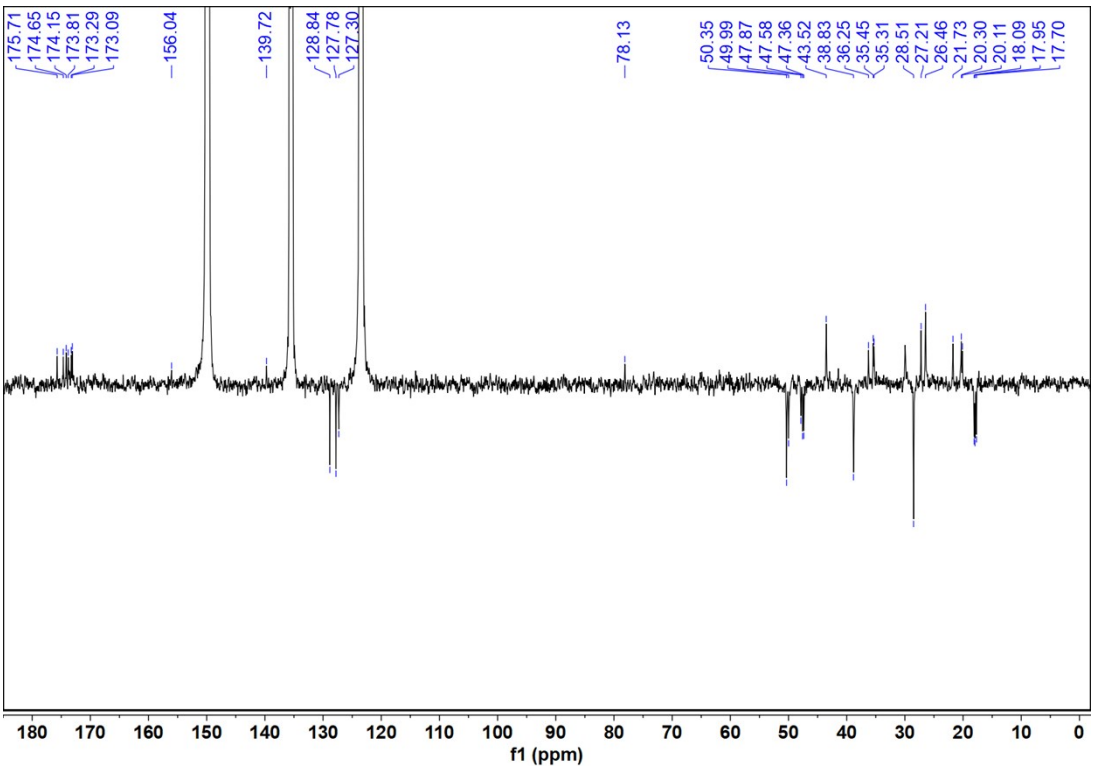

Tetrapeptide ester **3E** (in $CDCl_3$)

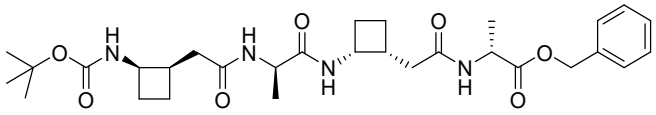

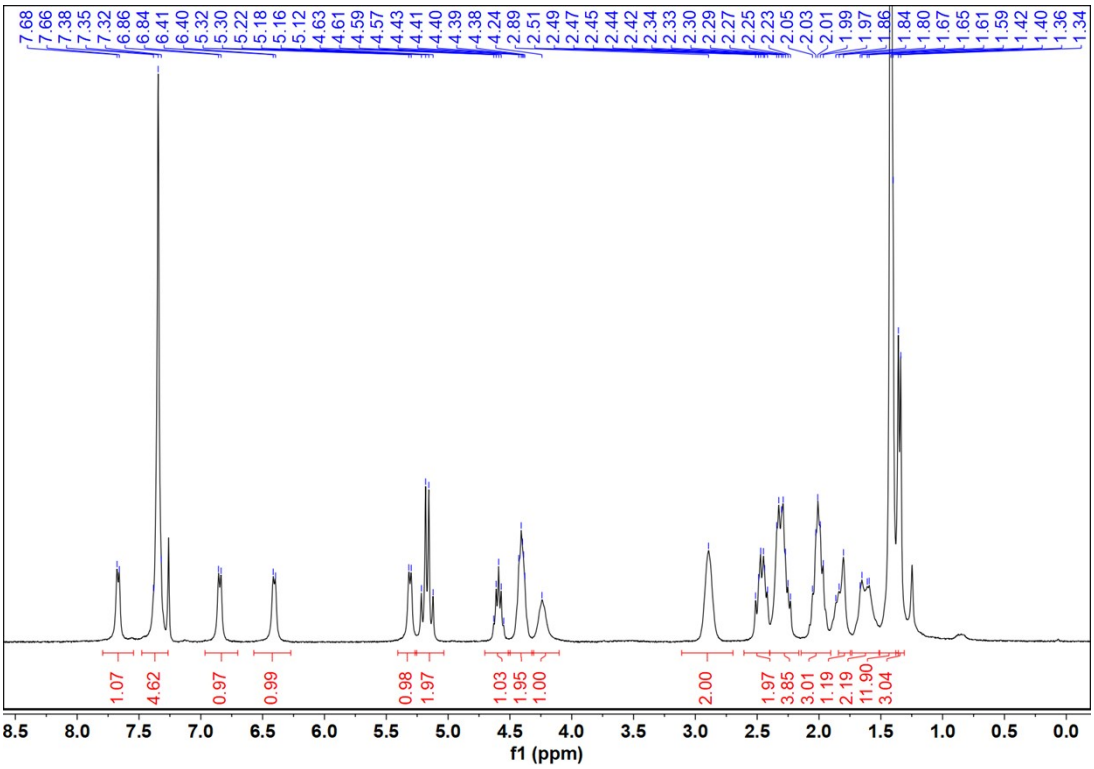

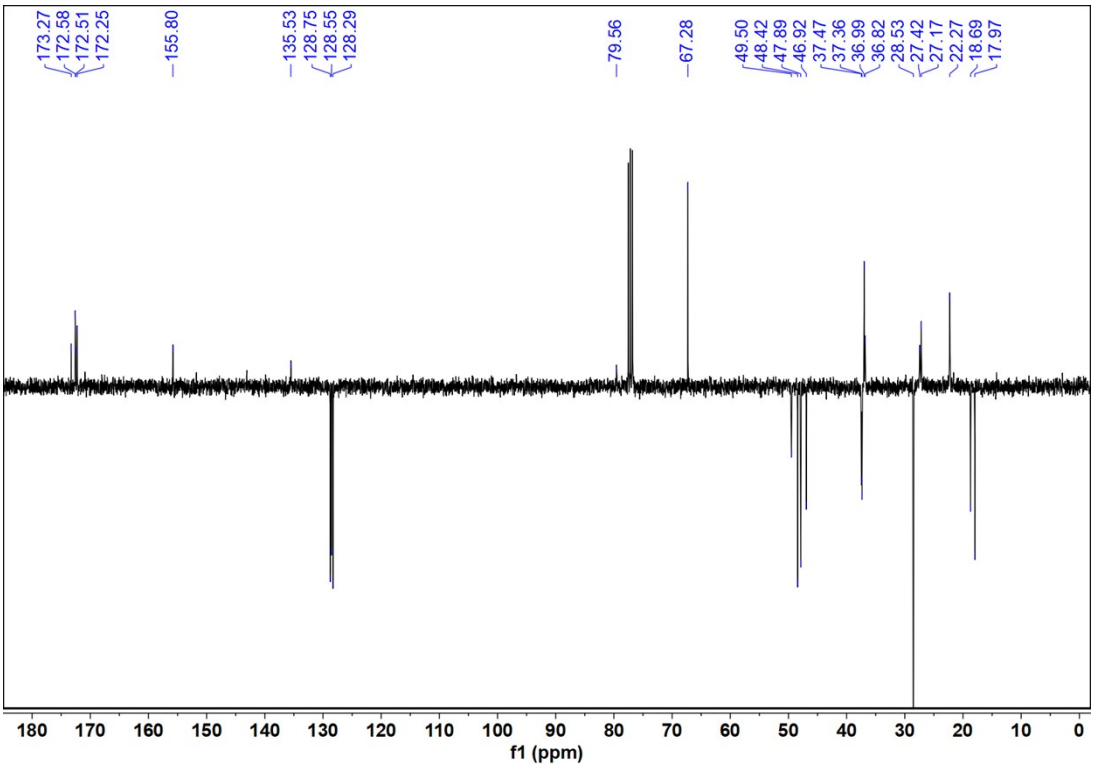

Tetrapeptide amide **3A** (in pyridine-d_5)

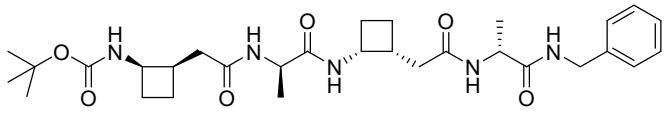

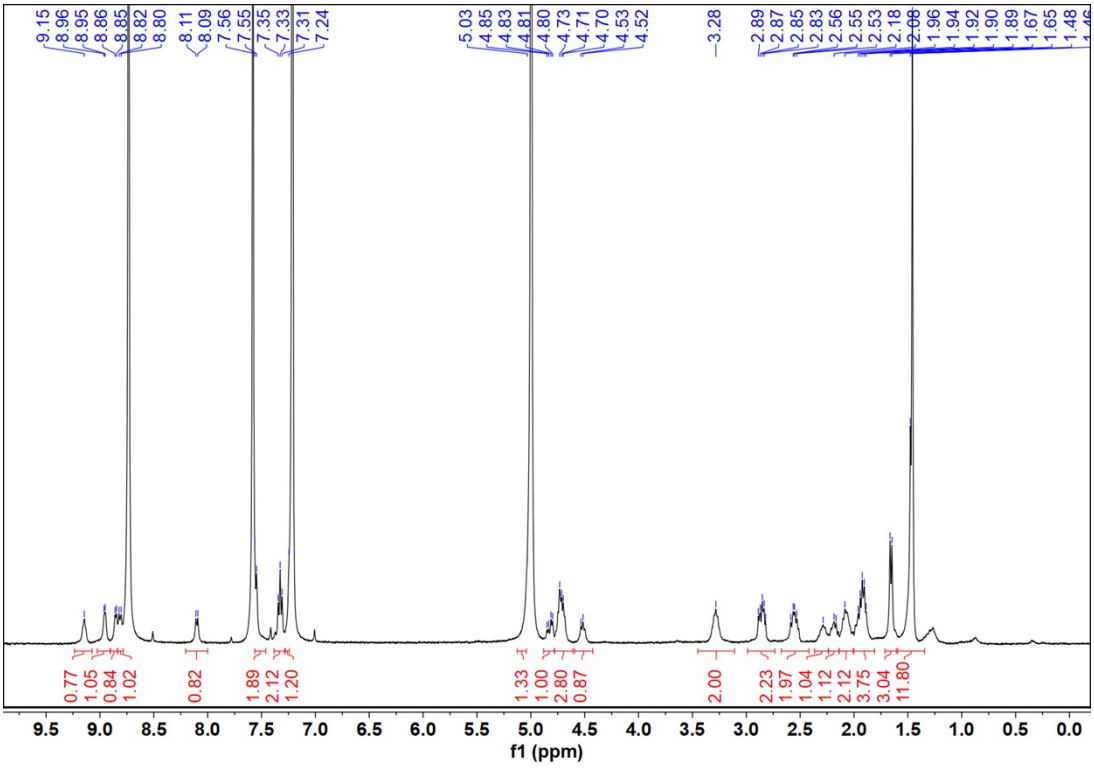

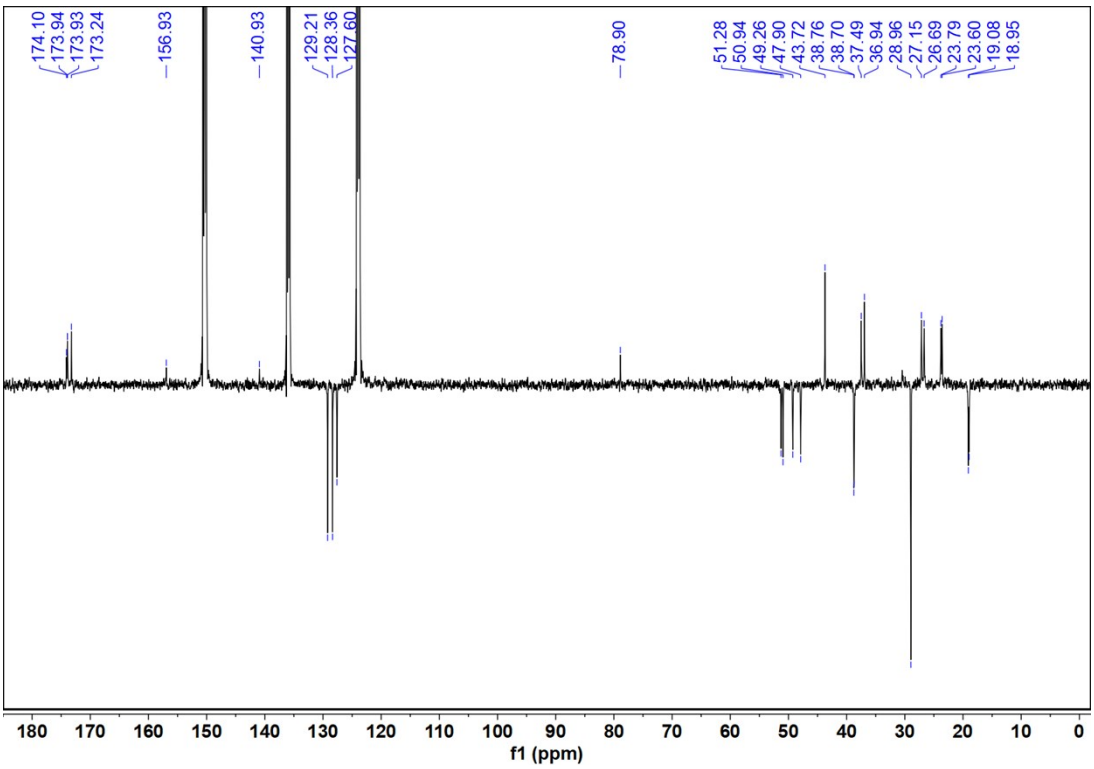

Hexapeptide ester **4E** (in DMSO-d_6)

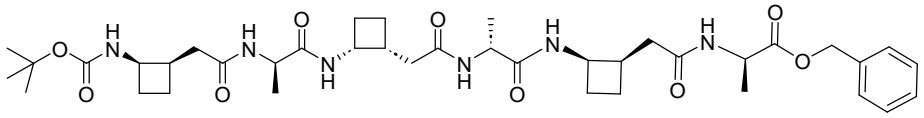

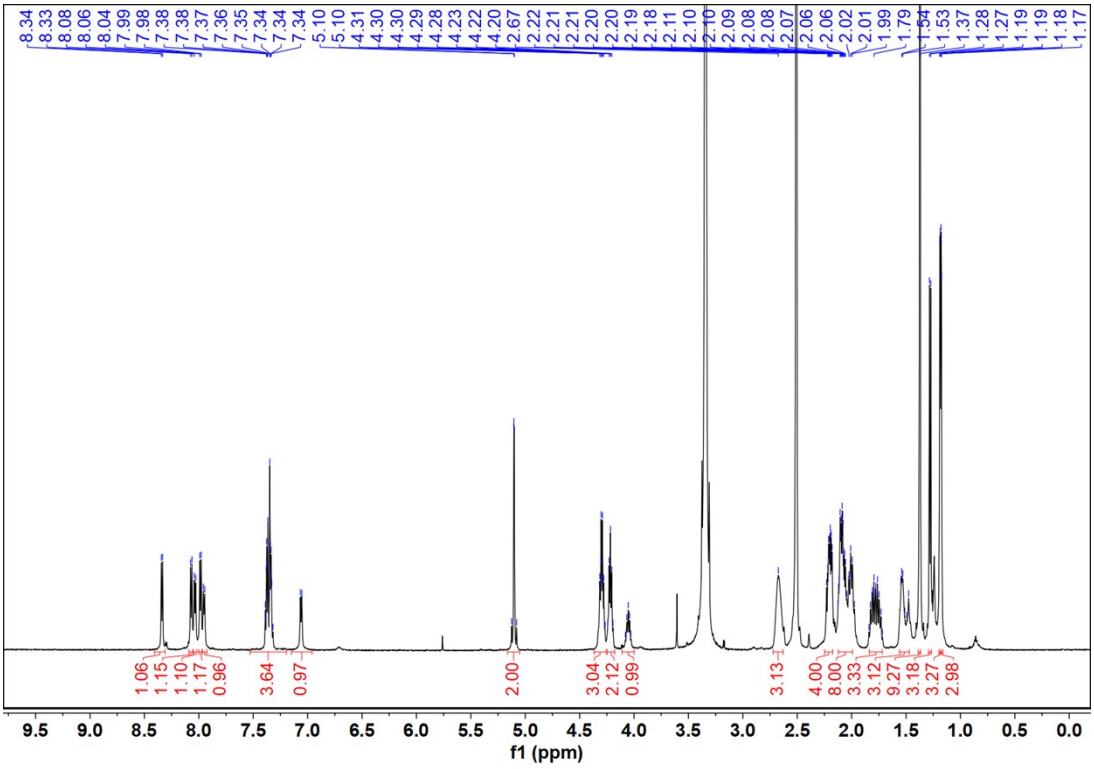

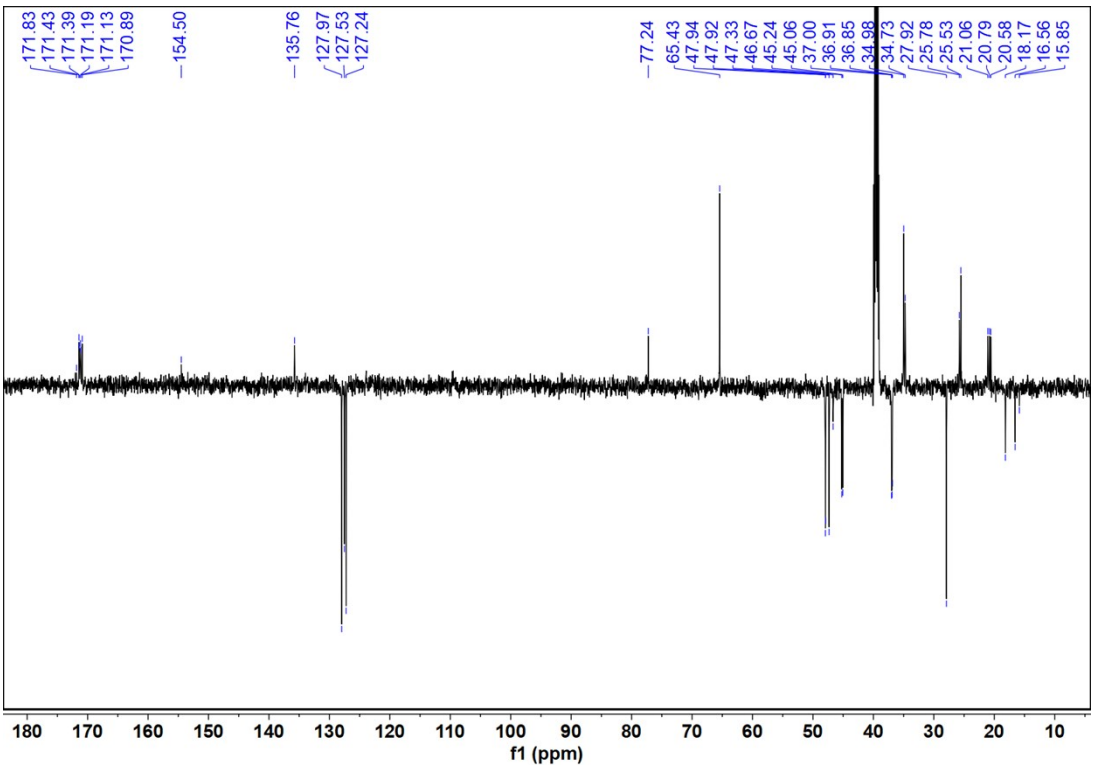

Hexapeptide amide **4A** (in DMSO-d_6)

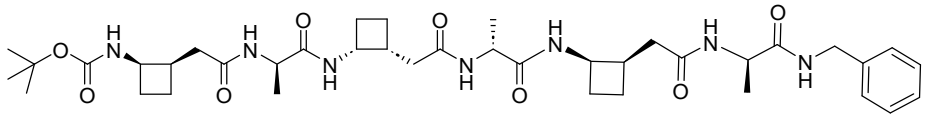

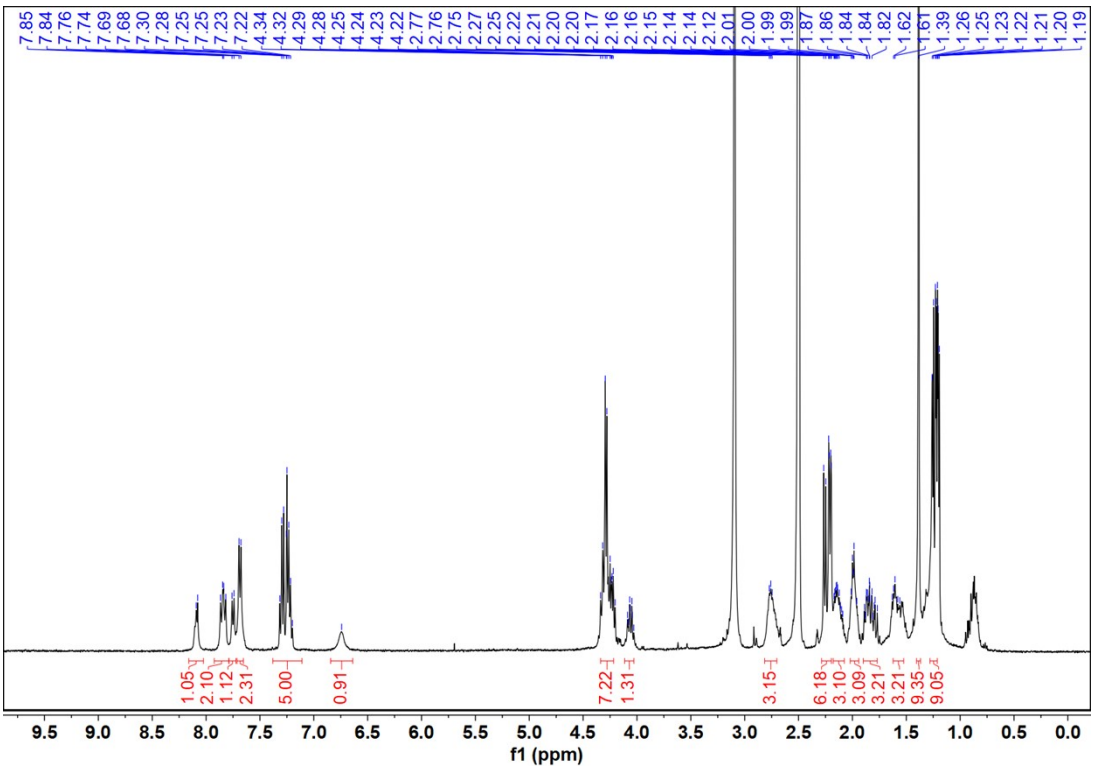

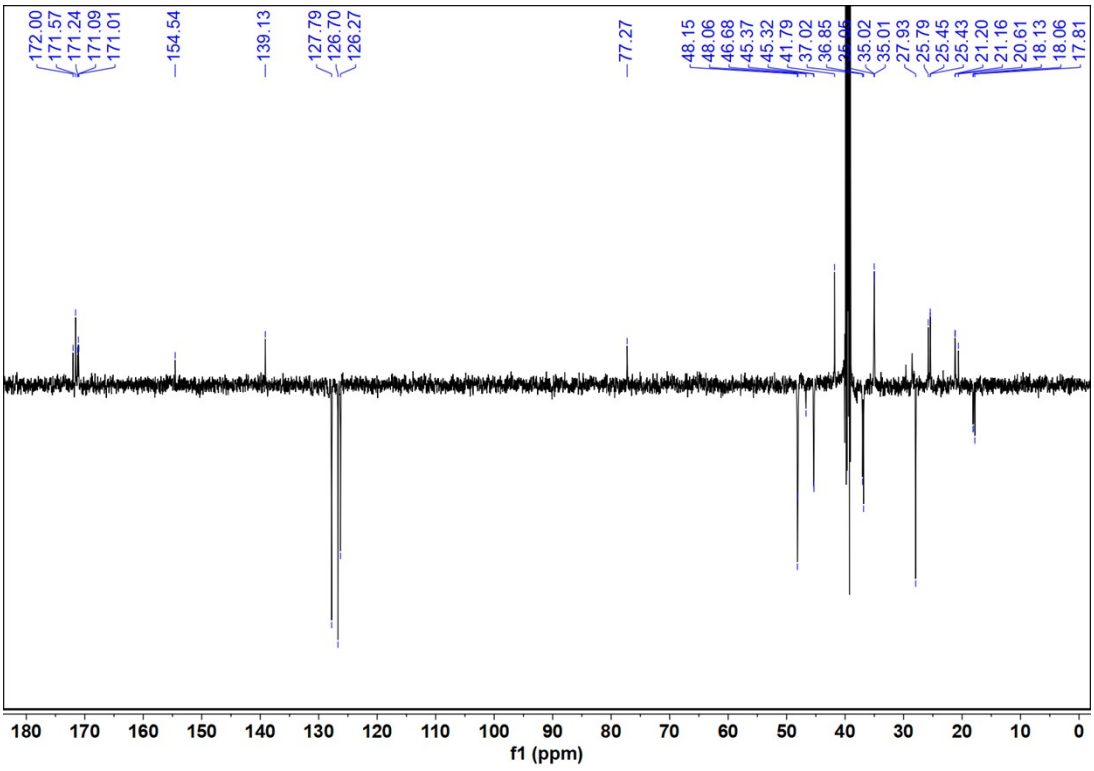

3. Solution state spectroscopic studies

3.1 IR spectra

Solution state infrared spectra of peptides were recorded at 295 K on a Fourier-transform Perkin Elmer Spectrum Two spectrometer, using 1-3 mM solutions in analytical grade $CHCl_3$ held in Omni-cell Specac 1 mm path-length NaCl plates. The absorbance bands in the amide A, I and II regions are shown in Figure S3.1.

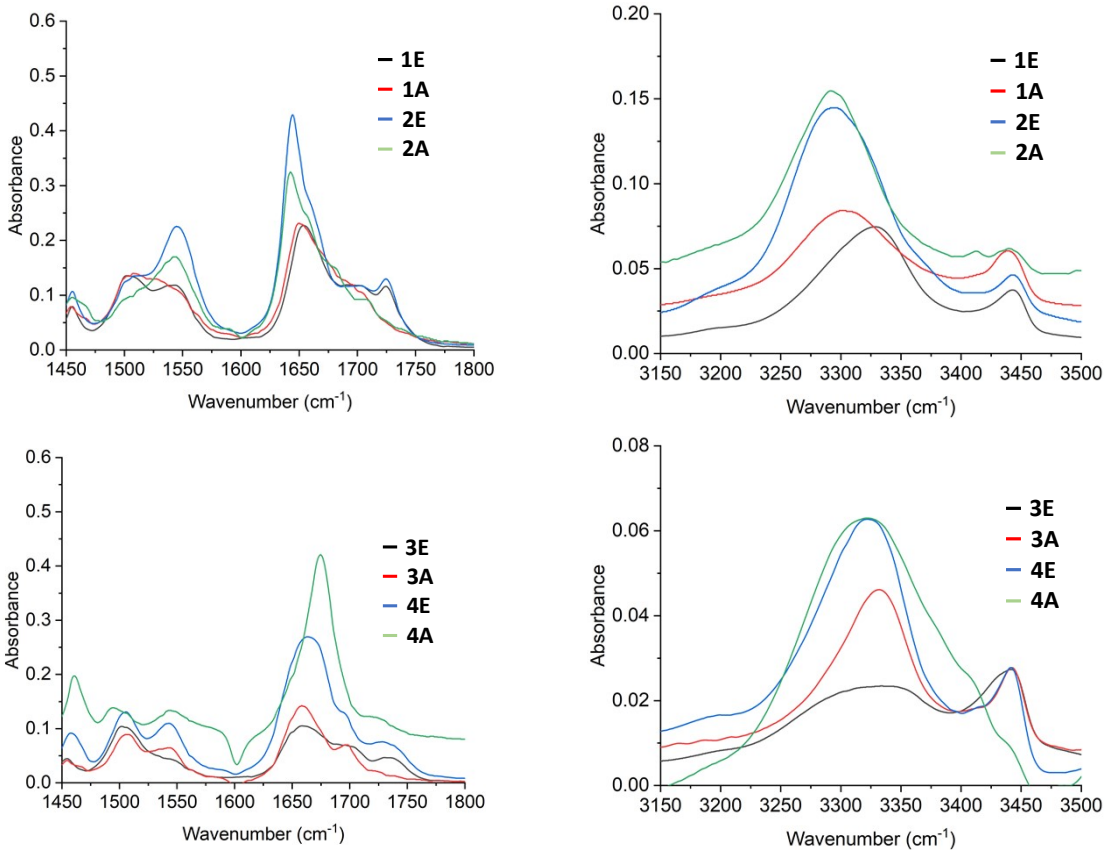

Figure S3.1. Solution state IR absorption spectra of peptides 1A/E to 4A/E; left panels show the amide I and II regions, right panels show amide A regions; upper panels are (*R,R,S*) series peptides, lower panels are (*R,R,R*) series peptides.

To verify the absence of intermolecular interactions in the conformational behavior and IR spectroscopic signatures, a dilution experiment was carried out on a representative example from each series: tetrapeptide amide **1A** for the (*R,R,S*) series and tetrapeptide amide **3A** for the (*R,R,R*) series. No concentration effects were in evidence in the IR spectra of these compounds recorded for 2 mM and 0.4 mM solutions in analytical grade $CHCl_3$, suggesting that any folding preferences were due to intramolecular interactions.

The absorbance bands in the amide A, I and II regions are shown in Figure S3.2.

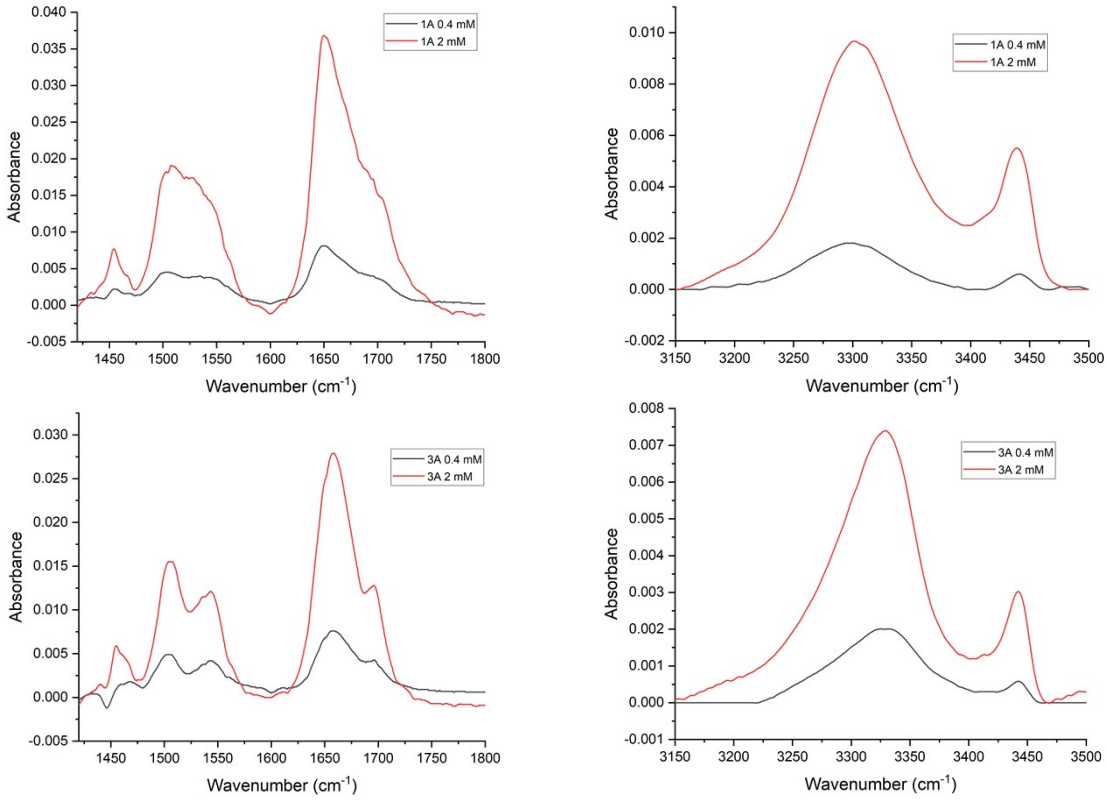

Figure S3.2. Solution state IR absorption spectra of (*R,R,S*) peptide 1A (above) and (*R,R,R*) peptide 3A (below) at 2 mM and 0.4 mM concentrations (red and black curves, respectively); left panels show the amide I and II regions, right panels show amide A regions.

3.2 NMR titration experiments

A DMSO-d_6 titration experiment was conducted on a representative peptide from each series: tetrapeptide amide **1A** for the (*R,R,S*) series and tetrapeptide amide **3A** for the (*R,R,R*) series. Starting sample solutions were prepared at a concentration of 2 mM in $CDCl_3$ (400 µL). Successive aliquots of DMSO-d_6 (6 × 2 µL, 2 × 4 µL, 2 × 10 µL) were added to the NMR tube; after each addition the sample was agitated rapidly then the ^{1}H NMR spectrum re-recorded. All spectra were recorded at 300 K.

In the (*R,R,S*) series, a 12/10 helical conformation of compound **1A** would implicate a hydrogen-bonded status for carbamate proton NH^4 and amide protons NH^{15} and NH^{22}, whereas amide protons NH^{11} and NH^{26} would be free and solvent exposed. Titration with DMSO-d_6 induced a low-to-negligible shift for the former three signals ($\Delta\delta$ = 0.26, 0.02 and 0.00 ppm, respectively). In contrast a significant downfield shift was observed for the latter two signals ($\Delta\delta$ = 0.46 and 0.76 ppm, respectively). These data are in full agreement with a 12/10 helical conformation for compound **1A** (Figure S3.3).

In the (*R,R,R*) series, a 12 helical conformation of compound **3A** would implicate a hydrogen-bonded status for amide protons NH^{15}, NH^{22} and NH^{26}, whereas carbamate proton NH^4 and amide proton NH^{11} would be free and solvent exposed. Titration with DMSO-d_6 induced a negligible shift for the former three signals ($\Delta\delta$ = 0.06, –0.12 and 0.10 ppm, respectively). In contrast a significant downfield shift was observed for the latter two signals ($\Delta\delta$ = 0.83 and 0.91 ppm, respectively). These data are in full agreement with a 12 helical conformation for compound **3A** (Figure S3.4).

The helical assignments are supported by the chemical shift data observed in $CDCl_3$ solution. Whatever the helical pattern, free amide NH signals (6.72, 6.88 ppm for **1A**; 5.91 ppm for **3A**) appear upfield compared to H-bonded amide NH signals (8.17, 7.86 ppm for **1A;** 7.74, 7.74, 7.28 ppm for **3A**). Similarly, the free carbamate NH signal (4.99 ppm) for **3A** appears upfield compared to the H-bonded carbamate NH signal (5.74 ppm) of **1A**.

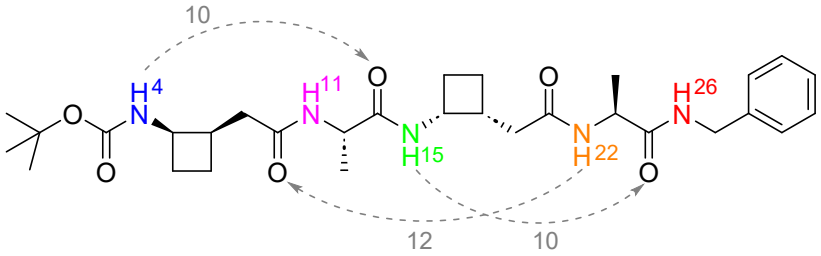

Compound **1A** (*R,R,S*) showing the hydrogen bonding system of a 12/10 helix

	DMSO-d_6 (%, v/v)											
	0	*0.5*	*1*	*1.5*	*2*	*2.5*	*3*	*4*	*5*	*7.5*	*10*	*Δδ*
*δ*NH4	5.74	5.75	5.77	5.78	5.81	5.83	5.85	5.89	5.93	5.98	6.00	0.26
*δ*NH11	6.72	6.77	6.82	6.87	6.94	6.97	7.00	7.05	7.11	7.16	7.18	0.46
*δ*NH15	8.17	8.17	8.17	8.17	8.17	8.17	8.17	8.17	8.17	8.15	8.15	0.02
*δ*NH22	7.86	7.87	7.87	7.87	7.87	7.87	7.87	7.87	7.87	7.87	7.86	0.00
*δ*NH26	6.88	6.97	7.07	7.14	7.25	7.29	7.34	7.43	7.51	7.60	7.64	0.76

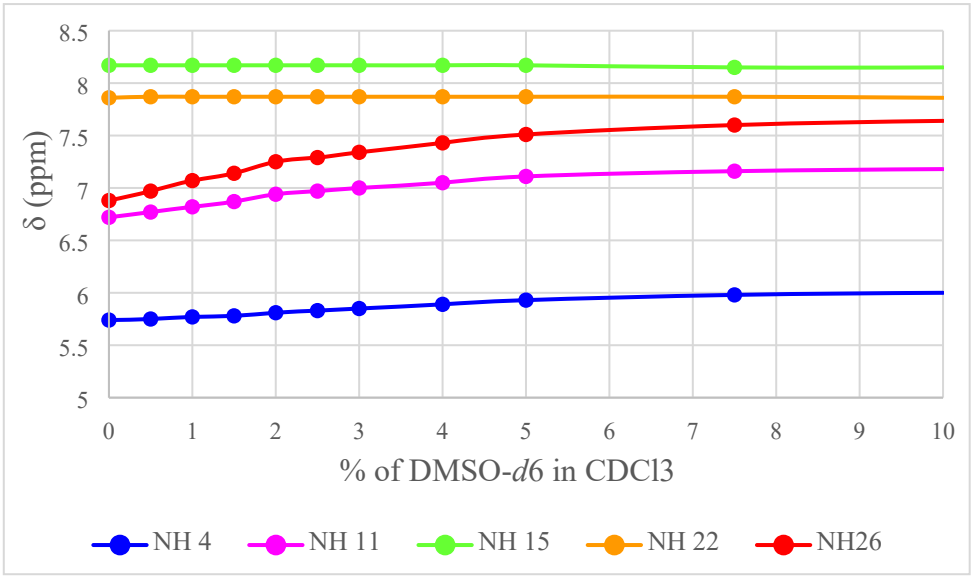

Figure S3.3. ^{1}H NMR DMSO-d_6 titration experiment on compound 1A.

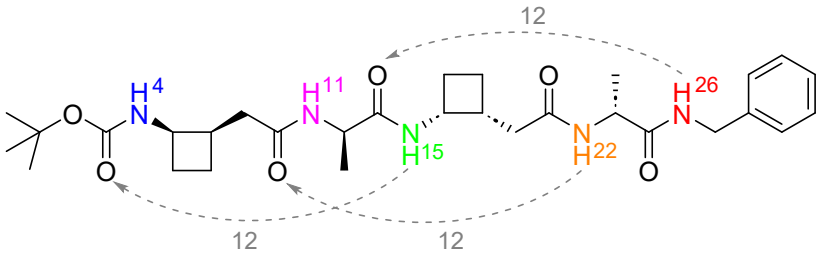

Compound **3A** (*R,R,R*) showing the hydrogen bonding system of a 12 helix

	DMSO-d_6 (%, v/v)											
	0	*0.5*	*1*	*1.5*	*2*	*2.5*	*3*	*4*	*5*	*7.5*	*10*	$\Delta\delta$
δNH4	4.99	5.22	5.31	5.38	5.44	5.48	5.55	5.62	5.67	5.76	5.82	0.83
δNH11	5.91	6.17	6.25	6.33	6.40	6.45	6.53	6.61	6.65	6.76	6.82	0.91
δNH15	7.74	7.77	7.79	7.79	7.79	7.80	7.81	7.81	7.82	7.82	7.80	0.06
δNH22	7.74	7.74	7.73	7.72	7.72	7.71	7.68	7.67	7.67	7.64	7.62	–0.12
δNH26	7.28	7.34	7.36	7.36	7.38	7.38	7.39	7.39	7.39	7.39	7.38	0.10

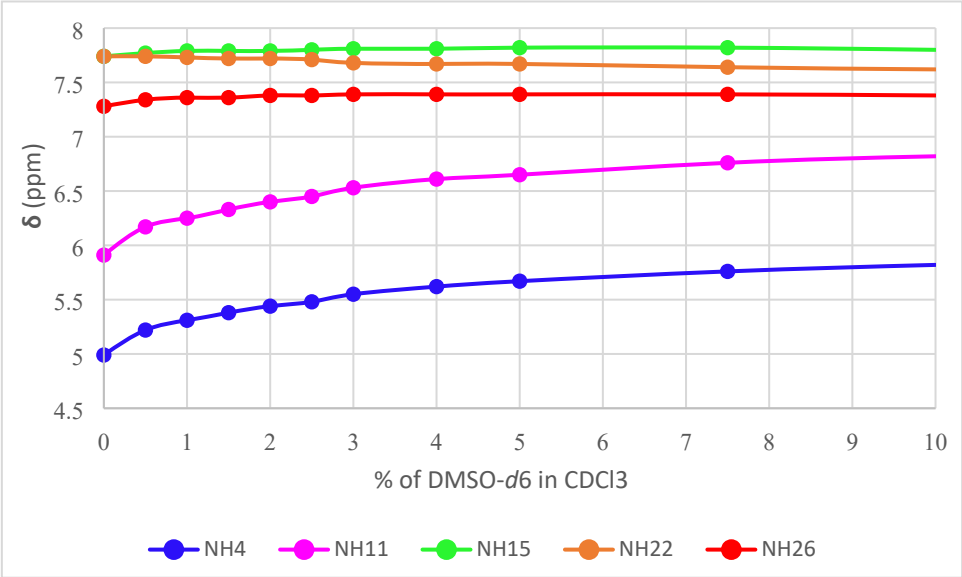

Figure S3.4. ^{1}H NMR DMSO-d_6 titration experiment on compound 3A.

3.3 ROESY NMR experiments

ROESY spectra of (*R,R,S*) series peptides **1E**, **1A**, **2E** and **2A** peptides were recorded on a Bruker 400 MHz spectrometer. Solutions were prepared in pyridine-d_5 at a concentration of 5 mM. The pulse sequence was roesyadjsphpr. The experiments were performed by collecting 2048 points in f2 and 256 points in f1.

All four peptides showed non-local correlations that were indicative of the presence of 12/10 helical conformations, according to literature precedents.[S14-S17]

These correlations are: CαH(*i*–2)—HNα(*i*), NγH(*i*–2)—HNα(*i*) and CγH(*i*–2)—HNα(*i*).

Tetrapeptide ester **1E**

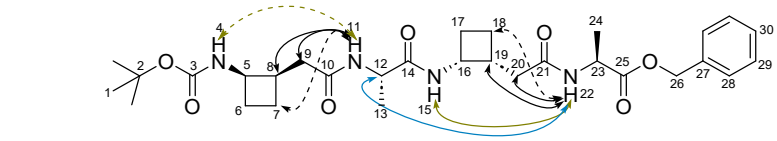

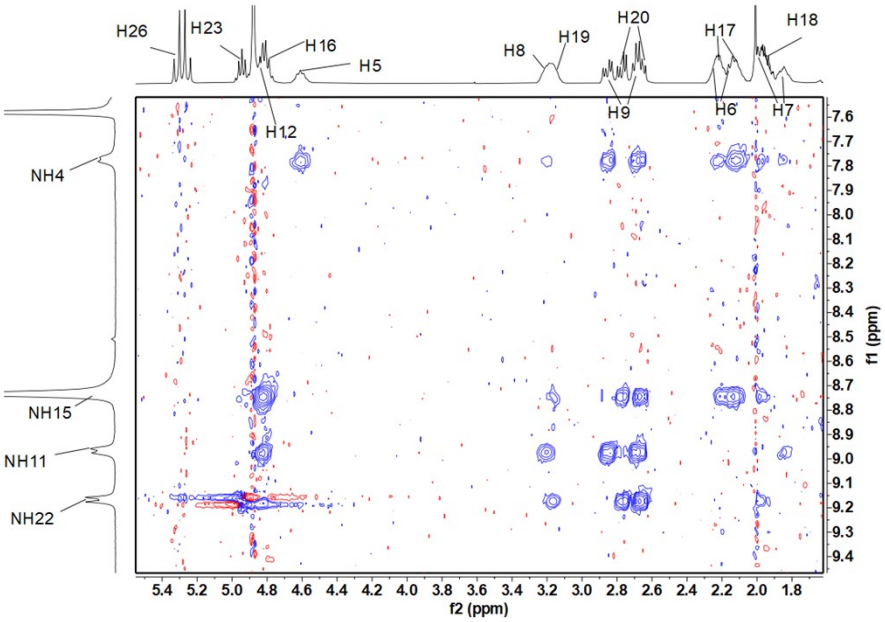

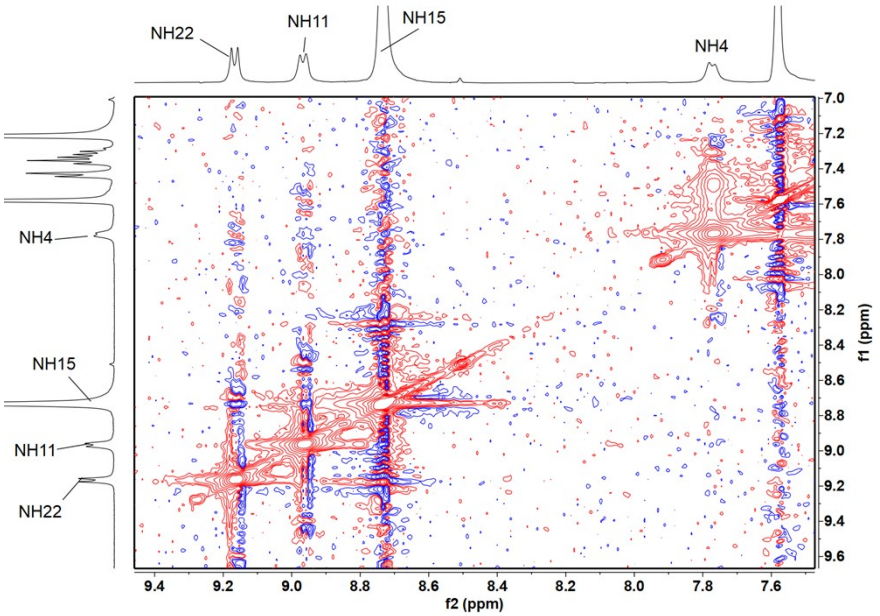

Tetrapeptide amide **1A**

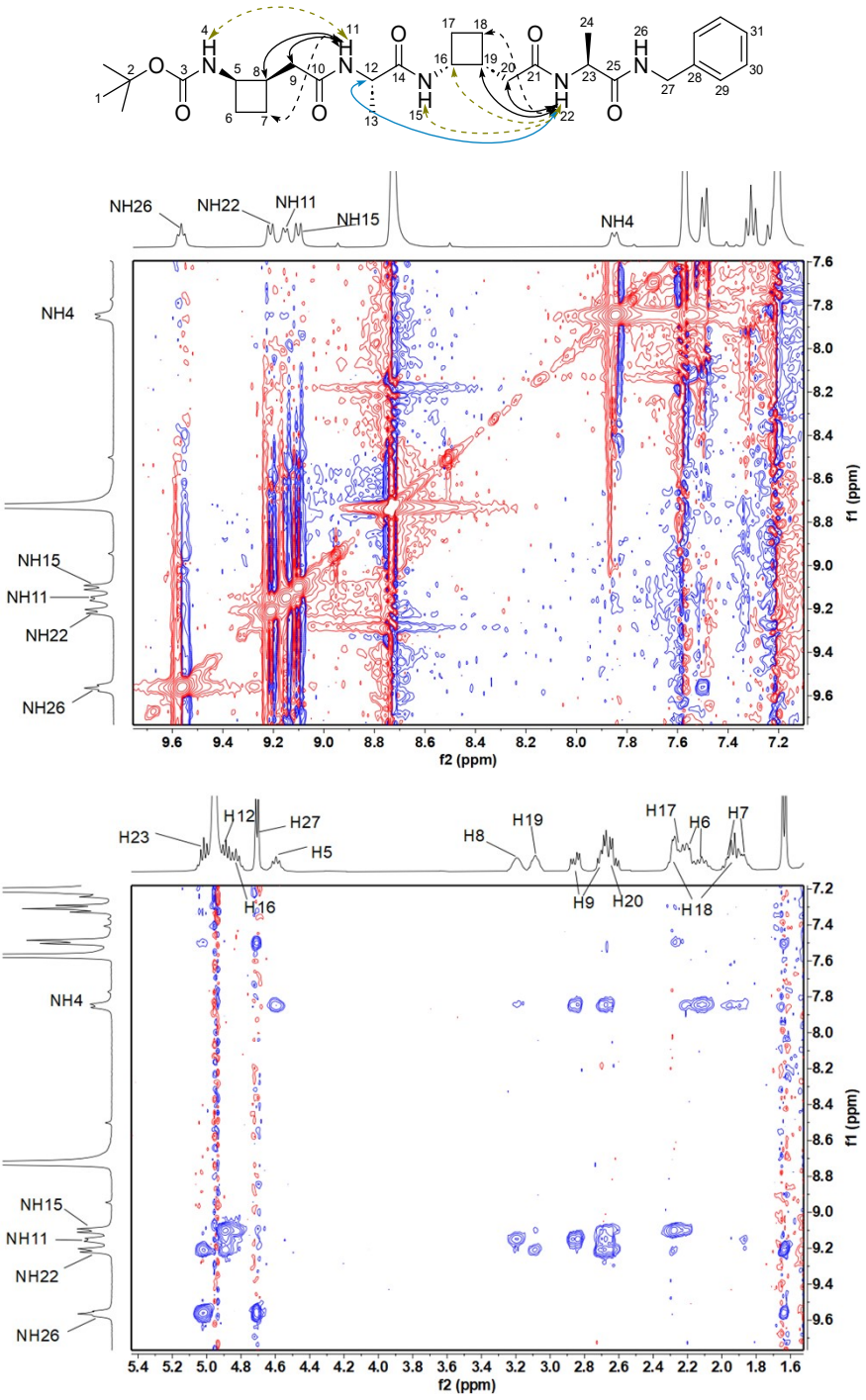

Hexapeptide ester **2E**

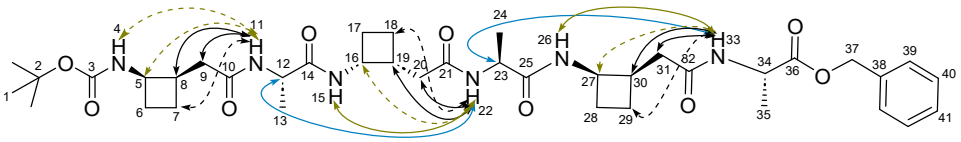

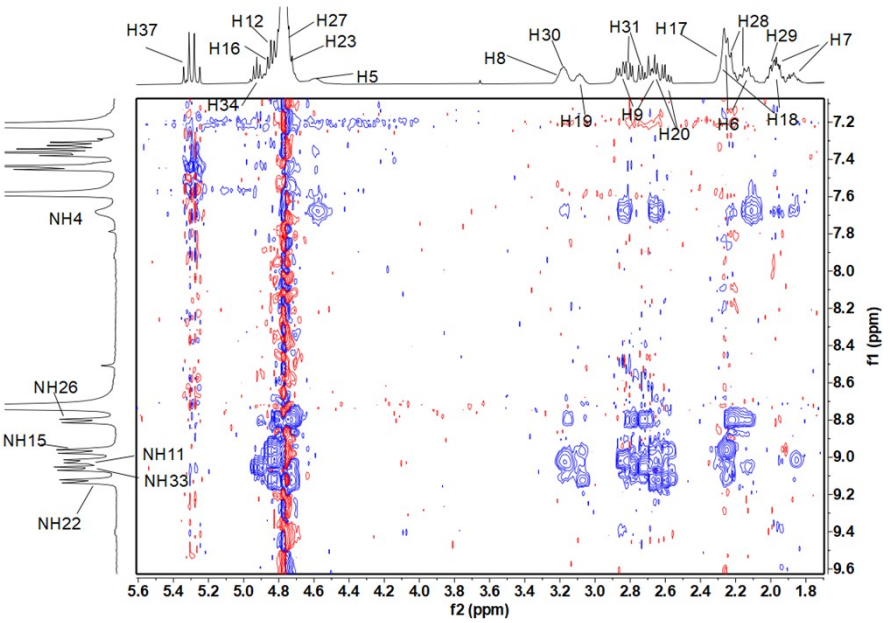

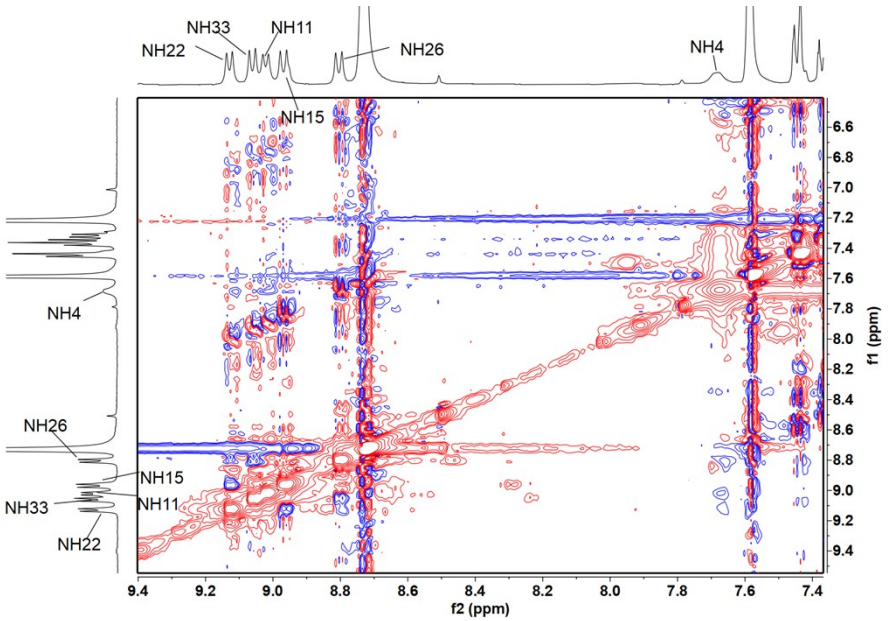

Hexapeptide amide **2A**

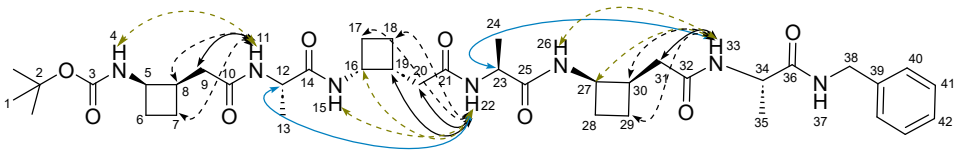

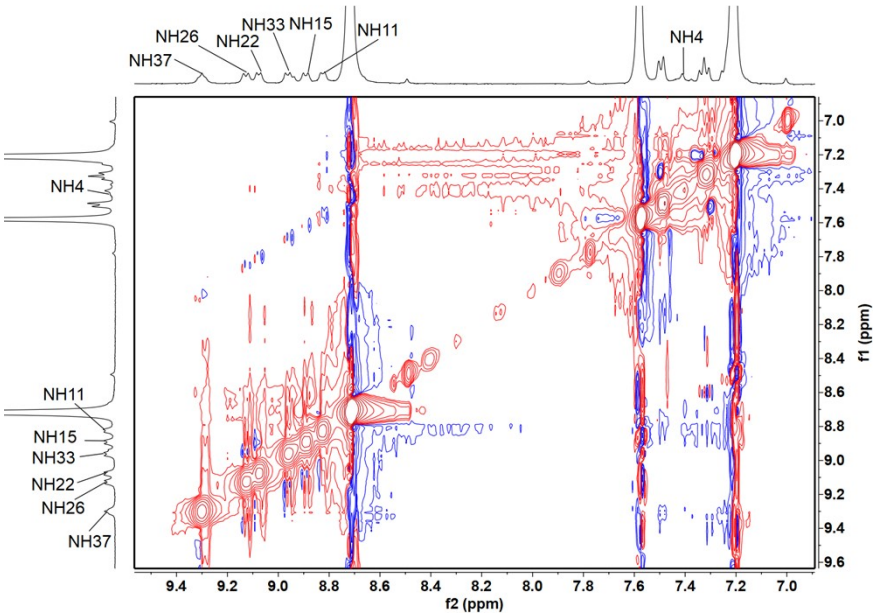
NH26
NH22
NH33 NH15
NH11
NH37
NH4
NH4
NH11
NH15
NH33
NH22
NH26
NH37
f2 (ppm)
f1 (ppm)

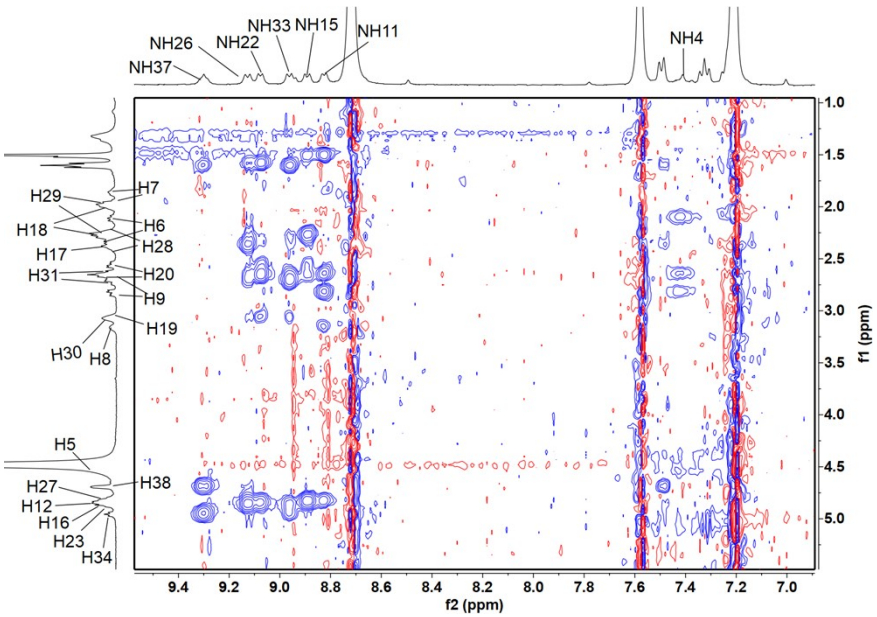
NH26
NH22
NH33 NH15
NH11
NH37
NH4
H29
H18
H17
H31
H7
H6
H28
H20
H9
H19
H30
H8
H5
H27
H12
H16
H23
H34
H38
f2 (ppm)
f1 (ppm)

3.4 Circular Dichroism

The far-UV electronic circular dichroism (ECD) spectra were recorded for 0.25 μM or 0.125 μM solutions in analytical grade MeOH in 1 mm sample cells at 298 K. The mean residue molar ellipticity $[\theta]$ (deg·cm^2·dmol^{-1}) was calculated according to the equation below, wherein θ*obs* = observed ellipticity (mdeg); *c* = concentration (mol·L^{-1}); *n* = number of residues; *l* = cell path length (cm).

$$[\theta] = \frac{\theta obs}{10 \times c \times n \times l}$$

The ECD spectra are shown in Figure S3.5. The (*R,R,S*) peptide series shows a fairly regular set of curves, with some heterogeneity for ester **1E**, but better homology for **1A**, **2E** and **2A**, featuring a single positive Cotton effect centered around 205 nm. The (*R,R,R*) peptide series is considerably more disparate, showing a positive Cotton effect that varied from 195 to 205 nm and, in some cases but not all, a negative effect at around 220 nm. There is no coherence in the strength of the Cotton effects with increasing hydrogen bonding options and no regularity in the ratio of the positive/negative Cotton effects.

There are only limited reports in the literature of ECD spectra of α/γ-peptides and precious few correlations between the signs of the Cotton effects and the helix handedness. We concur with the caution that has been advocated regarding the interpretation of ECD spectra of folded peptides and the limits of the technique in the evaluation of secondary structure.[S18-S21]

Methanolic ECD spectra of α/γ-peptides that adopt 12/10 helix structures feature a single Cotton effect centered around 205 nm.[S14, S17] A positive Cotton effect is considered to be indicative of a right-handed 12/10 helix, on the basis of an examination of the backbone dihedral angles obtained from a restrained molecular dynamics study.[S14] The regularity of the ECD spectra of the (*R,R,S*) peptide series, showing a positive Cotton effect centered at around 205 nm, suggests that the right-handed 12/10 helix observed for these compounds in chloroform solution may also prevail in the more polar solvent methanol.

Methanolic ECD spectra of α/γ-peptides that adopt 12 helix structures show a first Cotton effect centered at around 220 nm and a second Cotton effect, stronger and with the opposite sign, at around 195 nm.[S18, S22-S25] While some superficial similarities appear, the lack of heterogeneity in the ECD spectra for the (*R,R,R*) peptide series in methanol precludes confident assignment of any predominant folding pattern for these compounds in this polar solvent.

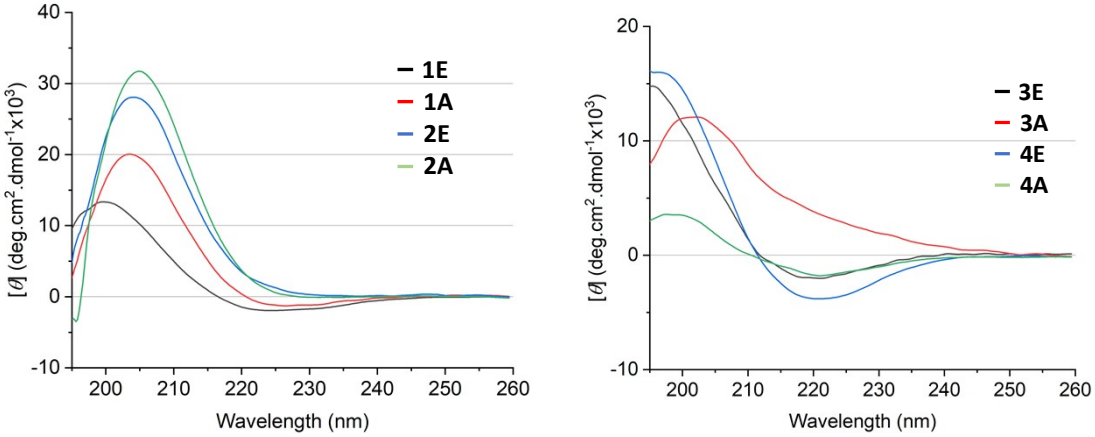

Figure S3.5. ECD spectra (0.125-0.25 mM in MeOH) of (*R,R,S*) series peptides 1E, 1A, 2E and 2A (*left*) and of (*R,R,R*) series peptides 3E, 3A, 4E and 4A (*right*).

4. References

S1. Turbomole V7.2, **2017**, a development of University of Karlsruhe and Forschungszentrum Karlsruhe GmbH, 1989-2007, Turbomole GmbH, since 2007; available from http://www.turbomole.com.

S2. S. Grimme, S. Ehrlich and L. Goerigk, *J. Comput. Chem.*, 2011, **32**, 1456.

S3. A. Schafer, C. Huber and R. Ahlrichs, *J. Chem. Phys.*, 1994, **100**, 5829.

S4. D. Rappoport and F. Furche, *J. Chem. Phys.*, 2010, **133**, 134105.

S5. M. Sierka, A. Hogekamp and R. Ahlrichs, *J. Chem. Phys.*, 2003, **118**, 9136.

S6. K. Eichkorn, O. Treutler, H. Ohm, M. Haser and R. Ahlrichs, *Chem. Phys. Lett.*, 1995, **240**, 283.

S7. K. Eichkorn, O. Treutler, H. Ohm, M. Haser and R. Ahlrichs, *Chem. Phys. Lett.*, 1995, **242**, 652.

S8. K. Eichkorn, F. Weigend, O. Treutler and R. Ahlrichs, *Theo. Chem. Acc.*, 1997, **97**, 119.

S9. C. Baldauf, R. Günther and H. J. Hofmann, *J. Org. Chem.*, 2006, **71**, 1200.

S10. A. Klamt and G. Schuurmann, *J. Chem. Soc. Perkin Trans. 2*, 1993, 799.

S11. C. Fernandes, S. Faure, E. Pereira, V. Théry, V. Declerck, R. Guillot and D. J. Aitken, *Org. Lett.*, 2010, **12**, 3606.

S12. G. Goldsztejn, V. R. Mundlapati, V. Brenner, E. Gloaguen, M. Mons, C. Cabezas, I. León and J. L. Alonso, *Phys. Chem. Chem. Phys.*, 2020, **22**, 20284.

S13. H. Awada, S. Robin, R. Guillot, O. Yazbeck, D. Naoufal, N. Jaber, A. Hachem and D. J. Aitken, *Eur. J. Org. Chem.*, 2014, **2014**, 7148.

S14. G. V. M. Sharma, V. B. Jadhav, K. V. S. Ramakrishna, P. Jayaprakash, K. Narsimulu, V. Subash and A. C. Kunwar, *J. Am. Chem. Soc.*, 2006, **128**, 14657.

S15. B. F. Fisher, L. Guo, B. S. Dolinar, I. A. Guzei and S. H. Gellman, *J. Am. Chem. Soc.*, 2015, **137**, 6484.

S16. M. W. Giuliano, S. J. Maynard, A. M. Almeida, L. Guo, I. A. Guzei, L. C. Spencer and S. H. Gellman, *J. Am. Chem. Soc.*, 2014, **136**, 15046.

S17. R. Fanelli, D. Berta, T. Földes, E. Rosta, R. A. Atkinson, H. J. Hofmann, K. Shankland and A. J. A. Cobb, *J. Am. Chem. Soc.*, 2020, **142**, 1382.

S18. B. F. Fisher and S. H. Gellman, *J. Am. Chem. Soc.*, 2016, **138**, 10766.

S19. A. Glättli, X. Daura, D. Seebach and W. F. van Gunsteren, *J. Am. Chem. Soc.*, 2002, **124**, 12972.

S20. D. A. Niggli, M. O. Ebert, Z. X. Lin, D. Seebach and W. F. van Gunsteren, *Chem. Eur. J.*, 2012, **18**, 586.

S21. D. Seebach, B. Jaun, R. Sebesta, R. I. Mathad, O. Flögel, M. Limbach, H. Sellner and S. Cottens, *Helv. Chim. Acta*, 2006, **89**, 1801.

S22. B. Dinesh, V. Vinaya, S. Raghothama and P. Balaram, *Eur. J. Org. Chem.*, 2013, **2013**, 3590.

S23. A. Bandyopadhyay, S. V. Jadhav and H. N. Gopi, *Chem. Commun.*, 2012, **48**, 7170.

S24. S. V. Jadhav, A. Bandyopadhyay and H. N. Gopi, *Org. Biomol. Chem.*, 2013, **11**, 509.

S25. A. Malik, M. G. Kumar, A. Bandyopadhyay and H. N. Gopi, *Pept. Sci.*, 2017, **108**, e22978.